



COMPARATIVE LABORATORY PERFORMANCE CHARACTERISATION OF SILICONE RUBBER TEXTURED INSULATORS

BY

ADNAN SALAMA KRZMA

B.Sc., M.Sc., ELECTRICAL ENGINEERING

Thesis submitted to Cardiff University

In candidature for the degree of

DOCTOR OF PHILOSOPHY

ADVANCED HIGH VOLTAGE ENGINEERING RESEARCH CENTRE

SCHOOL OF ENGINEERING

CARDIFF UNIVERSITY

2016

DECLARATION

This work has not previously been accepted in substance for any degree and is not concurrently submitted in candidature for any degree.

Signed.....(ADNAN S. KRZMA) Date.....

STATEMENT 1

This thesis is being submitted in partial fulfillment of the requirements for the degree of PhD.

Signed.....(ADNAN S. KRZMA) Date.....

STATEMENT 2

This thesis is the result of my own independent investigations, except where otherwise stated. Other sources are acknowledged by explicit references.

Signed.....(ADNAN S. KRZMA) Date.....

STATEMENT 3

I hereby give consent for my thesis, if accepted, to be available for photocopying and for inter-library loan, and for the title and summary to be made available to outside organisations.

Signed.....(ADNAN S. KRZMA) Date.....

*In the name of Allah, the Most Gracious, the Most Merciful
Peace and blessings be upon our Prophet Muhammad
and upon his family and companions*

ACKNOWLEDGEMENTS

I would like to express my heartfelt gratitude and appreciation foremost to my supervisors Prof. A. Haddad and Dr. M. Albano for all their invaluable guidance, support and encouragement throughout the duration of this project. Their expert advice and recognised extensive knowledge in the field of outdoor insulation systems have been a permanent source of great assistance.

I would like to extend my sincere thanks to Prof. R. T. Waters, Dr. H. Griffiths, and Dr. D. Clark for their valuable discussion and constant guidance.

I would also like to thank my sponsor, the ministry of higher education and scientific research of Libya for giving me the opportunity to complete my PhD study, without their financial support this study would not have been successful.

Thanks to all my colleagues at Advanced High Voltage Engineering Research Centre (AHIVE) for their help and friendship. I would also like to thank the technicians and the members of the research office for their assistance and support.

Last but not least, I wish to express my love and gratitude to my beloved wife for her patience and moral support. Deepest love to my mother for her endless encouragement. Thanks also to Allah for his gift, my beloved son "Elias".

ABSTRACT

Silicone rubber (SiR) outdoor insulators are increasingly being deployed in new AC and DC high voltage transmission systems thanks to their superior performance in wet-polluted conditions compared to traditional porcelain and glass insulators. However, in severely polluted environments, sustained discharge activities and dry band arcing due to surface contamination cause tracking, erosion, and the loss of hydrophobicity on the SiR insulator surface. This degradation can accelerate damage to the insulator surfaces, increasing the probability of a flashover and enduring insulator failure.

This thesis presents an experimental study on the electric performance of polluted and aged outdoor SiR polymeric insulators using AC and DC voltages. The research involved an extensive review of the published literature and an investigation of the performance of SiR insulators subjected to different ambient conditions and identifies the modes where most failure and degradation occurred on SiR surfaces.

Experimental investigations were carried out to compare the aging performance of two 11kV SiR insulator designs using a rotating wheel dip test under AC and positive DC excitations. A standard polymeric insulator design was used and compared with insulators that had a textured surface. Both insulator designs were fabricated in-house using a vacuum casting machine. Several electrical parameters were measured during the test to characterise the performance of each insulator. Dry band arcing activities were mainly observed on the trunk surface of the conventional profile. A decrease in hydrophobicity was measured on the tested surfaces, and tracking and erosion defects were also observed on both insulator designs. Leakage current measurements showed that drying and discharge activity was greater for a conventional insulator compared with the textured insulator, and more severe degradation appeared under positive DC tests than under AC. These studies showed that insulators with a textured design can improve the performance of SiR insulators against tracking and erosion under AC and positive DC excitations.

The electric field and potential distributions along the leakage surface of the 11 kV SiR insulators under dry clean and wet polluted conditions were studied using finite element method COMSOL Multiphysics. The critical of high field regions on SiR surfaces were identified and the power dissipated in the pollution layer along insulator surface was calculated. This study showed useful information about surface heating, which could be used to predict of the formation of dry bands.

An investigation of the pollution layer characterisation on conventional and textured pattern designs is described. Several tests were conducted to evaluate the behaviour of the insulator surfaces under different conditions. ESDD and NSDD parameters were measured for different materials, and evaluations for each design were also performed. Leakage conductance measurements on surface designs were determined, and the distribution trends of surface conductance were also characterised. Different rectangular SiR samples were assessed, and an improvement for reducing the pollutant deposition on textured surfaces was observed. In 4-shed insulators, the textured design showed comparable ESDD value with conventional profile. Textured designs also showed slower growth of the leakage current than the conventional design.

Clean fog tests (based on a high voltage ramp test) were carried out to investigate the flashover performance of conventional and textured insulator designs. For different ranges of wetting and pollution severity conditions, the textured design showed an improvement in the flashover performance that could reach 16 % compared to the conventional surface. This indicates that the textured surface seems to be more effective under severe ambient conditions. It was also observed that the textured insulator design can improve the electrical performance of SiR insulators under AC and DC voltages.

PUBLICATIONS

A. S. Krzma, M. Albano, R. T. Waters, and A. Haddad, "Comparative performance of 11 kV silicone rubber polymeric insulators with HVAC and HVDC excitations using the rotating wheel dip test," in The 19th International Symposium on High Voltage Engineering (ISH), Pilsen, Czech Republic, 2015.

M. Albano, **A. S. Krzma**, R. T. Waters, H. Griffiths, and A. Haddad, "Artificial pollution layer characterization on conventional and textured silicone-rubber insulators," in The 19th International Symposium on High Voltage Engineering (ISH), Pilsen, Czech Republic, 2015.

A. S. Krzma, M. Albano, and A. Haddad, "Comparative performance of 11kV silicone rubber insulators using artificial pollution tests," in 2015 50th International Universities Power Engineering Conference (UPEC), Stoke On Trent, United Kingdom, pp. 1–6, 2015.

A. S. Krzma, M. Albano, and A. Haddad, "Comparative performance of 11kV silicone rubber polymeric insulators under Rotating Wheel Dip Test," in 49th International Universities Power Engineering Conference (UPEC), Cluj-Napoca (Romaina), pp. 1–5, 2014.

A. S. Krzma, M. Albano, and A. Haddad, "Comparative performance of 11kV silicone rubber polymeric insulators using Tracking Wheel Test," 7th Universities High Voltage Network - UHVNet 2014, Colloquium on Technologies for Future High Voltage Infrastructure, 15-16 Jan, Guildford, 2014.

TABLE OF CONTENTS

CHAPTER 1: INTRODUCTION	1
1.1. Outdoor insulation for high voltage: functions and problems	1
1.2. Impact of weathering on flashover performance of polymeric insulators	2
1.3. Objectives of the present work.....	4
1.4. Methodology	6
1.5. Thesis contributions.....	8
1.6. Thesis outline	9
CHAPTER 2: COMPATATIVE PERFORMANCE OF OUTDOOR INSULATORS: A REVIEW ...	12
2.1. Introduction.....	12
2.2. Outdoor insulators	13
2.2.1. Porcelain insulators	13
2.2.2. Glass insulators.....	14
2.2.3. Polymeric insulators	15
2.3. Composite insulation materials	16
2.3.1. Silicone rubber	18
2.3.2. Texturing of silicone rubber polymeric insulators	18
2.3.3. Construction of silicone rubber insulators	20
2.4. Pollution influences on silicone rubber insulators.....	23
2.4.1. Pollution cumulative on insulator surfaces	23
2.4.2. Categories of pollution severity levels.....	24
2.5. Outdoor insulators for direct voltages	26
2.5.1. Basic differences between DC and AC conditions	26
2.5.2. Flashover vulnerabilities on DC and AC systems.....	28
2.5.3. Deterioration features on DC systems	30
2.6. Aging and degradation of polymeric insulators.....	31
2.6.1. Polymeric insulators failure modes	32
2.6.2. Loss and recovery of hydrophobicity.....	35
2.6.3. Polarity effect on the aging of Silicone rubber insulators.....	36
2.7. Flashover mechanism of silicone rubber insulators.....	40
2.8. Monitoring and assessments	42
2.8.1. Visual inspections.....	42
2.8.2. Hydrophobicity evaluation.....	43
2.8.3. The leakage current measurement	45
2.9. Artificial pollution testing methods of polymeric insulators.....	46

2.9.1.	Flashover tests methods.....	47
2.10.	Performance of silicone rubber insulators under AC and DC energisation	48
2.11.	Summary	55
CHAPTER 3: EXPERIMENTAL FACILITIES, SAMPLES AND TEST ARRANGEMENTS		56
3.1.	Introduction.....	56
3.2.	Experimental test summary	57
3.3.	Textured design.....	57
3.3.1.	Textured Trunk (TT) profiles	59
3.3.2.	Textured Trunk and Shed (TTS) profiles.....	60
3.4.	The Rotating Wheel Dip Test (RWDT).....	60
3.4.1.	Test insulators	61
3.4.2.	Insulator preparation.....	62
3.4.3.	Rotating wheel dip test set-up and facilities	65
3.4.4.	Electric circuit of RWDT	66
3.4.5.	Motor control program and data acquisition system.....	67
3.5.	Surface conductance measurement tests	74
3.5.1.	Surface conductance meter	74
3.6.	Measurement of insulator pollution level.....	75
3.7.	Fog chamber test.....	76
3.7.1.	Test samples	76
3.7.2.	The preparation of pollution suspension	76
3.7.3.	The fog chamber	77
3.7.4.	The test circuit diagram	78
3.7.5.	The data acquisition system	79
3.7.6.	Thermal and visual cameras records	80
3.8.	Summary	80
CHAPTER 4: COMPARATIVE PERFORMANCE OF SILICONE RUBBER POLYMERIC INSULATORS UNDER HVAC AND HVDC ENERGISATIONS USING THE ROTATING WHEEL DIP TEST		82
4.1.	Introduction.....	82
4.2.	Experimental conditions.....	83
4.3.	Experimental procedure.....	84
4.4.	Rotating wheel dip tests under AC excitation	85
4.4.1.	Leakage current.....	85
4.4.2.	RMS leakage current.....	87
4.4.3.	Peak current magnitude.....	88
4.4.4.	Power dissipation	89

4.4.5.	Power factor angle.....	90
4.4.6.	Cumulative dissipated energy.....	91
4.5.	Rotating wheel dip tests under positive polarity DC excitation	91
4.5.1.	Leakage current.....	91
4.5.2.	Cumulative dissipated energy.....	92
4.6.	Visual and infrared (IR) observations of aging	93
4.6.1.	Visual and infrared (IR) observations.....	93
4.6.2.	Electrical discharge activities and temperature distribution	96
4.7.	Hydrophobicity tests	97
4.8.	Localised surface conductance evaluation tests	99
4.9.	Computation of electric field distribution over the polluted surface of silicone rubber insulator	101
4.9.1.	Insulator geometry and material properties.....	102
4.9.2.	Boundary conditions	103
4.9.3.	Simulated model.....	104
4.9.4.	Simulation results and	105
4.10.	Conclusion	109
CHAPTER 5: ARTIFICIAL POLLUTION LAYER CHARACTERISATION ON CONVENTIONAL AND TEXTURED SILICONE RUBBER INSULATORS.....		113
5.1.	Introduction.....	113
5.2.	Equivalent Salt Deposit Density (ESDD) and Non-Soluble Deposit Density (NSDD) evaluation	114
5.2.1.	The requirements to measure the pollution severity degree.....	115
5.2.2.	Application and removal of pollution layer.....	115
5.2.3.	Equivalent Salt Deposit Density (ESDD) on rectangular plain samples	117
5.2.4.	Equivalent Salt Deposit Density (ESDD) on 4-shed insulators.....	119
5.3.	Leakage conductance evaluation tests under AC and DC voltages	122
5.3.1.	Fog density.....	122
5.3.2.	Wetting process.....	123
5.3.3.	AC and DC leakage conductance evolutions	125
5.4.	Surface conductance evaluation tests	128
5.4.1.	Test procedure	128
5.4.2.	Test results and discussion	129
5.5.	Conclusion.....	131
CHAPTER 6: PERFORMANCE OF ARTIFICIALLY POLLUTED SILICONE RUBBER POLYMERIC INSULATORS USING THE CLEAN FOG CHAMBER FACILITY		133
6.1.	Introduction.....	133
6.2.	High voltage tests	134

6.3.	Clean insulator fog test.....	134
6.4.	High voltage flashover tests with ramp control under different pollution conditions.....	136
6.4.1.	Test classification	137
6.4.2.	Test techniques	138
6.4.3.	Flashover performance of tested insulators	139
6.4.4.	The influence of pollution severity level on the flashover of SiR insulators 142	
6.4.5.	Flashover voltage (FOV) variation with salt deposit density (ESDD)	144
6.4.6.	The influence of the wetting rate on the flashover of SiR insulators	145
6.4.7.	Electrical properties calculated associated with FOV	146
6.4.8.	Visual observations of pre-flashover	150
6.5.	Performance of silicone rubber polymeric insulators under AC and positive DC tests	150
6.5.1.	Artificial pollution of tested insulators	151
6.5.2.	HVAC clean-fog test results.....	152
6.5.3.	HVDC clean-fog test results.....	153
6.5.4.	Visual appearance and infrared (IR) observations	155
6.6.	Conclusion.....	157
CHAPTER 7: GENERAL DISCUSSIONS, CONCLUSION AND FUTURE WORK		160
7.1.	Performance in the rotating wheel dip tests	160
7.2.	Artificial pollution layer characterisation over the insulator surfaces.....	162
7.3.	Performance under clean fog.....	163
7.3.1.	Tests procedures.....	163
7.3.2.	High voltage ramp tests conclusions.....	164
7.3.3.	Performance of SiR insulators under clean fog test using AC and DC voltages	166
7.4.	Future work	167

LIST OF FIGURES

CHAPTER 2

Figure 2-1: Standard design cap-and-pin porcelain insulators.	14
Figure 2-2: Cap-and-Pin glass insulators.	14
Figure 2-3: Chemical structure of silicone rubber.	18
Figure 2-4: Cross-section of 11kV silicone rubber insulators.	21
Figure 2-5: Relationship between ESDD and NSDD (pollution type A) and the site pollution severity levels [2-115].	25
Figure 2-6: An overview of various factors effects on the aging of polymeric insulators [2-63].	31
Figure 2-7: Most common failure modes of polymeric insulators [2-68, 2-69, 2-70].	34
Figure 2-8: Model of the IP test setup illustrating the flow direction of for the contaminant and the ion under (a) positive DC and (b) negative DC voltages [2-82].	38
Figure 2-9: Captures of the electrodes (a) before the IP test, (b) after seven hours of IP test under positive DC, (c) after seven hours of IP test under negative DC [2-82].	39
Figure 2-10: Flashover development on SiR insulators [2-88].	42
Figure 2-11: Sessile water drop on the insulator surface [2-7].	43
Figure 2-12: AC leakage current bin count data for tested insulators during a period of 150 days [2-83].	49
Figure 2-13: Positive DC leakage current bin count data for tested insulators during a period of 150 days [2-83].	49
Figure 2-14: Negative DC leakage current bin count data for tested insulators during a period of 150 days (Note that data for the insulator SiR 75 are not presented) [2-83].	50

Figure 2-15: Time of day average of 10 minutes peak leakage currents for insulator SiR 29 for test period of 150 days [2-83].....	51
Figure 2-16: Time of day average of 10 minutes peak leakage currents for insulator SiR 87 for test period of 150 days [2-83].....	51
Figure 2-17: Peak current waveforms for SiR 87 insulator during a pollution event [2-83].	52
Figure 2-18: Maximum leakage current of the SiR insulator under AC [2-119]. ..	52
Figure 2-19: Maximum leakage current for SiR insulator under DC both polarities [2-119].	53
Figure 2-20: Erosion on the insulator SiR 87 [2-83].....	54
Figure 2-21: Visual appearance of the SiR insulator at the end of the test [2-119].	54

CHAPTER 3

Figure 3-1: Hemispherical protuberances: square-intersection pattern [2-25]. ...	58
Figure 3-2: 4 mm textured trunk design (TT4) [2-81].....	60
Figure 3-3: 6 mm textured trunk shed design (TTS6) [2-81].....	60
Figure 3-4: Pigtail and pin aluminium end fitting design.	61
Figure 3-5: Test samples for conventional (a) and textured trunk (b) insulators.	62
Figure 3-6: (a) the vacuum casting machine: (1) the top mixing chamber (2) the lower injection chamber (3) touch control panel; (b) oven; (c) conventional insulator; and (d) textured insulator.....	64
Figure 3-7: Circuit diagram of RWDT.....	65
Figure 3-8: Test set-up of Rotating Wheel Dip Test on 11kV polymeric insulator.	66
Figure 3-9: The graphical LabVIEW program of the motor control of RWDT.	68
Figure 3-10: Flow chart of the motor control program.	69
Figure 3-11: The LabVIEW block diagram code for acquiring, monitoring and saving the leakage current and applied voltage signals.	71

Figure 3-12: The post-processing LabVIEW programming code: analysing and storing functions of the electrical properties.	72
Figure 3-13: The arrangement of surface conductance meter.....	74
Figure 3-14: Test set-up of fog chamber tester (Cardiff University High Voltage Laboratory).....	77
Figure 3-15: The test circuit diagram of fog chamber.....	78
Figure 3-16: Arrangement of data acquisition system.	79

CHAPTER 4

Figure 4-1: Schematic diagram of rotating wheel dip test [3-1].....	85
Figure 4-2: Leakage current and voltage applied waveforms during the 15 th wheel revolution.....	86
Figure 4-3: Typical RMS leakage current for conventional and textured insulators.	87
Figure 4-4: Typical variation of the absolute peak magnitude of leakage current.	88
Figure 4-5: Average power dissipated by conventional and textured insulators.	89
Figure 4-6: Power factor angle for conventional (a) and textured (b) insulators..	90
Figure 4-7: Total cumulative dissipated energy during 190 wheel revolutions under AC excitation (10 hours).	91
Figure 4-8: Typical variation of leakage current for both insulators under DC excitation.	92
Figure 4-9: Total cumulative dissipated energy during 190 cycles test under DC excitation (10 hours).	93
Figure 4-10: Infrared record and temperature distribution along the surface profile of tested insulators during rotating wheel dip tests, of different instants. .	94
Figure 4-11: Visible discharges activities during rotating wheel dip test.	95
Figure 4-12: The visual appearance of tested samples at the end of the test.....	96

Figure 4-13: Temperature distribution and leakage current waveforms of the conventional insulator when (1) partial arcing was formed and (2) a hot spot due to partial arcing developed.....	97
Figure 4-14: Hydrophobicity comparisons between tested insulators.....	98
Figure 4-15: Average surface conductance measurements for the top sheds of tested insulators.	100
Figure 4-16: Average surface conductance measurements for the bottom sheds of tested insulators.....	100
Figure 4-17: Average surface conductance measurements for the trunk of tested insulators.	101
Figure 4-18: An 11 kV silicone rubber insulator: (a) insulator geometry (b) cross-sectional profile and dimensions.....	102
Figure 4-19: Two dimension (2D) axis symmetric model for a polluted insulator	104
Figure 4-20: Equipotential lines along the surface profile of the clean dry and wet polluted SiR insulator.....	105
Figure 4-21: Voltage profile along the SiR insulator surface.....	106
Figure 4-22: Tangential electric field along the leakage path for insulator under wet polluted surface condition.....	107
Figure 4-23: Surface power dissipation in pollution layer along polluted insulator surface.....	109

Chapter 5

Figure 5-1: Swabbing of the pollutant on insulator surface [3-2].....	116
Figure 5-2: Procedure for measuring non- soluble deposit density (NSDD).	116
Figure 5-3: Rectangular samples with flat (left) and textured (right) surfaces. ...	117
Figure 5-4: ESDD on rectangular samples versus pollutant suspension conductivity.....	118

Figure 5-5: ESDD values for conventional insulators of material A (in blue) and material B (in red) versus conductivity of the pollutant suspension applied.	120
Figure 5-6: ESDD values for all insulator designs versus pollutant suspension conductivity applied.	121
Figure 5-7: Wetting on TTS6 insulators.....	124
Figure 5-8: Verifying the fog uniformity in the fog chamber tests.....	125
Figure 5-9: AC leakage current of a conventional insulator versus applied fog time; ESDD 0.21 mg/cm ²	126
Figure 5-10: AC leakage current for ESDD 0.21 mg/cm ² : conventional (CONV) and texture (TTS6).....	126
Figure 5- 11: AC leakage current for ESDD 1.20 mg/cm ² : conventional (CONV) and texture (TTS6).....	127
Figure 5-12: DC leakage current for ESDD 0.21 mg/cm ² : conventional (CONV) and texture (TTS6).....	128
Figure 5-13: Surface conductance measurements on sheds and trunk of conventional insulators at peak time (red) and after 1 hour-test (white).	130
Figure 5-14: Surface conductance measurements on sheds and trunk of textured insulators at peak time (red) and after 1 hour-test (white).	130

Chapter 6

Figure 6-1: Voltage RMS and leakage current RMS records during a clean SiR insulator fog-test.	135
Figure 6-2: Visual records of a clean SiR insulator at 42 kV.....	135
Figure 6-3: High voltage flashover tests.....	137
Figure 6-4: Mean FOV curve of 4 ramp voltage test series for a conventional SiR insulator. Each ramp test series consisted of 12 flashovers.	139
Figure 6-5: Ramp voltage test series for fog rate 9 l/h: effect of pollution severity level on FOV. Red curve ESDD 0.21 mg/cm ² , Green curve 0.64 mg/cm ² , and Blue curve 1.15 mg/cm ²	143

Figure 6-6: FOV variation with ESDD value at fog rates of 4 and 9 l/h using CONV and TT6 insulators.....	144
Figure 6-7: Average FOV of 3 test series for CONV and TT6 SiR insulators: effect of wetting rate on FOV. ESDD 0.64 mg/cm ² . Fog rates 4, 7 and 9 l/h.	145
Figure 6-8: Ramp 1 and 2 of test series for CONV insulator under conditions of ESDD (0.64 mg/cm ²) and fog rate (7l/h). Ramp 1: FOV 26.96 kV at 303s; Ramp 2: FOV 30.76 kV at 407s.....	147
Figure 6-9: Ramp voltage test series for CONV SiR insulator under conditions of ESDD (0.64 mg/cm ²) and fog rate (7 l/h).....	148
Figure 6-10: First voltage ramp of test series for CON and TT6 insulators. ESDD (0.64 mg/cm ²); fog rate (7 l/h): CONV: FOV 26.96 kV at 303 s, TT6: FOV 29.29 kV at 421 s.	149
Figure 6-11: Captures images of the conventional insulator during flashover fog test at 32 kV: (a) sparks bridging part of insulator trunk (b) bridging of sheds (c) small streamer discharges.....	150
Figure 6-12: Typical variations of rms leakage current for conventional and textured insulators.	152
Figure 6-13: Total cumulative dissipated energy during one-hour test under AC energization.....	153
Figure 6-14: Typical variation of leakage current under positive DC excitation.	154
Figure 6-15: Total cumulative dissipated energy during 1-hour test under positive DC energization.....	155
Figure 6-16: Visible image, infrared record and temperature distribution along the surface profile.....	156
Figure 6-17: The Visual appearance of tested insulators.	157

LIST OF TABLES

Table 2-1: Examples of typical environments.....	25
Table 2-2: Criteria for estimation the hydrophobicity classification (HC)	44
Table 2-3: Silicone rubber test insulators [2-83].....	48
Table 3-1: Characteristics of 600A/B silicone rubber material.....	61
Table 3-2: Dimensions of tested insulators	62
Table 4-1: Evaluated hydrophobicity level of samples after 10-hour test.....	99
Table 4-2: Material properties for the used insulator.....	103
Table 5-1: SiR insulator specifications.....	119
Table 5-2: The amount of NaCl requires for pollutant suspension conductivity	119
Table 6-1: High voltage flashover tests results	141

LIST OF ABBREVIATIONS

Abbreviation	Expansion
SiR	Silicone Rubber
HV	High Voltage
AC	Alternating Current
DC	Direct Current
RWDT	Rotating Wheel Dip Test
EPDM	Ethylene-Propylene-Diene-Monomer
ESDD	Equivalent Salt Deposit Density
NSDD	Non-Soluble Deposit Density
IEC	International Electrotechnical Commission
STRI	Swedish Transmission Research Institute
EPR	Ethylene-Propylene Rubber
RTV	Room Temperature Vulcanised
HTV	High Temperature Vulcanised
ATH	Alumina Trihydrate
LMW	Low Molecular Weight
NaCl	Sodium Chloride
SPS	Site Pollution Severity
UV	Ultra-Violet
IP	Inclined Plane
SEM	Scanning Electron Microscopy
EDX	Energy Dispersive X-ray
IR	Infra-Red
HC	Hydrophobicity Classification
FOV	Flashover Voltage
TT	Textured Trunk
TTS	Textured Trunk and Shed
CONV	Conventional
GRP	Glass Reinforced Plastic
DAQ	Data Acquisition
TDMS	Technical Data Management Streaming
RMS	Root Mean Square
THD	Total Harmonic Distortion
HTM	Hydrophobicity Transfer Materials
FEM	Finite Element Method

1.1. Outdoor insulation for high voltage: functions and problems

When high voltage electricity was first utilised, it was quickly realised that there was a need to design a device that could insulate the conductors from ground potential. However, while any solid non-conductive material would be able to insulate a potential of few kilovolts between the conductor and ground under dry test conditions, it was difficult to design an effective insulator for wet-polluted conditions. In the early stages, the highest operating test voltages had been between 50 kV and 60 kV. Nonetheless, over the years, an increase in operating voltages was necessary. This led to the development of insulators with high electrical and mechanical stress ratings and the introduction of new transmission system designs [1-1].

Increased pollution also raised other challenges for insulator design. Higher production from agricultural and industrial resources increases the amount of pollution deposited on insulators. Thereby, the environmental influence is an important factor for selecting an insulator [1-1].

Silicone rubber (SiR) insulators are widely adopted for outdoor insulation. This is due to their superior surface properties for water repellency and their ability to transfer the hydrophobicity to the adhering pollutants. Unlike hydrophilic insulators (ceramic), SiR forces water to be deposited as discrete beads on the insulator surface, which means that it is difficult for a continuous thin layer of water to be formed. The reduction of surface wetting, therefore, leads to a reduction in the discharge activity and dry band arcing on the polymeric surface and ultimately improves the anti-pollution performance.

Pollution flashover constitutes the predominant parameter for the design and dimensioning of high voltage insulators [2-7]. A widespread review work by CIGRE [1-2, 2-42], adopted by the recently revised international standard [3-2],

has overturned the traditional method where the creepage distance between the insulation terminals determined the selection process for polluted environments. It is now accepted that other elements strongly affect the pollution performance as well. These are related to the electrical system requirements, the type of environment and pollution, and the insulator design [2-81].

The aging of SiR insulators under AC and DC excitation, however, is still not fully understood. Little is known about the aging mechanisms involved at the different stages and their influence on the lifetime of polymeric insulators. Results obtained from aging test methods are generally accepted, showing that there is a good relationship between the field and laboratory aging results [1-3]. This gives the motivation to investigate the aging of insulator materials under High Voltage Alternating Current (HVAC) and High Voltage Direct Current (HVDC) excitation using the Rotating Wheel Dip Test (RWDT) and other tracking and erosion tests.

1.2. Impact of weathering on flashover performance of polymeric insulators

The adoption of polymeric insulators in transmission systems started in 1970 . SiR and ethylene-propylene-diene monomer (EPDM) are the main classifications used in housing materials. Most users have employed EPDM insulators for relatively clean areas. However, SiR insulators have been utilized in both clean and contaminated environments. The superior hydrophobic properties of SiR insulators make them an attractive option for difficult environments where other types of insulators (including glass and porcelain) have exhibited problems related to the leakage current and flashovers [1-4].

However, in contrast to ceramic insulators, the surface of polymeric insulators is known to be changeable with time due to aging. It is also well known that in SiR insulators, the pollutants may be covered by a layer of silicone oil (LMW). In

polymeric insulators, the pollution removal is more difficult than on glass and porcelain insulators. This denotes that there is an interaction between the contaminant and the polymeric surface. The performance of polymeric insulators is dependent on all these features [1-4].

The housing materials of polymeric insulators have been extensively observed, and it was found that they change due to exposure to weathering outdoors. Extensive degradation, such as cracking, crazing, tracking, and erosion, might be noticed on their surfaces. In turn, surface degradation encourages water accumulation and increases the possibility of flashover. In some places, flashovers have been seen in the early morning time during wet and misty conditions [1-4].

There have been many investigations of the flashover performance of polymeric insulators [1-5, 2-1]. Some have achieved good evaluations and have revealed that the flashovers are mostly on EPDM insulators. As this type of insulator is still used in service, predicting its future flashover performance is very important for system stability and reliability.

It has also been recognised that, in some cases, the non-soluble component of surface pollutants affects the pollution performance. Non-soluble deposit density (NSDD), which refers to the amount of non-soluble material per unit surface area, is used as an indicator of the inert component of contamination. NSDD is calculated by filtering the water obtained from the equivalent soluble deposit density (ESDD) measurement, drying the filter, and measuring the weight increase. However, ESDD is not a sufficient index of pollution severity on composite insulators exhibiting high hydrophobicity, and it may not provide all benefits of polymeric insulators performance.

Other approaches are needed to characterize the aging and pollution performance of composite insulators. Measuring the surface resistance at low

voltage in the absence of discharges through the measurement of the leakage current under wet conditions has been proved to be a successful method [1-4,1-6]. The leakage current measured represents the actual leakage conductance of the surface, taking into account the variations of the surface wettability and the interaction between the pollutant and the polymeric surface.

1.3. Objectives of the present work

Over the last four decades, extensive efforts have been made to achieve a better understanding of the aging in composite outdoor insulation materials, by utilising different methods to investigate the materials' properties and their surface changes due to degradation [1-7, 1-8]. Several experimental techniques have been conducted to assess the surface degradation due to discharge activities and dry band arcing, where the heat represents a predominant factor of degradation. There is a lack of information regarding the heat developed at the surface of SiR insulators during the dry band activities. However, with the use of modern thermal imaging tools, it has become easier to identify thermal stress on the insulator surfaces.

The textured insulator (characterised by 4 mm or 6 mm square textured patterns on the shed and/or shank regions) was proposed by Cardiff University as a novel design for SiR polymeric insulators [2-25]. Its pattern aims to improve the electrical performance and flashover voltages by reducing both the electric field strength and the leakage current density in the shank regions of an insulator. An increase in the length of creepage distance can reduce the field stress under severely polluted conditions while an increase in surface area could reduce the leakage current density in the susceptible shank region.

In tests based on IEC 62730 RWDT tests [3-1], textured insulators have been examined to investigate their electrical performance against other conventional insulator designs in order to identify any design that is inappropriate for use in

overhead transmission lines. Textured insulators have demonstrated a significant reduction in the leakage current and the surface degradation.

The research programme of this thesis, that is, investigating the performance of SiR polymeric insulators under different test conditions is diverse; with tasks including fabrication of insulators as well as designing software routing using LabVIEW programming for analysing the acquired data, computing the field distribution over the insulator surface using modelling based on the finite element method, devising low voltage tests for evaluating the surface and the pollution layer conductance, and conducting high voltage tests (RWDT, flashover ramp test, and clean fog test).

The main objectives of this research work are as follows:

- (a) to investigate the long-term aging performance of SiR polymeric insulators with different profiles, with textured and non-textured designs using a RWDT and to compare the surface degradation under AC and positive DC excitations
- (b) to evaluate the localised surface conductance on conventional and textured insulators by identifying and understanding the variation trends of the conductance and its distribution across the surface of each insulator
- (c) to evaluate the electric field distribution along the creepage path of the insulator using COMSOL Multiphysics software and to identify the critical high field regions and any useful information about surface heating, which might help to detect the formation of dry bands on the SiR surfaces
- (d) to extend the study of the ESDD and NSDD on textured and conventional insulator designs and their influence on the flashover level under different pollution conditions
- (e) to characterise the leakage layer conductance on conventional and textured insulators under different fog conditions and for a wide range of artificial pollution levels using AC and DC low voltage sources, and

to verify the uniformity of the pollution layer on different areas of the insulator surface during the artificial pollution test

- (f) to investigate the flashover performance of textured SiR insulators in the clean fog tests and make a comparison with the performance of the conventional design, and to quantify the effect of the pollution severity level and the wetting rate
- (g) to explore and compare the aging performance of textured and conventional SiR insulator designs when energised by alternating and positive direct voltages under artificial pollution conditions
- (h) to develop powerful data acquisition software codes using the LabVIEW programming language and so acquire and monitor the waveforms of the leakage current and voltage applied signals and to then store the data into TDMS files for further post processing analysis. For the RWDT, the software would require a program for controlling the motor

1.4. Methodology

In order to achieve the objectives of the present work, a series of laboratory experiments were conducted in the high voltage laboratory at Cardiff University. These experiments were performed using different test facilities including the RWDT, the surface conductance meter device, and the climate fog chamber facility.

The main methods used are summarised as follows:

- A series of standard RWDT at voltages of 13 kV AC and 13 kV positive DC were performed on two different SiR insulator designs (conventional, and textured) to study their aging performance and the degradation levels on each insulator surface, and thereby to identify the optimum design used in this work
- In addition, a series of high voltage tests were applied to both insulator designs under the rotating wheel dip test and a conductance meter device was

used for surface evaluation. This helped to investigate the performance of each insulator design when subjected to severe test conditions. Results for conventional smooth SiR insulator designs were compared with the textured designs.

- The electric field and potential distribution along a defined leakage path of SiR insulators under dry and wet polluted conditions were studied using a finite element analysis, COMSOL Multiphysics software.
- Based on the modified IEC 60507 solid layer method, an artificial uniform pollution layer was applied to the SiR rectangular samples and 4-shed insulators with smooth conventional surfaces and with textured patterns in order to evaluate the ESDD and NSDD parameters according to the procedure described in IEC 60815 for identifying pollution severity levels and so determine the pollution performance on each surface design.
- A series of low voltage tests using sources of 200 V AC and 320 V positive DC voltages were carried out on conventional and textured insulators that had been artificially polluted to investigate the evolution of the leakage layer conductance under various pollution levels and different fog rates and to determine the possible impact of texturing on the insulator performance.
- A series of high voltage flashovers tests with ramp control were conducted under different test conditions to understand the flashover phenomena on conventional and textured SiR insulators and to examine the factors that influence the flashover, such as the wetting rate and the pollution conductivity.
- A series of standard clean fog tests at voltages 12 kV AC and 12 kV positive DC were carried out on textured and non-textured SiR insulators to compare and analyse the electrical performance of each design under polluted conditions.
- Monitoring and inspecting techniques, including a visual video camera, thermal infrared camera, and hydrophobicity measurements, were used in order to detect any indications of aging on the surface of the tested insulators.

1.5. Thesis contributions

- 1- Comparisons were made of RWDT between conventional insulators and textured insulators showing that textured insulator profiles can improve the performance of polymeric insulators against tracking and erosions under AC and positive DC excitations.
- 2- Electric stress regions on the SiR insulator were investigated and revealed by means of computer simulations. Good correlation was achieved between simulated results and practical observations on the discharge activity.
- 3- Based on the extensive tests carried out on conventional and textured surfaces to investigate the pollution layer characterisation, the effectiveness of textured designs was clearly observed; it reduces the aging of the surface and consequently, it reduces the pollution deposition on the insulator surface, thereby, improves the pollution performance of polymeric insulators.
- 4- A high voltage ramp test procedure was conducted to investigate the flashover performance of SiR insulators. Comparison between conventional and textured designs was evaluated showing that the textured design can improve the flashover performance of polymeric insulators under various test conditions.
- 5- Using clean fog artificial pollution tests, textured insulators were found to exhibit a better electrical performance compared with conventional insulators under AC and positive DC voltages. Therefore, textured designs can improve the performance of polymeric insulators used in outdoor insulation.
- 6- Using the LabVIEW software, a novel code program was developed to control with very good accuracy, the DC motor of the rotating wheel and to acquire the data during the test.

1.6. Thesis outline

This thesis is structured into the following chapters. In this chapter, a general introduction of this thesis is given. Moreover, the research objectives, the methodology, and the main contributions of this work are briefly described.

Chapter 2: Comparative performance of outdoor insulators: A review

In this chapter, a review of published literature related to the research work is presented. Specific subjects relevant to the technology of outdoor SiR polymeric insulators are demonstrated, including the polymeric insulation materials, the chemical composition structure of SiR surfaces that ensure a unique long-term performance over different conditions, the loss and recovery of SiR surface hydrophobicity, and the contamination processes of SiR insulators under AC and DC excitations that contribute to the aging or the degradation process. Furthermore, the research work and design principles of textured profiles that preceded this work are also described. The impact of the environmental conditions and the electrical stress factors on polymeric insulator performance is also discussed. Flashover vulnerabilities on DC and AC systems and the flashover mechanism on SiR insulators are also investigated. The performance of the SiR insulators when energised by AC, positive DC and negative DC voltages is also discussed.

Chapter 3: Experimental facilities, samples and test arrangements

The SiR insulator designs with the smooth conventional surface and with textured patterns used in this work, in addition to the experimental facilities and techniques used for evaluating the performance of SiR insulators under different conditions are described. The RWDT facilities have been selected to investigate the suitability of the material and/or the design of SiR insulators for use on overhead transmission lines under AC and positive DC excitations. The fog chamber facility has been selected to simulate the climatic conditions, with the

systems used for generating the electrical stress on tested insulators and measuring the leakage current on the surfaces. Details are given of the possible arrangement of the conductance meter and its technique, which was used for evaluating the surface conductance on tested samples. The motor control program and its interfacing with the data acquisition systems specially designed for RWDT and the fog chamber used to acquire, monitor, and store live test data are illustrated. The post processing software system that was used to analyse the stored data together with the thermal and visual cameras records are also presented. The in-house making of the SiR insulators using an MCP 5/01 vacuum casting machine is described. Furthermore, details are given of the preparation of pollution suspension and of the techniques used to measure the pollution level on the insulator surfaces.

Chapter 4: Comparative performance of silicone rubber insulators under HVAC and HVDC energisation using the Rotating Wheel Dip Test

This main purpose of this chapter is to compare the aging performance of SiR polymeric insulators under AC and positive DC energisation. The well-established IEC RWDT test, that was used to evaluate two different SiR insulator designs (conventional and textured), are presented, and the results of long-term performance testing are reported. Estimation of hydrophobicity using the STRI hydrophobicity classification guide is also presented. Moreover, details are given of the measurements of localised surface conductance that were evaluated using a surface conductance meter to understand the variation trends in the conductance and its distribution on each insulator surface. In addition, presents the investigation of electric field stress on silicone rubber insulators by using computer simulations and laboratory test conditions. A commercial finite element software is employed for insulator modeling to determine the electric potential and field distribution along the leakage path under dry and wet polluted surface conditions. The simulation results are discussed in this chapter.

Chapter 5: Artificial pollution layer characterisation on conventional and textured silicone rubber insulators

In this chapter, investigations of pollution layer characterisation on conventional and textured insulator designs are described. In accordance with the clean fog testing method, many tests were carried out to evaluate the changing behaviour of the insulator surfaces under different conditions. ESDD and NSDD parameters are measured for different materials and each design is evaluated. Low voltage tests using AC and positive DC excitations to assess the conductance characteristic of SiR insulators are also conducted. In addition, details are given of the surface conductance measurements that are evaluated to provide a better understanding of the flashover voltage performance of textured and conventional designs.

Chapter 6: Performance of artificially polluted silicone rubber polymeric insulators using the clean fog chamber facility

The flashover performance of SiR insulators is investigated using clean fog tests based on a modified version of IEC 60507 solid layer methods. Extensive series tests of the flashover ramp test were performed under different conditions to evaluate the effect of the pollution severity level, fog rate, and insulator profiles on the flashover performance. The comparative aging studies of different insulator designs using alternating and positive direct voltages under artificial pollution conditions were also explored. Moreover, visual and thermal cameras were employed to monitor and inspect any feature of aging on the insulator surface during the test.

Chapter 7: Conclusion and Future work

The final chapter presents the overall conclusions based on the findings of this research study and outlines some suggestions for future work.

CHAPTER 2: COMPATATIVE PERFORMANCE OF OUTDOOR INSULATORS: A REVIEW

2.1. Introduction

The growth of the energy sector is facing many challenges. The integration of systems that generate power from renewable sources, the trend of using high voltage direct current (HVDC) transmission networks, and the environmental legislation regarding the effect of carbon dioxide emissions are just a few examples of these concerns that will figure in the future of the energy challenge. However, there are also problems that, although they have been known since the early stages of high voltage power systems, they have not been overcome. Thus, the performance of outdoor high voltage insulators under polluted environmental conditions is still an issue of concern.

It has been proven that the pollution flashover of outdoor insulators can contribute to power disruption and outages. The most common causes of flashover are over-voltages due to switching and lightning surges and the contamination of the insulator surfaces under severe environmental conditions.

Contamination flashover is an important element in the selection and design of outdoor insulators for power distribution and transmission systems. Polymeric insulators have been extensively used over the last decades due to their superior flashover performance for polluted environments compared with their ceramic counterparts; however, under severely polluted conditions, surface discharge activities and pollution flashovers are not completely removed.

Considerable work has been done, both to understand causes of failure of insulation systems and to improve the insulator performance for use in severely polluted areas without any flashover. Different artificial pollution test methods have been conducted to simulate the ambient test conditions under realistic withstand voltages. In such tests, the insulator is energised by

an appropriate voltage source (AC or DC), and its contaminated characteristics are evaluated by recording the voltage and leakage current.

2.2. Outdoor insulators

The demand for electrical energy has been increasing gradually. For transmitting a massive amount of electricity, high voltage transmission systems have been extensively used. In the transmission system, high voltage apparatus, such as insulators, play a significant role for attaining normal operation of the power supply [2-1].

Outdoor insulators are widely used in power transmissions and distribution networks. They help in providing mechanical support to the overhead line conductors, and they isolate them electrically from the tower. This section aims to provide an insight into three different insulating materials in use today: porcelain, glass, and polymers. Porcelain and glass are also known as ceramic insulators, and polymeric insulators are known as composite or non-ceramic insulators. Different profiles of insulators are selected based on the environmental conditions and the application for which they are used, for instance, suspension, tension, and post types. Insulators are also available with different dimensions and designs according to the voltage rating [2-2, 2-3].

2.2.1. Porcelain insulators

Porcelain insulators have been well known in the power system industry for a long time and are still the most widely used. This inorganic material has demonstrated relatively higher thermal resistance and strength regarding degradation of the surface. Porcelain is a highly glazed surface [2-2, 2-4]; this gives the insulator better self-cleaning properties in heavy pollution areas and helps reduce the discharges activities at sharp edges. Moreover, the glaze is chemically inert due to the strong molecular bonds that form the porcelain

material. Therefore, the insulator is mechanically solid and has a good resistance surface against corrosion [2-2, 2-5, 2-6]. Figure 2-1 shows a typical standard profile of a cap-and-pin porcelain insulator, with the main components of a glazed porcelain shed and metal cap-and-pin, which are all embedded together with the mortar [2-7]. The insulators are joined in series to achieve a string. The number of units used in the string varies based on the system voltage.

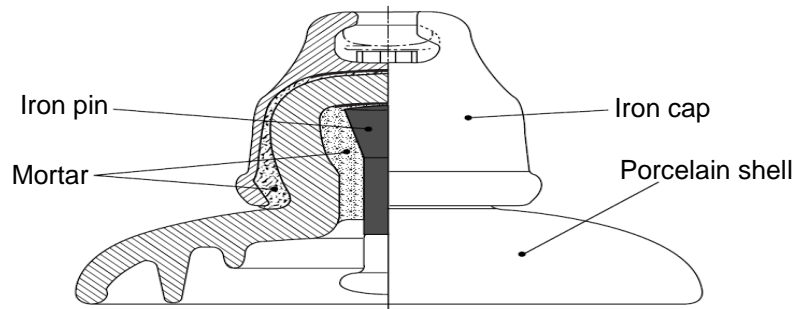


Figure 2-1: Standard design cap-and-pin porcelain insulators.

2.2.2. Glass insulators

Glass insulators have been used in service for up to 70 years, as is discussed in detail in [2-8]. These insulators offer great resistance due to the thermal handling they receive. With this handling, insulators have enhanced their mechanical properties compared with porcelain cap-and-pin insulators [2-2]. Toughened glass insulators (Figure 2-2) have the advantage of facilitating the inspection of the electrical lines even in the case of breakage. Though the glass disc smashes into small parts, the mechanical strength of the insulator remains the same as for the unbroken insulator [2-2].



Figure 2-2: Cap-and-Pin glass insulators.

Nonetheless, glass has a lower melting point than porcelain, making it more susceptible to surface erosion owing to the heat produced by surface discharges [2-2]. Thus, problems occur in contaminated environments where channelling of the glass surface, particularly the undersides, undermines the mechanical strength of the unit [2-8].

The flashover performance of ceramic (glass and porcelain) insulators under polluted conditions is substantially reduced, and a larger number of units is required resulting in a heavy insulator string. Therefore, to reduce the size of high voltage apparatus systems, the use of polymeric insulators have been introduced. These insulators are light in weight and have a water repelling surface, which ensures excellent performance in polluted environments.

2.2.3. Polymeric insulators

Due to the increased demands for electricity, it is becoming important to raise the capabilities of power transmission and distribution networks, which has led industrialists to develop and design lighter insulators that have good mechanical and electrical properties compared with porcelain and glass insulators. In 1970, the first generation of commercial polymeric insulators was introduced [2-9, 2-10]. With this inception, developments of composite or non-ceramic insulators increased rapidly [2-11].

Currently, polymeric insulators are being used in various applications, which include housings, bushings, and simple insulators. This is due to the numerous advantages that they have over porcelain and glass insulators, namely, reduced weight, excellent electrical strength, easy handling and transportation, reduced breakage, and improved resistance to vandalism; recently, they also have improved contamination performance. Nonetheless, despite these advantages, they have a limitation in the form of aging [2-12, 2-13, 2-14], that is, degradation,

which has a negative influence on their performance and makes them liable to damage.

2.3. Composite insulation materials

Since the development of lightweight composite insulators has increased widely, various types of polymeric materials have been used for overhead insulation systems. These include epoxy resins, ethylene-propylene rubber (EPR), and silicone rubber (SiR) [2-15, 2-16, 2-17]. Each material provides particular characteristics to protect the insulator rod from the degradation that may occur due to the environment and electrical discharges.

Currently, epoxy resin materials are suitable for distribution insulation with a voltage up to 69 kV, and their long-term performance in clean environments is relatively successful. However, in polluted environments, their performance is unsatisfactory. This is because of hydrolysis, in which de-polymerization of the cast resin occurred then, will ultimately lead to electrical tracking and poor ultraviolet resistance of epoxy resin. Therefore, the use of these materials has been restricted to apparatus like bushings and bus insulators [2-15].

There are three types of EPR in common use in overhead outdoor insulations: ethylene-propylene-diene monomer (EPDM), ethylene propylene monomer (EPM), and a copolymer of silicone [2-15, 2-16]. These materials are appropriate for distribution and transmission systems with up to 765 kV [2-15]. The long-term performance of EPR in clean and dry conditions has been proven, whereas the performance in polluted conditions is not known. SiR for overhead insulation systems is represented by three common categories: liquid silicone rubber (LSR), room temperature vulcanised rubber (RTV) and high temperature vulcanised rubber (HTV). Both RTV and HTV categories have high levels of alumina trihydrate (ATH) and fumed silica, and they are the most commonly used.

However, LSR is still in the early stages, though its usage is increasing rapidly [2-15].

Unlike other types of polymeric materials for electrical insulation, SiR has been shown to be the most reliable material for outdoor electrical insulation systems [2-15]. This is attributed to the superior performance it offers under contaminated environments. For example, SiR materials have demonstrated an excellent water repellent surface. This feature prevents the formation of polluted water films on the insulation surface, hence, increasing the possibility of suppressing leakage current activities and, thereby, limiting flashovers and power outages [2-17]. During the transient period, wherein the water repellence is temporarily lost, the ATH filler protects the silicone from degradation while the discharge activity and dry band arcing occurs on the insulation surface. After a short drying period, the silicone material recovers its water repellence, and the protection is restored [2-15].

Significant improvements in the performance and quality of polymeric materials have been made since their first introduction for use in high voltage distribution and transmission systems. However, the long-term behaviour of these materials is not fully understood, and further research is required regarding the following aspects [2-18, 2-116, 2-117, 2-118]:

- understanding polymeric materials' mechanical, chemical, and electrical aging
- investigating the composition of polymeric materials
- Choosing an appropriate insulator design and manufacturing
- improving the monitoring techniques of the performance of in-service insulators

2.3.1. Silicone rubber

SiR material now seems to be the preferred option for overhead insulators due to its excellent hydrophobic properties compared with other polymeric materials. Many researchers [2-7, 2-19, 2-20, 2-21] believe that the hydrophobicity of SiR is due to the low molecular weight (LMW) silicone chains that are diffused to the surface. The migration of LMW silicone oil from the bulk to the surface allows the material to recover its hydrophobicity if it is lost. Figure 2.3 shows the chemical composition of SiR, in which LMW comprises methyl groups (CH_3) attached to silicone (Si) and oxygen (O) atoms. The chemical structure of SiR contains a repeating (Si-O) chain backbone [2-18]. This chain is very stable, giving the material a greater ability to resist the effects of heat, ozone, and ultra-violet (UV) radiation, thereby, ensuring a long-term stable performance over an extensive range of in-service conditions [2-22].

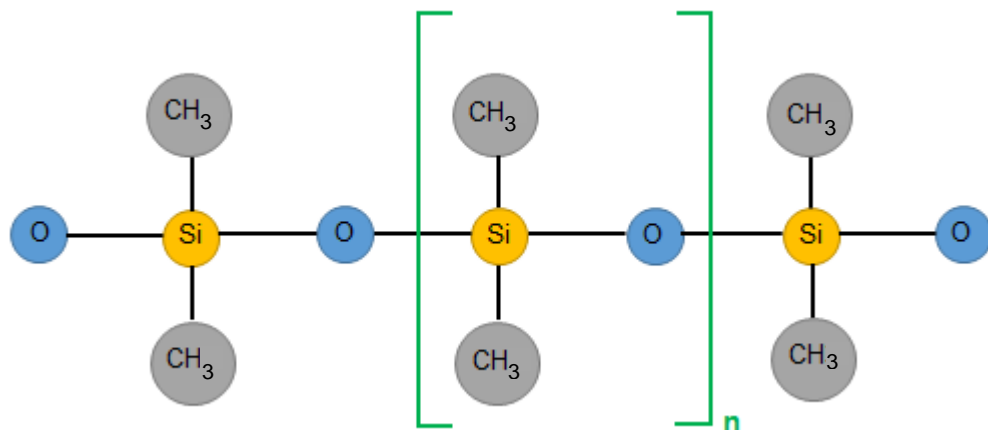


Figure 2-3: Chemical structure of silicone rubber.

2.3.2. Texturing of silicone rubber polymeric insulators

The widespread use of SiR insulators for overhead lines and distribution systems has not led to the complete elimination of discharge activities and dry bands even with the use of superior hydrophobic materials. Therefore, the surface degradation and insulator flashover due to these discharges is still a subject of concern. Harsh environmental conditions would still result in discharge activities

on the insulator surface, and the design of SiR insulators remains very simple due to the moulding limitations, which prevent the development of complex insulator profiles [2-23].

The leakage current and the electric field strength on the polluted surface of SiR insulators have the greatest density in the regions of the smallest contour edges around the shank areas, resulting in increased surface power dissipation. Consequently, localised heating leads to the formation of dry bands, and this, with surface discharge, may eventually cause degradation of or damage to the insulator surface [2-23, 2-24].

Textured insulators are a novel approach [2-25] to the design of polymeric insulators and have brought many advantages to improving insulator performance. Various textured designs of the polymeric surface may be achieved by using a pattern comprising an array of contiguous or overlapping protuberances.

The aim of this design is to reduce the power dissipation by reducing both the electric field strength and the current density in the shank regions. This may be managed by increasing both the surface area and the creepage distance of the insulator without increasing its overall longitudinal length [2-23].

Furthermore, it is observed that compared with conventional samples, textured patterns might mitigate the damage induced on polymeric materials due to surface discharges by presenting multiple paths for current conduction: when one current path initiates drying as a result of Joule heating, its resistance will increase. At this instant, the current flow will shift to a different path of lower resistance before significant thermal degradation occurs [2-23].

2.3.3. Construction of silicone rubber insulators

Long-rod SiR insulators, which are used for different overhead lines and distribution systems, have the same design structure, but the size of these insulators and the end fitting shapes are variously based on the application for which they are used [2-2]. A cross-section of the standard SiR insulator used in this work is shown in Figure 2-4.

The SiR polymeric insulators are composed of three main components [2-12]:

- 1- The fibreglass reinforced core, which is an internal part of a polymeric insulator, is intended to provide the mechanical strength.
- 2- The metal end fittings are usually forged steel or aluminium alloy and are selected to convey the mechanical load to the core. Their shape is very important to limit the corona discharges that cause the polymeric material to become fragile and possibly to crack, thereby, damaging the insulator due to moisture ingress into the fibreglass core [2-26].
- 3- The housing, which is the external part of the core, consists of weather sheds and a sheath. The weather sheds provide the required leakage distance, and the sheath is an insulating material between the core and the weather sheds.

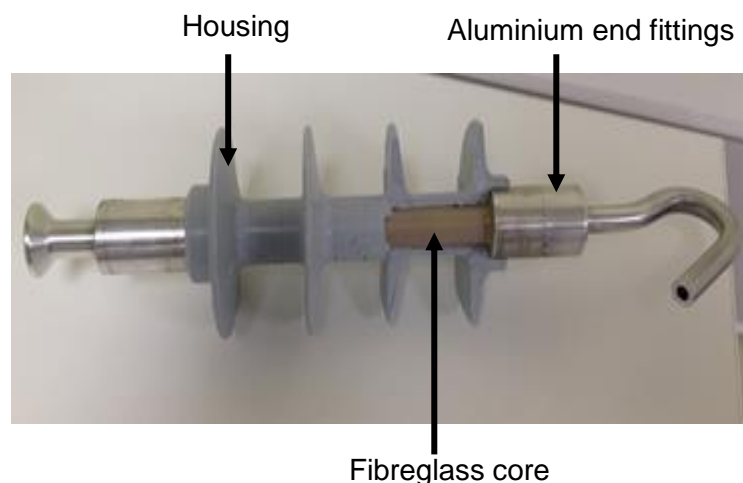


Figure 2-4: Cross-section of 11kV silicone rubber insulators.

Composite SiR insulators can be manufactured using several techniques. However, today, the most commonly used technique involves moulding the insulator housing directly around the fibreglass core. In this manner, the housing can be chemically joined to the core [2-12, 2-27].

Metal end fittings, which are made of forged steel or aluminium, can be attached to the core in different ways. Crimping is the strongest method and is most commonly used for the attachment to the rod [2-1, 2-28].

The SiR material used for this work has significant advantages over porcelain and glass insulators. The most significant advantages of SiR insulation are associated with the reduced weight. The weight of a polymeric insulator is usually about 10% of its porcelain or glass equivalent. This makes it attractive in many ways, especially regarding cost reduction [2-29]. In addition, polymeric insulators offer several other advantages over traditional ceramic insulators and so have generated considerable interest among utilities, including the following:

- lower cost of design towers, construction transportation, and maintenance
- increased transmission capacity of existing lines by providing a light and practical tower design, which requires little space and is sufficiently flexible to accept more circuits [2-30, 2-31]
- high mechanical strength, which allows the construction of long spans of towers [2-9, 2-12]
- reduced vulnerability to severe damage from vandalism that causes the insulator shatter and drop the conductor [2-32]
- improved contamination performance for outdoor service due to their low surface energy, which means they can maintain a good hydrophobic surface property in severely polluted environments [2-33, 2-34]
- better ability than glass and porcelain insulators to withstand higher voltage [2-35]

- improved flashover performance under polluted and wet conditions by limiting the formation of a continuous film of water [2-2, 2-36, 2-37, 2-38]

Nonetheless, despite these advantages, some problems arise with the use of polymeric insulators:

- exposure to dry band arcing and weather conditions; these may cause changes in their chemical composition, thereby, reducing the electrical performance of the insulator [2-39]
- tracking and erosion, which may lead to flashover and ultimate degradation of the insulator [2-11]
- crazing and chalking of the insulation surface, which is attributed to increased pollutant collection, arcing, and flashovers
- weakening of the mechanical strength and bonding breakdowns along the shed rod interface [2-10]
- loss of hydrophobicity due to the exposure of UV radiation, heat, moisture, and electric discharge activities that may occur on the insulator surface
- unknown long-term endurance and life expectancy are unknown and difficulty in detecting faulty insulators

Due to utilities' increased experience with these insulators through extensive research conducted in laboratory and field test stations, several problems, included tracking, erosion, loosening of end fittings, cutting of the corona and inadequate bonding between the fibre core and shed materials have almost been eliminated by the use of new manufacturing techniques and excellent materials [2-27, 2-28]. The new technology of polymeric insulators has possibilities for use in many applications of high voltage systems. However, their expected lifetime is still an issue of concern to some power utilities. Therefore, an additional understanding of their long-term reliability would be valued and could stimulate further growth in their use [2-12].

2.4. Pollution influences on silicone rubber insulators

In order to increase the reliability of power grids, much research has focused on high voltage insulators. This key element of the transmission and distribution system is still susceptible to various environmental conditions [2-40]. Indeed, outdoor insulators suffer from natural and industrial pollution with serious problems of flashover occurrence. The natural pollutants are classified into two main types, namely, soluble and non-soluble. The soluble component is commonly expressed in terms of equivalent salt deposit density (ESDD), which refers to the amount of sodium chloride (NaCl) in milligrams (mg) per unit surface area of the insulator (cm^2). The non-soluble component, such as Kaolin, is normally defined in terms of non-soluble deposit density (NSDD), which corresponds to the number of milligrams of kaolin removed from a certain surface of the insulator divided by the area of this surface (cm^2) [2-115].

2.4.1. Pollution cumulative on insulator surfaces

The contaminant elements are transferred to the insulator surfaces by the influence of the air; the larger amount of pollution is usually deposited in the shed regions. The main process of contaminant deposition can be described with the following steps [2-2, 2-41]:

- 1- The material particles are transported towards the surface of the insulator by the air.
- 2- The particles flow close to the energised surface due to the action of three major forces; the wind, electrostatic and gravitational forces.
- 3- The part of the airborne particles that is relatively heavy is deposited at the surface point where no force will to remove it.

Much more importantly, it was identified in [2-2], which investigated the standard of ceramic insulator types, that the effects of the vortex to the air flow may increase the deposition of smaller particles at the edges of the skirts and sides of

the insulator surface whereas, with the technology of polymeric insulators, this has been overcome by the introduction of smooth aerodynamic profiles.

The importance of aerodynamic influences in pollution depends not only on the electrical conditions, to which the airborne particles are subjected to but also of their long range. In addition, many contaminant particles are electrically charged by friction effects and by a combination of ions caused from industry.

Such particles will be enhanced by any electric force added to their aerodynamic and gravitational forces; they will be attracted when they are exposed to the range of charged DC electrodes, but will stay free under AC fields. In contrast, the corona activity that causes copious flows of ions and very heavy dirt deposition is seen in DC, but is not observed in AC tests [2-43]. For this reason, pollution patterns under AC and DC excitations are significantly different [2-2].

2.4.2. Categories of pollution severity levels

The site pollution severity (SPS) is defined as the maximum values of ESDD and NSDD measured according to the methods detailed in [2-115]. The measurements are recorded over a minimum of one year to take into account any climate changes. The SPS is classified into five types as follows [2-115]:

- a. very light
- b. light
- c. medium
- d. heavy
- e. very heavy

According to [2-115], values of both ESDD and NSDD below 0.01 mg/cm^2 are considered very light, while values of ESDD above 0.1 mg/cm^2 are considered heavy. Figure 2-5 shows the corresponding classes of ESDD and NSDD values in terms of the site pollution severity levels for long-rod insulators.

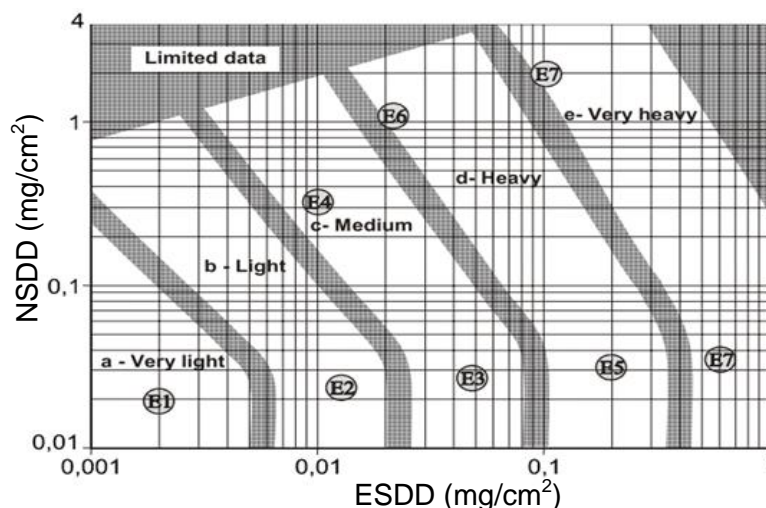


Figure 2-5: Relationship between ESDD and NSDD (pollution type A) and the site pollution severity levels [2-115].

Based on the CIGRE Task Force 33.04.01 and IEC 60815 standards [2-42, 2-115] for insulation selection, the typical pollution can be identified as shown in Table 2-1.

Table 2-1: Examples of typical environments [2-115]

Example	Typical environments
E1	greater than 50 km ^a from any desert, sea or dry land greater than 10 km from a major city that causes man-made pollution sources ^b Within a shorter distance than the stated above of pollution sources, but: <ul style="list-style-type: none"> • predominant wind is not directly from these pollution • regular monthly rain washing
E2	10-50 km ^a from the desert, a sea or open dry land 5-10 km from man-made pollution sources (major city pollution sources) Within a shorter distance than E1 from pollution sources ^b
E3	3-10 km from the desert, a sea, or dry land and 1-5 km from man-made pollution sources.
E4	Further away from pollution sources than stated in E3, but: <ul style="list-style-type: none"> • Drizzle often occurs after along dry pollution accumulation season (several weeks) • Heavy rain with high conductivity happens • High NSDD level, between 5-10 times the ESDD
E5	Within 3 km of the desert, a sea, and dry area 1 km of man-made pollution sources
E6	With a greater distance from pollution sources than stated in E5, but: <ul style="list-style-type: none"> • Dense fog often occurs after along dry pollution accumulation season • High NSDD level, between 5-10 times the ESDD
E7	the same distance of pollution sources as identified for the heavy area and: <ul style="list-style-type: none"> • directly exposed to sea-spray or thick saline fog • or directly exposed to pollutants with high conductivity, or cement type dust with high density, and with regular wetting by fog or drizzle • desert regions with fast accumulation of sand and salt, and regular condensation

a= during the storm, ESDD may reach a higher level, **b=** the presence of a major city will have an influence over a longer distance.

2.5. Outdoor insulators for direct voltages

2.5.1. Basic differences between DC and AC conditions

The service experience of the insulators under DC excitation is limited compared with that of AC insulators. This is because the reliability of test results under DC has been restricted by the difficulty and high cost of providing a number of test facilities. The insulators that are exposed to DC energization are different from the corresponding AC condition in several aspects [2-2]:

- pollution mechanism and propagation process of discharges
- surface erosion and metal terminals corrosion process
- aging process of the dielectric

The contamination process on the insulator surfaces under DC will have more severe effects than on AC even under the same test conditions [2-44]. This is because electrically charged airborne particles on DC insulators will deviate to the electrodes under the steady electric field. Any discharge activities that occur on the insulator surface will produce considerable flows of ions, which consequently will attach to the particles and cause more deposition [2-2, 2-44, 2-45]. In [2-82], the authors state that the deposition of the pollutants on the insulator surface under DC is 1.2 to 1.5 times that under AC for the same field conditions.

It seems that the case from which voltage is applied directly (DC) must be most promising for flashover. The absence of current zeros and polarity reversals under DC exacerbates the progress of primary discharge activities to complete flashovers [2-46, 2-47]. Since the distributed voltage along the insulator surface depends only on the resistance when DC is applied, more extensive variations have to be expected than under AC. However, it is very difficult for flashovers to occur under alternating voltage with the presence of voltage zeros, polarity reversals and stress variations, as the propagation process is fairly slow, and

many cycles have to be achieved from the inception to the completion of a flashover event [2-2].

So far, the operating experience with DC excitation systems has made clear that the degradation of the insulation surface is expected to be more severe than with AC [2-2, 2-13, 2-48]. This is attributed to the nature of surface discharges, which are likely to be steadier under DC. Glass and polymeric insulators suffer seriously from the direct effects of discharges and from the electrochemical elements that accumulate close to the electrodes. The electrolysis of salt, for instance, can generate Sodium hydroxide (NaOH), which rapidly damages many polymers and glass materials [2-2]. Decreased electrical strength under contaminated conditions, the corrosion of metal terminals, surface erosion, and the degradation of the dielectric materials used for outdoor insulation from both laboratory and field studies have been reported in [2-49]. In addition, several studies have extensively investigated the performance of the materials usually used in DC insulators [2-36, 2-50, 2-51, 2-52]. According to reports [2-53, 2-83] from laboratory and field experiences, the expected lifetime of polymeric insulators used in DC networks is relatively shorter than for AC insulators [2-83].

The corrosion process of the end fitting materials has been a subject of many research programmes [2-54]. Damage to the metal hardware due to electrolytic corrosion is usually observed on DC lines. Corrosion is caused by the flow of the leakage current on the insulator surface [2-55, 2-56, 2-57]. Swelling of the pin metal due to corrosion and growth in the cement itself have also been detected. The effect of polarity on the stress of DC has also been noted; breaking of the head of cap-and-pin insulators under positive polarity has been noticed in very severely polluted conditions [2-2]. However, by using the technology of a zinc sleeve pin, insulators have exhibited good performance on DC systems under various polluted conditions.

Changes in the behaviour of ceramic insulators under DC excitation have been widely investigated [2-2, 2-58]. As both porcelain and glass materials have moving ions, migration will occur under a steady-state situation (DC). Phenomena such as the discharge of ions close to electrodes have chemical and physical effects, and trees will form in ceramic materials. The most concern issue is what the rates of such defects will be at temperatures from which the insulator normally operates. The following sections will consider the flashover liability and the deterioration level of the insulators used on DC systems in contrast with those for AC systems [2-2].

2.5.2. Flashover vulnerabilities on DC and AC systems

As specified in section 2.5.1, it should be noted that the characteristics of AC and DC arc propagation are clearly different. Thus, the DC flashover process of polluted insulators differs from the AC process. When the flashover voltages are compared by AC and DC excitations using a specific type of insulator and pollution severity level, the factor $F = V_{ac} / V_{dc} = (\text{peak AC flashover voltage}) / (\text{peak DC flashover voltage})$ is found to differ with the insulator shape [2-2]. Salt fog tests in [2-8] show the values of F to vary from between 1.2 to 1.7. A report in Japan [2-59] confirmed that F changes with the shape of the insulator, and the severity level reaches above 2 at highly contaminated areas. It also showed the influence of the polarity, with negative stress exhibition 10%-20% reduction than the positive.

For artificial pollution tests, a huge difference in local deposit density was obtained; values of DC can be ten times higher than the average in AC applications [2-2]. Studies of the influence of shape have proposed that the distance between the tips of the skirts for DC insulators should be increased to mitigate bridging due to frequent arcs. Pargamin, Huc and Tartier in CIGRE

illustrated that the significant differences in the behaviour are affected not only by the shape but also by the material of the insulator [2-2].

Polymeric insulators normally offer better performance than ceramic ones. Pargamin's results under a salt fog test can be correlated to other work in [2-60] for anti-fog shapes that showed good performance: F values of between 2 and 2.8 were obtained at a severity level of 28 kg/m^3 [2-2]. An investigation was done by Verma [2-2] to study the flashover liability and insulator diameter effects on DC stress for long-rod and disc-type insulators. It was found that the values of F in highly severe conditions varied from between 1.7 and 2.5 for the anti-fog type while they varied from 1.4 to 2.1 for long rod and standard discs. The reduction in flashover voltage due to the increase in the core diameter was relatively high [2-2]. General summaries on the vulnerability to flashover events under DC can be given as follows [2-2]:

- All insulator categories are much more susceptible to flashover under DC application than under AC. In the case of overhead lines, long-rod insulators have to be provided at severely polluted conditions.
- Up to 300 kV, the linearity is confirmed under DC stress, but for higher voltages, the behaviour might be changed with an increased possibility of flashover.
- Using polymeric insulators or coating may offer some improvement; however, the effects of aging are likely to be more harmful.
- Some shapes for DC may allow an acceptable increase in a flashover voltage, especially for overhead line insulators. However, in the case of substation insulators, the shape is seen as an unattractive option due to the effect of large diameters.

2.5.3. Deterioration features on DC systems

Extensive information is available on the degradation rate and the fracture of overhead line insulators. A study by Peixoto, Pargmin, Marrone and Carrara in CIGRE presents some analyses and statistics about the physics of deterioration under DC excitation, and these can be summarised as follows [2-2]:

- The annual failure rates for glass insulators in Africa, Scandinavia, and Italy are relatively ten times higher under DC energisation than for AC lines.
- Different causes of damage under DC have been identified, including severe erosion close to the electrodes and fracture due to the swelling process and ionic migration. However, only the first is known to cause damage under AC.
- Handling includes a reduction in the ionic migration by increasing the volume resistivity of the dielectric and elimination of voids from glass could be useful while a large increase of volume resistivity can cause a major change in the composition of the glass since it would interface with the toughening process.
- Glass insulators, even with their liability to suffer from severe erosion, will still sustain last longer on DC than on porcelain, in which the stress is less but the mechanical crack is much greater.
- Long-rod insulators would be more useful on DC systems since they are subject to only slight degradation from ionic migration and have no hidden metal parts that may be corroded.
- Some long-rod polymeric insulators have provided very good results on DC networks; thus, these might be useful on DC applications especially when the pollutant effects, such as salt, can be overcome.

2.6. Aging and degradation of polymeric insulators

The use of polymeric insulators in high voltage transmission networks differs between countries. They have being to be a highly developed alternative to traditional insulators in all voltage transmission levels for AC and DC applications. However, they still have concerns about their long-term aging behaviour which, unlike that of ceramic insulators, is not well understood [2-61, 2-62].

Aging is a very important issue; it refers to the degradation of an insulator by different environmental factors and electrical stresses, as shown in Figure 2-6. Weathering (temperature, moisture, UV sunlight, and humidity), mechanical stresses, and discharge activities in the form of surface arcing or corona activity are the most important factors leading to aging. These factors also have an interactive effect that can accelerate the degradation [2-63].

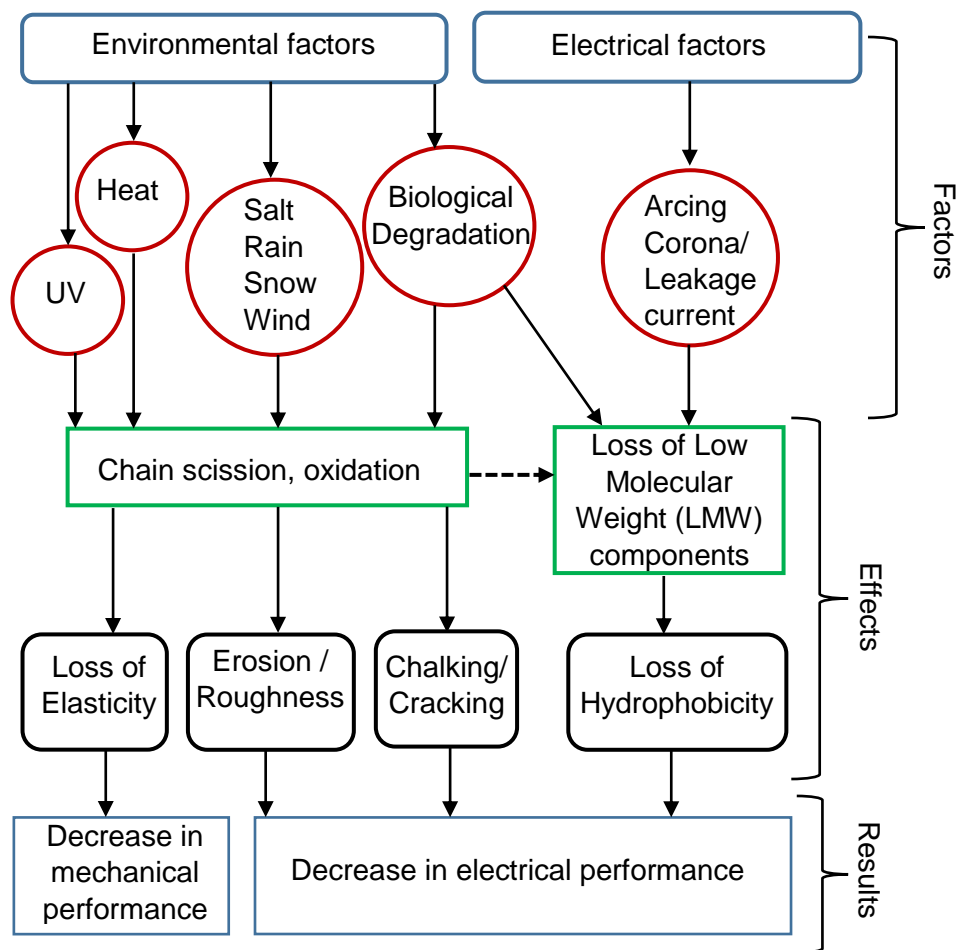


Figure 2-6: An overview of various factors effects on the aging of polymeric insulators [2-63].

Unlike porcelain and glass, a polymeric insulator is an organic material, and there can be changes to its electrical and mechanical strength with time under severe stress. Of the two properties of a polymeric insulator, electrical and mechanical, it has been proved that the fibreglass core will not be damaged, and there will be no reduction in the mechanical strength if the applied stress is lower than the degradation limit [2-64]. Therefore, the mechanical aspects will not be a main concern. Instead, the main issue of concern is the long-term electrical performance, which is mainly related to the insulator housing and design.

Aging of the housing material can decrease the ability of the insulator to provide the services voltage, thus leading to flashovers, and it can cause degradation of the housing by tracking and/or erosion. So these two aspects, namely, flashover and degradation, are the main influence on the overall electrical performance. However, these two aspects are not necessarily dependent on each other. Service experience in [2-65] has indicated that polymeric insulator flashovers can occur without any substantial degradation (tracking or/and erosion), and in some situations, surface erosion has occurred without leading to a flashover.

2.6.1. Polymeric insulators failure modes

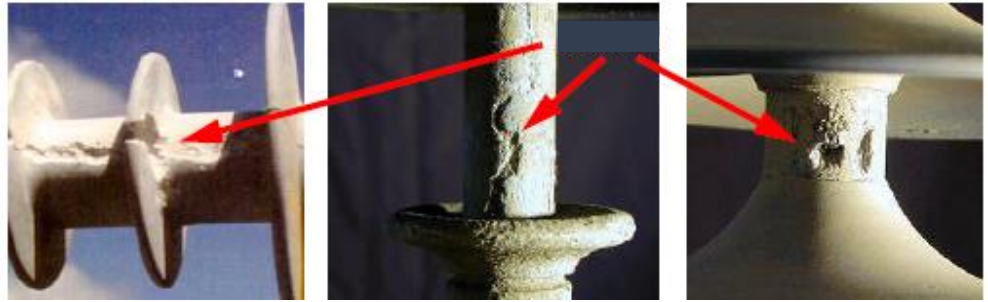
In the early stages of polymeric insulators being used as electrical insulation, they were believed to have an excellent resistance to degradation caused by the conditions found in service. Polyethylene, for instance, was widely used in underground cables, as it was considered safe with regard to degradation under service conditions [2-66]. However, recent research has shown that all polymeric insulators are susceptible to damage under the multiple factors applied and/or induced in service, which ultimately leads to failure. The most common factors that affect the polymeric insulators include discharges, humidity, and other environmental and electrical stresses. In [2-67], the authors have reviewed the main aging factors leading to the failure of polymeric insulators. Figure 2-7 shows

the most significant failure/degradation modes that occur in polymeric insulators [2-68, 2-69, 2-70]:

- Tracking/carbonizing: irreversible degradation mode caused by the formation of conductive paths initiating and developing on the insulation surface even in dry condition [3-1]. See Figure 2-7(a).
- Erosion: irreversible and non-conducting degradation of the insulator surface that occurs due to the major loss of materials; it can substantially reduce the thickness of the polymeric sheath. See Figure 2-7(b).
- Chalking: appearance of a rough and whitish powdery surface due to the exposure of filler materials from the insulator housing and caused by UV radiation and electrical activity [2-72]. See Figure 2-7(c).
- Cutting/splitting: cracks or breaks in the insulator housing (sheath or/and shed), which may consequently lead to the removal of materials and so significantly reduce the creepage distance. See Figure 2-7(d).
- Cracking: shallow cracks (micro-fractures) on the surface of the insulator, with a depth of less than 0.1 mm. See Figure 2-7(e).
- Colour changes: changes in the colour of the housing materials of the polymeric insulators due to environmental and chemical influences [2-73]. See Figure 2-7(f).
- Puncture: hole in the insulator sheds or/and shank/sheath. See Figure 2-7(g).
- Brittle fracture: this leads to mechanical degradation of the fibreglass core rod and is characterised by some smooth fracture surfaces. This failure mode is attributed to an attack by nitric acid generated by corona discharge activity in a moist environment [2-94]. The exact source of the acid has been a topic of much debate. However, it is now thought [2-94] that the brittle fracture may be due to a combination of factors and is not always described by a single mechanism. See Figure 2-7(h).



(a) Tracking



(b) Erosion



(c) Chalking

(d) Splitting/Cutting



(e) Grazing



(f) Changes of colours



(g) Puncture



(h) Brittle fracture

Figure 2-7: Most common failure modes of polymeric insulators [2-68, 2-69, 2-70].

2.6.2. Loss and recovery of hydrophobicity

Hydrophobicity is defined as the ability of polymeric materials to repel water on their surfaces, forming discrete droplets rather than a continuous film [2-71]. Polymeric insulators are considered to have good hydrophobic properties and so have an excellent pollution flashover performance compared to that of traditional hydrophilic insulators made from porcelain and glass.

On the ceramic high voltage insulators, water readily forms a continuous film on the hydrophilic surface. In the presence of contamination, a leakage current develops, which may ultimately lead to a flashover of the insulator. The hydrophobic surface properties of polymeric insulators prevent the formation of a continuous film, and so the water remains as individual droplets, which may simply drop away from the surface [2-72, 2-73].

However, this hydrophobicity might be lost temporarily as a result of aging. Electrical discharge activity causes oxidation of the polymeric insulator, and the surface becomes gradually more hydrophilic. The surface will recover its hydrophobicity after sufficient recovery time has passed without any excessive electrical discharge activities [2-74].

Two prevalent polymeric materials used for outdoor insulation are EPDM and SiR. While both EPDM and SiR in service offer an excellent pollution performance due to their hydrophobic properties under aging stress, SiR has been preferred for use in composite insulators in harsh ambient conditions [2-7, 2-75]. This is because its hydrophobicity is preserved for a long time. In addition, it demonstrates a higher hydrophobicity recovery rate than EPDM [2-76]. The investigation in [2-33] showed that the SiR insulator preserved its hydrophobicity for more than seven years in outdoor tests and could be energised to +300 kV_{DC} while EPDM became totally hydrophilic. It was reported [2-20] that, after a long-term aging test with HVAC and HVDC, SiR retained

a good performance while EPDM insulators failed. These superior characteristics of SiR have also led to the development of RTV silicone rubber coating to improve the performance of porcelain insulators [2-77, 2-78].

The hydrophobicity of SiR is associated with the low molecular weight (LMW) of the silicone chains as described in section 2.3.1. When electrical discharge activities occur on the polymeric surface, these chains may be broken resulting in a loss of hydrophobicity, but new bonds of LMW diffuse to the surface [2-79]. The way the LMW is transferred to the pollutant remaining on the surface of an SiR insulator is not entirely understood, but options related to diffusion and evaporation have been studied in [2-80]. In some conditions, the pollutant has a significant non-soluble component, which may cover the SiR surface and so disturb the process of hydrophobicity recovery [2-80, 2-81].

2.6.3. Polarity effect on the aging of Silicone rubber insulators

HVDC is often a good option for long distance power transmission lines, in preference to high HVAC. The pollution performance of high voltage insulators is a significant issue in the insulation coordination of power networks, especially of HVDC systems. In the case of HVAC systems, lightning and switching performances are usually the determining factors for deciding the insulator dimensions, while pollution performance is often the determining element in the case of HVDC [2-83].

Although HVDC has brought many benefits to long distance transmission systems, the line insulators used in a DC network face many challenges. As discussed in section 2.5.1, the static field under DC is constant and unidirectional. This attracts many adjacent airborne pollutants onto the insulator surface, which will result in an inferior voltage withstand performance. The results obtained in [2-83] showed useful information about the performance of

SiR insulators energised by positive DC and negative DC voltages. The polarity effect was confirmed regarding pollution performance and insulator aging [2-84].

Vas et al. [2-82] showed that the eroded mass for the SiR samples under positive DC energisation is more severe than for those under negative DC. Studies by Bruce et al. [2-84] also performed inclined plane (IP) tests on SiR materials using DC and confirmed that the positive DC tests have the highest peak leakage current and show a significant degree of surface degradation. Moreno and Gorur [2-13] studied the performance of polymeric housing materials under AC and DC tests, and they identified that the positive polarity DC is usually considered to be more severe than the negative. In addition, Gustavson et al. [2-85] tested cylindrical SiR samples in a coastal environment under AC and DC voltage; the DC stressed samples exhibited a higher leakage current and more severe surface degradation compared with those exposed to the AC voltage. Similarly, an investigation conducted by Elombo et al. [2-83] at Koeberg pollution test station in South Africa showed that the leakage currents for SiR insulators under positive polarity were greater than those obtained under the negative DC. In addition, more erosion was observed on the SiR that was energised by positive DC. Studies by Meyer et al. [4-9] reported a correlation between the surface temperature of SiR samples and the eroded mass, and the leakage current values obtained under positive DC were higher compared to negative DC. An increased leakage current may lead to surface heating and, therefore, an increased temperature for the surface profile.

Scanning Electron Microscopy (SEM) analysis conducted on the eroded area of the SiR samples after seven hours of IP tests revealed that the samples under positive DC were extensively degraded, and many cracks were found on their surfaces. This demonstrates that a higher temperature prevails under positive DC [2-82].

Energy dispersive X-ray (EDX) studies on samples tested under positive DC have shown a migration of conductive ions from both the pollutant and the electrodes. This may have resulted in an increase in the surface conduction, and, therefore, a higher leakage current in the case of positive DC. In contrast to the observations under positive DC, no ion migration was observed for the samples under negative DC [2-82]. This migration of ions under positive DC excitation may be due to electrolysis, as suggested by Bruce et al. [2-84]; they demonstrated that there is a definite relationship between the electrode erosion and the cumulative charge under positive DC. The presence of ions in the event of positive DC can be clarified as follows. The normal condition for electrolysis process is that both electrodes should exist in an ionic solution. This condition is satisfied to a certain degree in this case since there is a certain electrode-pollutant interface close to the HV electrode. However, near the ground electrode, this interface is sporadic. Significant heating due to the dry band arcing may lead to evaporation of the contaminant near the ground electrode. The direction of ion flow and pollutant flow for both DC voltage polarities is shown in Figure 2-8.

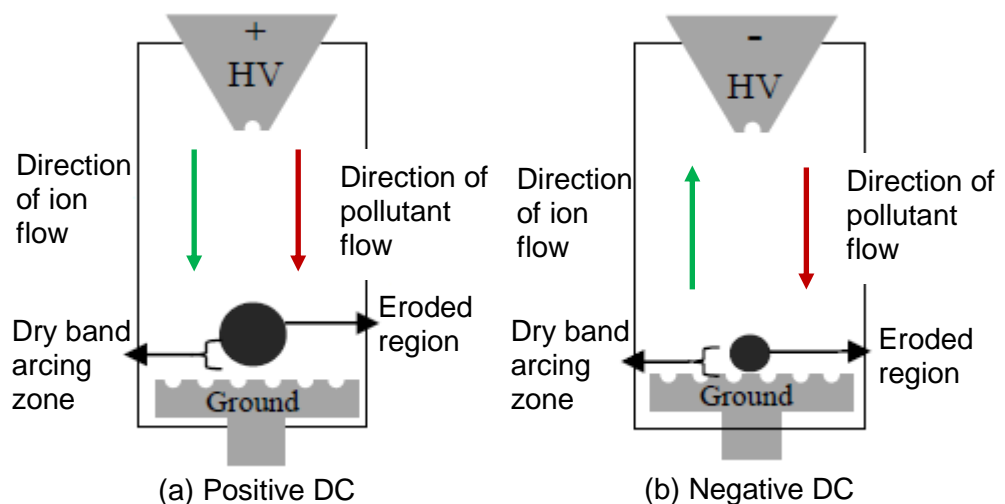


Figure 2-8: Model of the IP test setup illustrating the flow direction of for the contaminant and the ion under (a) positive DC and (b) negative DC voltages [2-82].

Under positive DC, as the interface often occurs close to the HV electrode, the ions flow into the solution, thus, generating an ionic current. However,

as they reach the ground electrode, the pollutant dries up due to the heating caused by dry band arcing. The ions are deposited close to the eroded surface, and the current path is finished by the arcing current.

Under negative DC, the ion has to be released from the ground electrode, but because of the strong arcing, this region is entirely dry. Since there is no interfacing between the electrode and the pollutant, the ion is unable to flow into the solution. Therefore, the electrolysis process will not occur under negative DC. Figure 2-9b illustrates the erosion of the HV electrode surface under positive DC, which is correlated to the gradual removal of the electrode surface into the solution due to the electrolysis process, while Figure 2-9c shows that under negative DC, the erosion is caused more by oxidation than by electrolysis. It seems that the probability of electrolysis under negative DC excitation is very limited. In addition, as there is no migration of ions under this case, the leakage current is much less, and so a better tracking and erosion resistance is observed in the samples under negative DC [2-82]. However, the ground electrode was seen to be eroded under negative DC. This could be due to the oxidation of the electrode as a consequence of the intense arcing that occurs close to the pit.

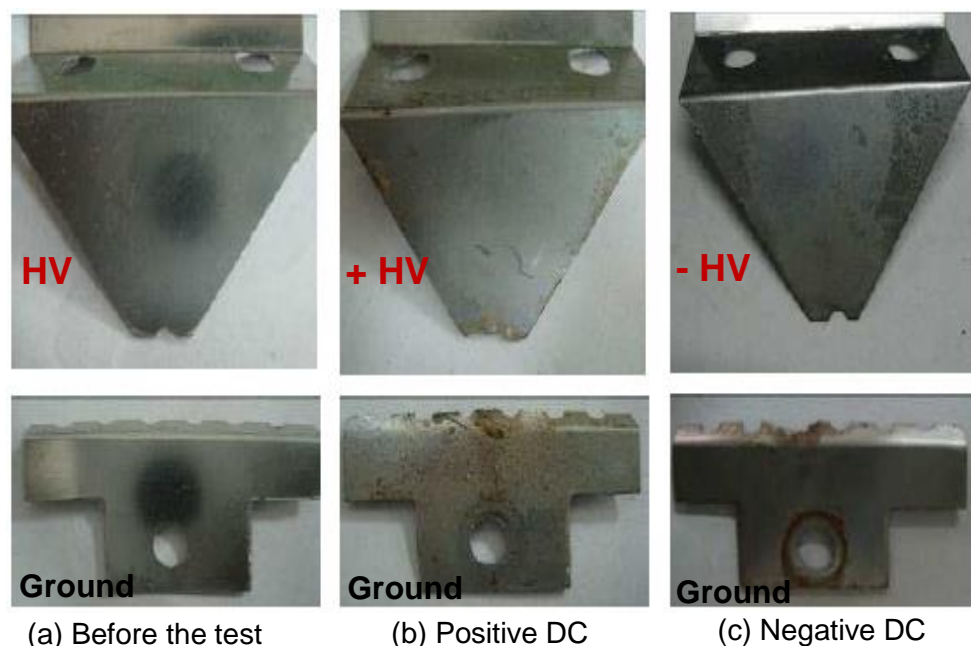


Figure 2-9: Captures of the electrodes (a) before the IP test, (b) after seven hours of IP test under positive DC, (c) after seven hours of IP test under negative DC [2-82].

2.7. Flashover mechanism of silicone rubber insulators

A flashover is defined as a disruptive discharge that occurs over the surface of a solid insulator as a result of water drop accumulation and/or due to overvoltage. The pollution flashover mechanism and the dry band formation of hydrophilic (porcelain and glass) insulators have been studied and are well understood [2-86, 2-87]. However, the nature of the hydrophobic surface of SiR insulators suggests that a different flashover mechanism occurs. The pollution flashover is a multi-step process for an SiR insulator. The main steps in the most common flashover phenomenon are explained as follows [2-88, 2-89, 2-90, 2-91]:

- 1) Contamination builds up: The wind transfers dust or other industrial pollutants onto the surface of the insulator. Fog and dew also wet the pollution deposition. The interaction between pollutants and water creates a solid surface layer, and the insulator is usually covered by a uniform pollution layer.
- 2) Diffusion of LMW chains: Diffusion is the natural behaviour of SiR insulators and may cause the LMW polymeric chains to migrate out of the weather shed material. The LMW chains produce a thin layer above the pollution layer, which ensures that the surface recovers hydrophobicity after an arc-free period.
- 3) Wetting of the surface: Early morning fog, dew, high humidity, or light rain creates water droplets on the hydrophobic surface of the polymeric insulator, as shown in Figure 2-10a. Salt from the pollutant dissolves in the water droplets, which become conductive. The remaining dry surface pollution is gradually wetted by the migration of the droplets. This produces a high resistive layer around each droplet, as illustrated in Figure 2-10b.
- 4) Ohmic heating: The small leakage current passes through a highly resistive layer of the insulator surface. As the electrolyte has a negative

thermal coefficient, the surface resistance will decrease gradually, and the leakage current will increase due to heating. At the same time, drying and loss of moisture increases the surface resistance. The two contrasting phenomena attain equilibrium at a lower level value of leakage current.

- 5) Electric field effect on water droplets: The development of the wetting process increases the water droplets' density and reduces the distance between them. The applied electric field results in a force, which flattens and lengthens the droplets. If the distance between the drops is small, the adjacent droplets gather together, and filaments are created, as shown in Figure 2-10c.
- 6) Spot discharges: Filaments minimize the distance between the electrodes, which may lead to an increase in the electric field among the neighbouring filaments. This field strength generates spot discharges between the filaments, as illustrated in Figure 2-10d.
- 7) Loss of hydrophobicity: Spot discharges age the polymeric layer around the droplets and reduce the hydrophobicity. This reduction of hydrophobicity joins the filaments together and increases the field strength. The high electric field around the electrodes causes corona discharges on the surface. These discharge activities destroy the hydrophobicity, which eventually leads to irregular shape formations in the wet region (Figure 2-10e).
- 8) Dry band formation: The region of the surface with the highest power dissipation remains dry. Since the dry band is an insulating region, the surface discharges will continue in the dry band area until the band develops to an adequate length to withstand the applied voltage. The consequent discharge activities cause surface erosion.
- 9) Flashover: Increasing the length of the filaments and formation of the wet regions ultimately leads to short the insulator by a conductive path. This electrolyte water surface provides the track of the arc, which propagates

along the surface of the conductive layer and causes flashover, as demonstrated in Figure 2-10f.

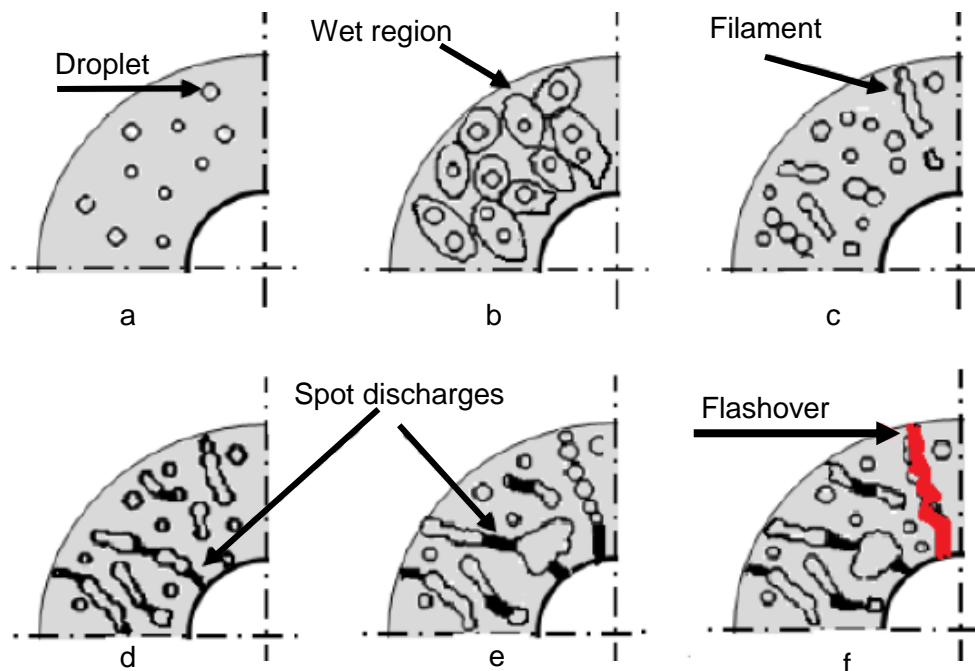


Figure 2-10: Flashover development on SiR insulators [2-88].

2.8. Monitoring and assessments

The aim of monitoring and diagnostics techniques is, in general, to provide useful information about the state of the insulator in the service. This means that the monitoring can help to make decisions about if and when replacement or maintenance of the insulator should be done. It is mainly correlated to reducing the risk of damage and minimizing the cost [2-27]. At present, most inspection methods used by the utilities are visual inspections that evaluate the hydrophobicity and measure the leakage current.

2.8.1. Visual inspections

This is the most common method used by utilities to identify defective polymeric insulators in service [2-29]. Visual inspections were found to be suitable for detecting visible faults on housing material, such as tracking, erosion, splitting, puncture, or any other obvious damage.

Imaging techniques, such as infrared thermography, UV, and light amplification equipment, were able to detect the presence of discharge activities on the insulator surface. IR imaging equipment was found useful for providing indications of internal faults, like tracking, that may potentially lead to failure of the insulator [2-27].

2.8.2. Hydrophobicity evaluation

Traditionally, the state of hydrophobicity on insulating surfaces is established through measuring the contact angle (θ). This angle is measured from where a small droplet of water meets the horizontal insulator surface, as shown in Figure 2-11. The contact angle is influenced by three factors of interfacial tension (λ) as described by the Young–Dupre equation [2-7]:

$$\lambda_{ia} = \lambda_{iw} + \lambda_{wa} \cdot \cos \theta \dots \dots \dots (2-1)$$

where a , i and w represent air, insulator and water, respectively. For a clean insulator surface, θ is around 30° for ceramic insulators and is greater than 90° for SiR. However, when the surface is covered by a layer of pollution, θ becomes always zero for the ceramic insulator (hydrophilic case), and it will recover to a considerable value for the SiR (hydrophobic case).

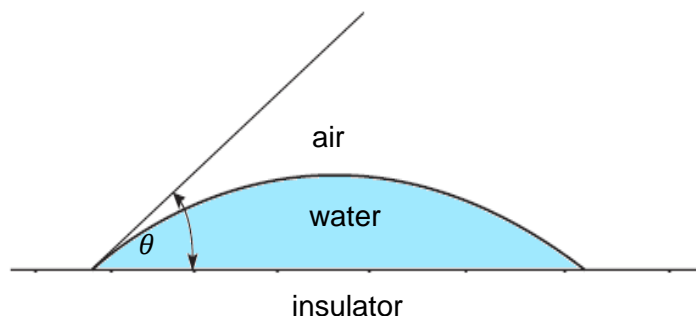
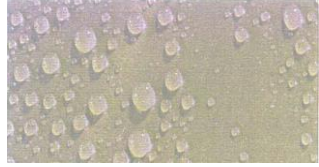
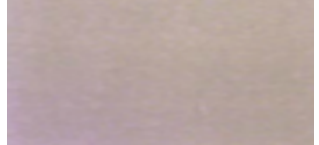


Figure 2-11: Sessile water drop on the insulator surface [2-7].

Since measurement of the contact angle technique is applicable only in the laboratory environment and is difficult to perform for the whole insulator surface, a simple test method for hydrophobicity classification (HC) has been introduced

by the Swedish Transmission Research Institute (STRI) [2-92], which has now has been adopted by the IEC [2-93]. Table 2-2 shows the STRI criteria for evaluating HC.

Table 2-2: Criteria for estimation of the hydrophobicity classification (HC) [2-92]

HC	Description	Pictures
1	Only discrete droplets are formed. This corresponds to $\theta_r = 80^\circ$ or greater for the majority droplets.	
2	The majority of the surface area is covered by discrete droplets. This corresponds to $50^\circ < \theta_r < 80^\circ$ for the majority of droplets.	
3	Only discrete droplets are formed. The majority of the surface area is covered by droplets that are no longer circular. This corresponds to $20^\circ < \theta_r < 50^\circ$.	
4	Both discrete droplets and wetted traces from the water runnels are noticed ($\theta_r = 0^\circ$). Entirely wetted area $< 2 \text{ cm}^2$. Together they cover less than 90% of the tested area.	
5	Both discrete droplets and wetted traces from the water runnels are observed. Some entirely wetted area $> 2 \text{ cm}^2$. Together they cover less than 90% of tested area.	
6	The wetted area covered is more than 90% (i.e. small unwetted areas (spots/ traces) are still noticed).	
7	Continuous water film is observed over the whole tested area.	

In this test, the hydrophobicity of the insulator surface is identified by comparing the surface with one of the standard photographs of the hydrophobicity classes (HC), which ranges between HC1 (hydrophobic class) and HC7 (hydrophilic class). The disadvantage of this technique is that the measurement

is based on the operator's judgment. To deal with this issue, Berg et al. in [2-95] proposed a digital image analysis technique for evaluating the hydrophobic measurement of the surface. Applications of such a process, where computer software can analyse the image, make the examination more objective and precise.

2.8.3. The leakage current measurement

Aging, which refers to the loss of hydrophobicity, tracking and erosion, leading ultimately to a flashover, is still a main concern with polymeric insulators. While the leakage current element is a cause of aging, it could be useful as an indicator of surface degradation [2-96]. Several efforts have been made to correlate leakage current parameters to the pollution level and to the surface damage, such as tracking, erosion, dry band arcing, and loss of hydrophobicity, and valuable information has been obtained [2-97]. Gorur et al. [2-11] found that both the magnitude of the peak current and the number of current pulses have presented good indicators of the surface condition and tracking damage of the EPDM insulators.

Bruce et al. [2-84] reported that the indication of material degradation can be evaluated by inspecting the nature of the leakage current pattern. This can be achieved by assessing the time distribution of the leakage current magnitude using the 15 samples per second recorder, which is an active method used to observe low-frequency surface behaviour. This data can then be illustrated as a measure of intermittency, making it possible to calculate the total duration time a sample spends in a non-conducting mode during the test. This gives precise information relating to the state of the surface of a conducting filament with or without a discharge present. Results from the literature [2-98, 2-99] confirm that the parameters of leakage current waveforms (e.g. peak and rms values)

provide valuable information that can be used to evaluate the polymeric insulator performance under different test conditions.

2.9. Artificial pollution testing methods of polymeric insulators

The pollution performance is an important factor for the selection and dimensioning of insulators, which increases the need to establish a common standard test method for evaluating outdoor insulation [2-100]. To evaluate the performance of polluted polymeric insulators, several types of artificial test methods are in use; the tracking wheel test, the inclined plane test, the salt fog and clean fog tests, and other approaches for evaluating tracking and erosion have been developed [2-101, 2-102, 2-103, 3-1, 3-9].

The subcommittee of the IEEE working group on lightning and insulator [2-104] reported that the most common artificial pollution tests employed are the clean fog test, the salt fog method, and the wet contamination test.

In the clean fog test technique, dry contaminated insulators under voltage stress are exposed to a fog generated from tap water. This test method simulates the condition in which a contaminant that has accumulated on the insulator surface is gradually wetted by natural sources of moisture leading to an increase in the possibility of the flashover phenomenon. In the salt fog test method, clean insulators are energised and subjected to a fog produced by atomising water [2-100]. This technique is mainly applicable to coastal environments, where insulators are subjected to direct salt spray. For the wet contamination method, which is not adopted as a standard test, insulators with a wet conducting coating are exposed to a voltage. This approach emulates the re-energisation of a line on which contaminated insulators have been subjected to a wetting agent, such as high humidity or rain [2-105].

2.9.1. Flashover tests methods

An increase in the number of problems associated with flashover incidents has encouraged many studies to obtain a better understanding of the phenomena leading to flashover, which causes a loss in the electrical performance of the insulators under different environments [2-106]. These studies normally include experimental investigations field observations and mathematical models. They have been established for the purpose of finding a way to avoid the problem of flashover [2-107, 2-108, 2-109, 2-110, 2-11, 2-112].

In one such study, Karady et al. [2-88, 2-89, 2-90] showed the results of an experimental study that aimed to provide a clear understanding of the flashover mechanism and explain the flashover phenomenon on the SiR surface. The results were found useful to improve the laboratory test procedures and to assess polymeric insulator performance under contaminated conditions.

Similarly, the authors in [2-113] presented a method for computing the electric field on an insulating surface in the presence of discrete water droplets. This technique was valuable for analysing the performance of outdoor insulation since the shape of the water droplet affects the magnitude of the electric field and, therefore, enhances the field as a force leading to moisture entry into the insulator surface.

Furthermore, in [2-114], the authors developed a dynamic arc model to analyse and predict the pre-flashover leakage current of polymeric insulators under wet polluted conditions. The model showed satisfactory results and the pre-flashover leakage current was easily predicted. This model might be helpful for simulating polymeric insulators designed for ultra high voltages outdoor applications.

2.10. Performance of silicone rubber insulators under AC and DC energisation

Extensive investigation studies were conducted at Koeberg Pollution Test Station, in Cape Town using natural pollution conditions with the aim to compare the aging performance of silicone rubber insulators under AC and DC (both polarities) energisation [2-83]. The AC test voltage was selected as 13.5 kV RMS. For both polarities DC, the voltage level was also chosen equal to the AC RMS value, based on the assumption that the aging performance of the insulator depends on the power dissipated over the insulator surface during electric discharge activities [2-83]. The comparison was performed with five insulators have different creepage distances and of the same manufacture as shown in the Table 2-3. The insulator dimensions complied in accordance with the IEC requirements. The insulators were energised by each voltage type, whereas being exposed to the environment for 310 days. The results data of 150 days were analysed with some reference to results of the entire test period [2-83].

Table 2-3: Silicone rubber test insulators [2-83]

Insulator	Creepage distance (mm)	Unified Specific Creepage Distance (USCD) (mm/kV)	Form Factor
SiR 87	1180	87	9.8
SiR 75	1010	75	8.7
SiR 58	780	58	6.4
SiR 46	615	46	5.5
SiR 29	395	29	3.3
GL 42	560	42	1.1

It was shown from the recorded data that the high leakage current level was measured in the summer due to the severe pollution level and high humidity. In contrast, during the winter, a lower level of leakage current was recorded, confirming the washing effect of the rain [2-83]. The leakage current data was

recorded at the sampling rate of 2 kHz, i.e 40 samples per 50 Hz cycle. The data was then post-processed and saved every 10 minutes. As can be seen in Figures 2-12, 2-13, 2-14, the highest leakage current of each test insulator was analysed and stored into bin classes at the termination of the test period.

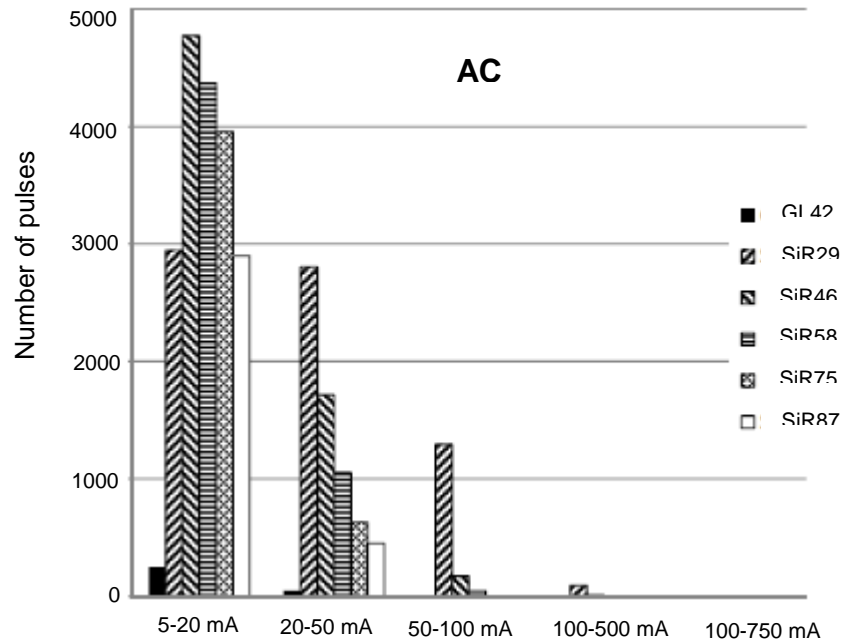


Figure 2-12: AC leakage current bin count data for tested insulators during a period of 150 days [2-83].

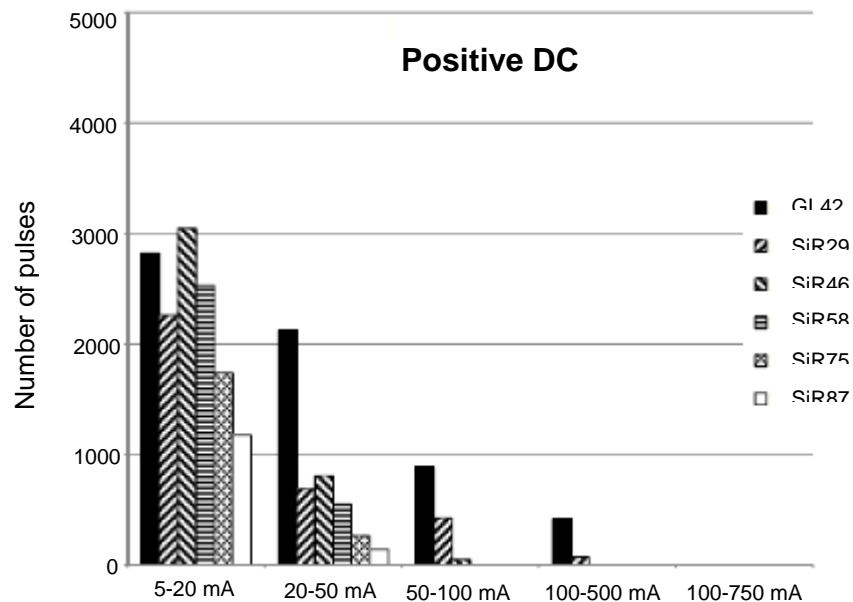


Figure 2-13: Positive DC leakage current bin count data for tested insulators during a period of 150 days [2-83].

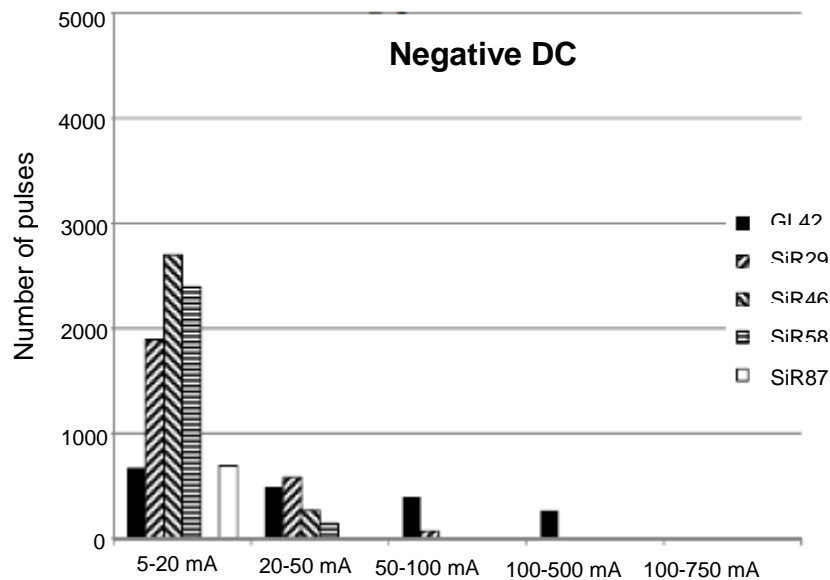


Figure 2-14: Negative DC leakage current bin count data for tested insulators during a period of 150 days (Note that data for the insulator SiR 75 are not presented) [2-83].

It is clear from the Figure 2-12, for the AC, the counts of the bin classes are less for the insulators with higher creepage distances. Only the exception occurs in the class of the 5-20 mA where insulator SiR 29 has a lower level count than the longer insulators. Arcs and discharge activities, driven by currents in mA range tend to be more damaging from an aging perspective than that associated with higher currents [2-83].

For the positive DC case, a similar tendency for the insulator SiR 29 has been noticed in the range of 5-20 mA. Figure 2-13, shows that the SiR 29 has a lower leakage current value than both SiR 46 and SiR 58 insulators. In the case of negative DC, SiR 29 has also lower leakage current counts in the 5-20 mA class, compared to the insulator SiR 46 (Figure 2-14).

Figures 2-15 and 2-16 show the peak of leakage currents for insulators SiR 29 and SiR 87, computed per 10 minutes interval for a complete day [2-83]. The values on the Figures were recorded by calculating the average of the peak leakage current for each instant. The highest leakage currents observe at 6 AM. The positive DC leakage current was the highest during the early morning time.

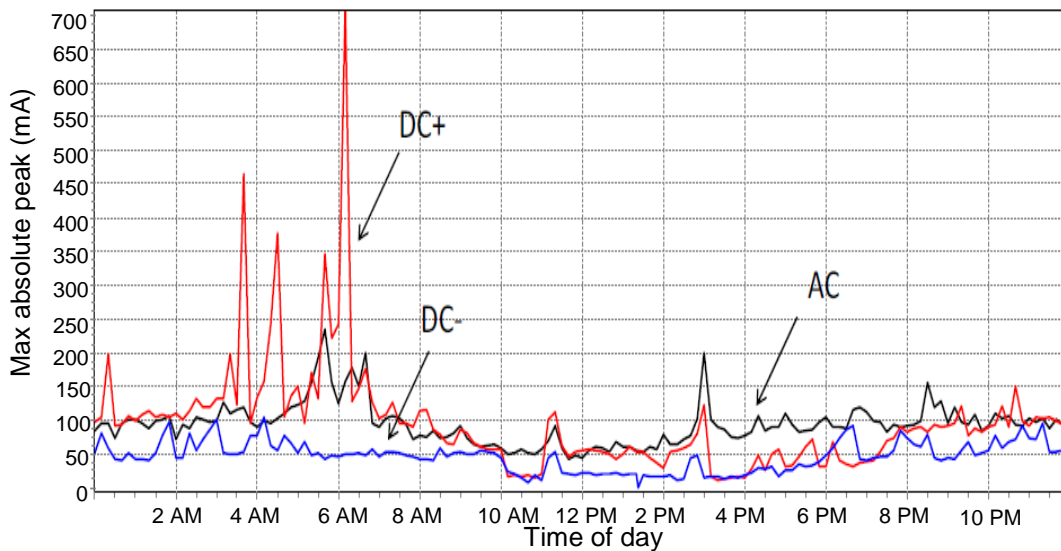


Figure 2-15: Time of day average of 10 minutes peak leakage currents for insulator SiR 29 for test period of 150 days [2-83].

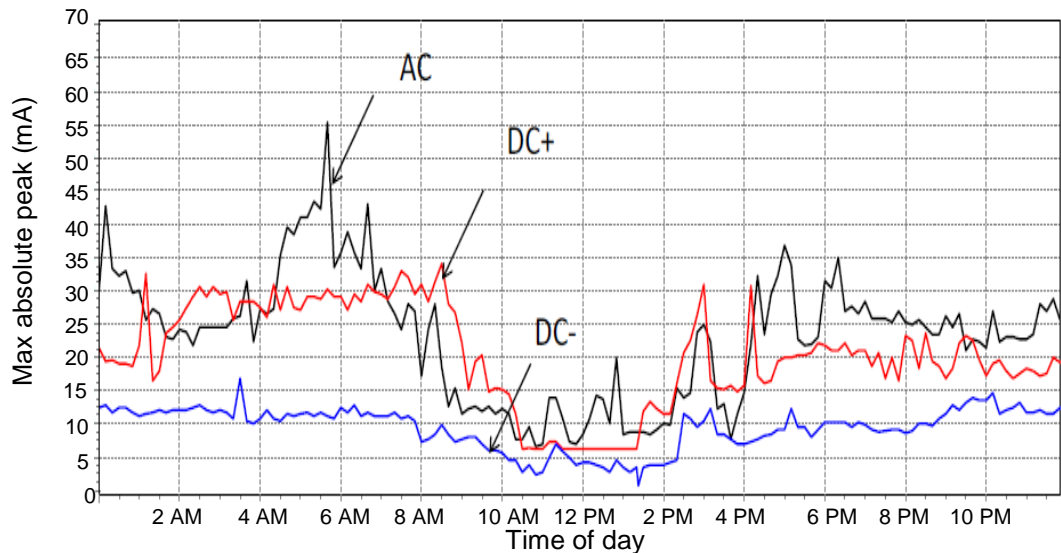


Figure 2-16: Time of day average of 10 minutes peak leakage currents for insulator SiR 87 for test period of 150 days [2-83].

For the both silicone rubber insulators (SiR 29 and SiR 87), the positive leakage current exceeds the negative DC current. This result is also confirmed by the finding results obtained in the Figures 2-13 and 2-14 and also by the peak waveforms of the leakage current during a pollution event as shown in Figure 2-17. For silicone rubber insulator SiR 87, in comparison to the shorter SiR 29 insulator, the AC peak leakage current exceeds the positive DC current [2-83].

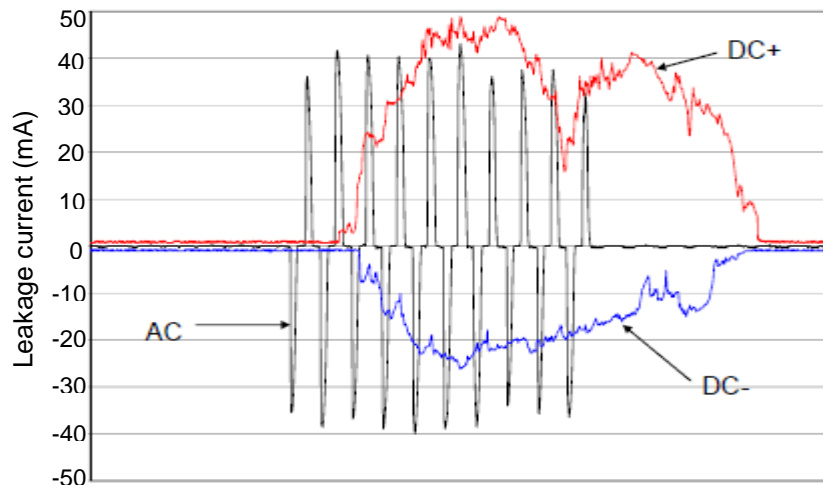


Figure 2-17: Peak current waveforms for SiR 87 insulator during a pollution event [2-83].

An interesting result found is that on the SiR insulators, the leakage current of the positive polarity DC was higher than that of the negative polarity DC [2.83]. This result is also confirmed in [2-119] by using the rotating wheel dip tests. The test was conducted on the SiR sample has a unified specific creepage length of 28 mm/kV. The test was approximately 7 weeks and the SiR sample was evaluated at the end of the test. The current traces recorded under AC, positive DC and negative DC voltages are shown in Figures 2-18 and 2-19. The highest leakage current value measured was 150 mA for the positive DC. While for the negative DC and AC cases, the maximum leakage current value was only 110 mA and 60 mA respectively [2-119].

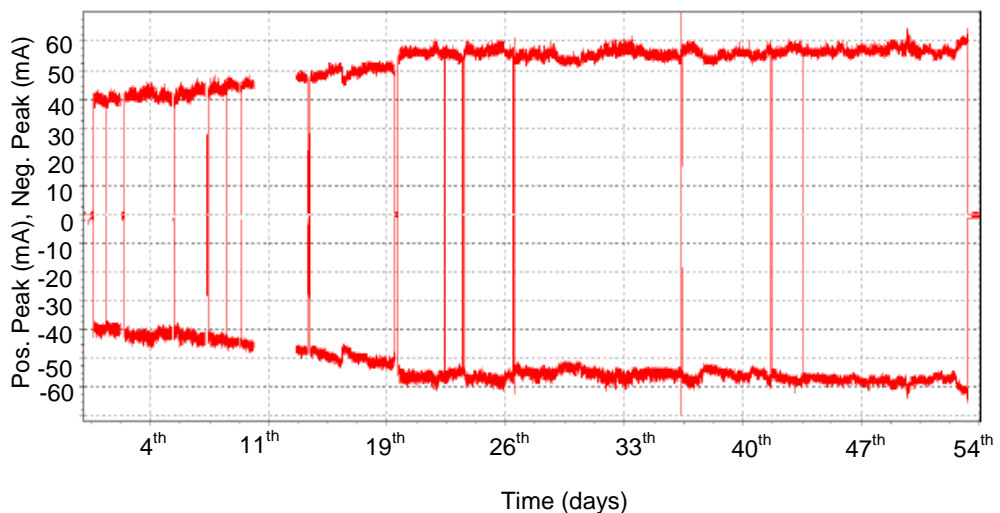
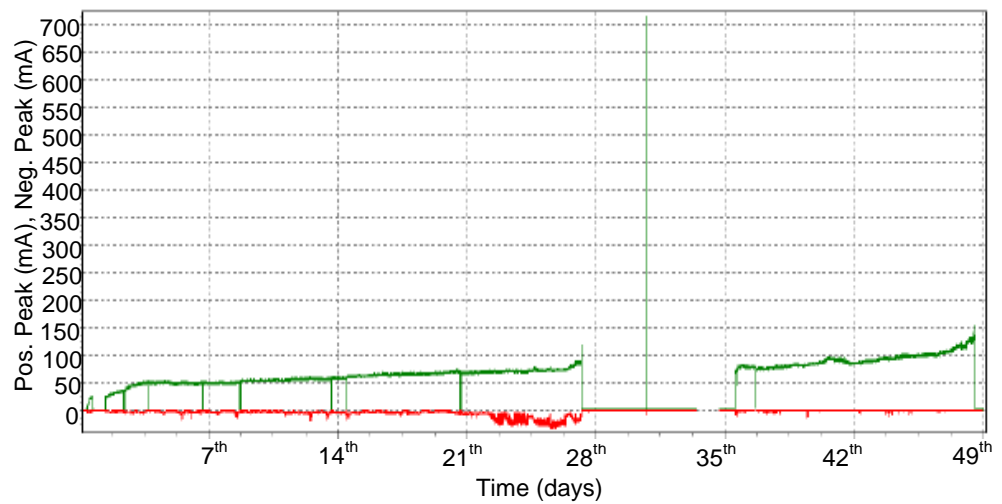
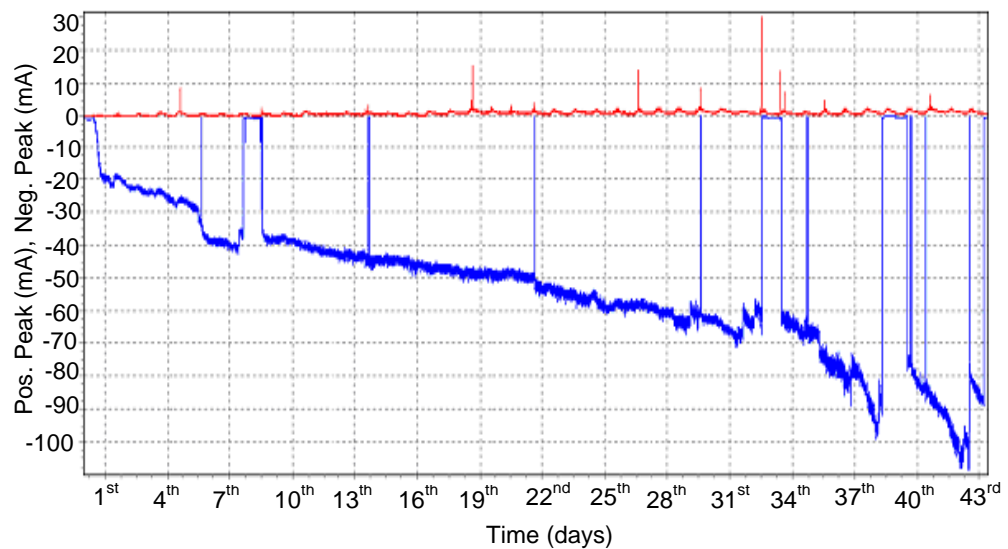


Figure 2-18: Maximum leakage current of the SiR insulator under AC [2-119].



(a) Positive DC



(b) Negative DC

Figure 2-19: Maximum leakage current for SiR insulator under DC both polarities [2-119].

For electrical discharge observations, both corona and dry band discharge activities mainly occurred on the sheds interfacing with both the high voltage and ground electrodes for all the SiR insulators [2-83]. These observations are particularly interesting in correlation with the finding of erosion detected on the tested insulators as shown in Figures 2-18. The measurement of hydrophobicity illustrated the upper surface of the sheds of the SiR insulators to be more hydrophobic than the bottom [2-83]. The rods of the longer insulators were also more hydrophobic than those of the shorter insulators. Hydrophobicity recovery was also faster for DC insulator surfaces than on the AC [2-83].



(a) Erosion AC (Week 22)



(b) Erosion -DC (Week 16)

(c) Erosion +DC (Week 18)

Figure 2-20: Erosion on the insulator SiR 87 [2-83].

As expected, significant erosion was observed on the rods near to the metal end fittings, though some cases were also noticed in the central parts of the longer insulators. For all insulators with all voltage types, the lowest erosion was observed on the SiR 29 insulator. This unexpected result might be related to the stationary nature of discharges, connected with the small leakage current range. This suggestion is supported by the fact that leakage current on SiR 29 in the range of 5-20 mA are less frequent than on others insulators. In general, SiR insulators were severely eroded when energised by positive DC voltage [2-83]. This severity of DC testing compared with the AC was also confirmed in [2-119]. The amount of erosion on the SiR insulator under positive DC was being the worst over all voltage classes (Figure 2-21).



(a) Shed puncture after 920 h

(b) Fails after 700 h

(c) Brown deposition and erosion after 910 h

Figure 2-21: Visual appearance of the SiR insulator at the end of the test [2-119].

2.11. Summary

The available literature review has shown that the electrical performance of SiR polymeric insulators is correlated to their surface properties. Insulators with hydrophobic surfaces have exhibited a superior performance for maintaining a lower leakage current and high resistance to flashover in polluted-wet conditions than insulators with hydrophilic surfaces.

The surface situation of polymeric insulators that are operated in severe environment conditions has been found to worsen with age. Aging has been found to reduce the overall electrical performance of polluted SiR insulators and cause an increased incidence of discharge activities and dry band arcing on the surface. This increase can degrade the housing material by tracking and/or erosion, which in severe cases, leads to damage to the insulator. So, the correlation between insulator surface condition and electrical performance is observed, in which the direct investigation of the state of the insulator surface is a useful technique in predicting insulator aging.

For AC and DC polymeric insulators, the literature has provided useful information about the performance of SiR insulators energised by AC, positive DC and negative DC voltages. The polarity effect has been confirmed relating to the pollution performance and the aging of SiR insulators. The severity of DC testing compared with AC has also been noticed.

The textured insulator is proposed by Cardiff University as a novel design for polymeric insulators, which aims to improve the flashover performance of SiR insulators by reducing the surface damage caused by discharge activities and dry band arcing. The present research describes the experimental investigations of textured insulators using standard and non-standard test methods and novel techniques to evaluate the expected improvement that may be achieved by using the textured designs.

CHAPTER 3: EXPERIMENTAL FACILITIES, SAMPLES AND TEST ARRANGEMENTS

3.1. Introduction

An understanding of the behaviour of silicone rubber (SiR) insulators using AC and DC excitations under different environment conditions is required for utilities and experimental facilities to implement outdoor insulators for high voltage applications.

This chapter presents the laboratory facilities, test arrangements, and experimental procedures developed for the following purposes:

- to fabricate the insulation samples with different shape profiles,
- to implement the mandatory test conditions,
- to carry out the experiments as they are designed,
- to measure the relevant electrical parameters, as these may be used as indicators of the aging performance of the polymeric insulators.

Leakage current and cumulative dissipated energy were observed and used to characterise each insulator. Visual and infrared cameras were also used to assess the discharge activity and temperature distribution along the insulator profile. A surface conductance meter was used to evaluate the variation in surface layer conductance on each insulator's surface. Equivalent salt deposit density (ESDD) and non-soluble deposit density (NSDD) parameters were also measured to determine the pollution severity levels.

For flashover performance tests, the magnitude of the flashover voltage (FOV) was used to evaluate the condition of the insulator. For all tested samples, silicone rubber materials were selected to make both rectangular samples and four-shed insulators.

3.2. Experimental test summary

Many experimental studies and investigations have been conducted in laboratories to examine the aging performance of SiR insulators as used in high voltage outdoor applications. These tests have been carried out under different environmental conditions to determine the electrical properties and the degradation level of the insulator surfaces. In this study, various types of four-shed SiR insulators (conventional and textured) were fabricated and subjected to the Rotating Wheel Dip Tests (RWDT) according to IEC 62730:2012 [3-1]. Surface conductance evaluation tests were also performed on the four-shed SiR insulators. The ESDD and NSDD tests were evaluated based on the standard described in IEC 60815 [3-2]. Tests were carried out using a high voltage fog chamber facility to investigate the performance of 11kV SiR insulators.

3.3. Textured design

With the aim of improving the pollution performance of polymeric insulators, a novel approach to controlling dry-band formation using a textured pattern design was investigated in [2-24, 2-25]. The geometrical pattern of textured insulators can achieve two valuable objectives; firstly, a substantial increase in the surface area can reduce the leakage current density in the susceptible shank region, and secondly, the textured surface increases the longitudinal creepage distance, which can, therefore, decrease the field stress, in particular areas of the insulator [2-23, 3-3, 3-4]. The textured samples comprised an array of hemispherical protuberances moulded with a square intersection of 4 mm or 6 mm in diameter, as illustrated in Figure 3-1.

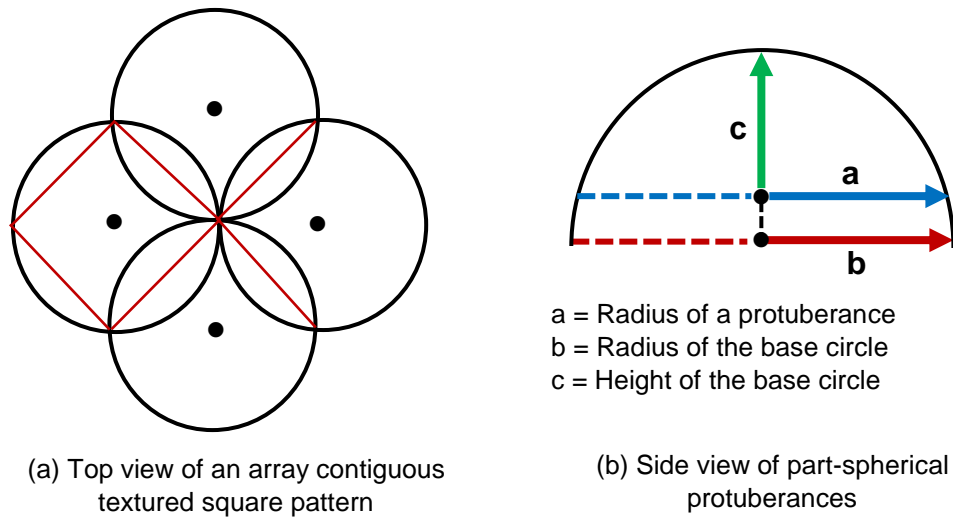


Figure 3-1: Hemispherical protuberances: square-intersection pattern [2-25].

The textured profile generally presents a significant improvement in the FOV compared with conventional SiR insulators under the clean-fog test conditions. It also shows a considerable reduction in the leakage current and surface degradation under RWDT.

For outdoor insulation under severe environmental conditions, a uniform pollution layer with volume conductivity σ (S/m) and thickness t (m) are assumed to coat both surface designs of textured and non-textured insulators. The layer conductance for both surfaces is specified by:

$$K = t \cdot \sigma \quad (\text{S}) \dots \dots \dots (3-1)$$

This layer can result in a significant conduction current (I) with non-uniform current density (J). The leakage current density inside the pollution layer at position (L) is given by:

$$J_{\text{layer}} = \frac{I}{L \cdot t} \quad (\text{A/m}^2) \dots \dots \dots (3-2)$$

By assuming the thickness of layer (t) to be constant, the surface leakage current density can be expressed as:

$$J = J_{\text{layer}} \cdot t \quad (\text{A/m}) \dots \dots \dots (3-3)$$

The contour of the circular surfaces along the insulator profile is varied because of the radius (r) and, therefore, the non-uniformity of electric field strength (E). The surface regions of the greatest J and E can cause a considerable heating of the pollution layer, which may ultimately lead to dry band formation on the insulator surface. The power dissipation P (W/m²) per unit area of the surface layer heating is given by:

$$P = EJ = J^2/\sigma \dots \dots \dots (3-4)$$

The aim of the textured surface was to reduce the power dissipation by reducing both field strength and leakage current density in the shank regions of an insulator. The reduction of the electric field and the current density was achieved by increasing the insulator surface area by a factor α ($\alpha=1.301$) and the creepage distance by a factor β ($\beta=2.222$) respectively [2-25]. With these increased factors (α , β), mitigation of the dry band formation and the surface degradation from the partial discharges was realized.

The surface profile of a textured insulator used the same standard design, with a textured surface moulded either on the insulator trunk (TT) or on both trunk and shed surfaces (TTS) [2-23].

3.3.1. Textured Trunk (TT) profiles

For the TT profiles, the three trunk sections of the insulator surface were moulded using a square intersection pattern with dimples of 4 mm (TT4) or 6 mm (TT6) in diameter. Figure 3-2 shows the textured trunk design (TT4) with 4 mm dimples. With this texture, the creepage distance of the insulator profile increased to 471 mm.

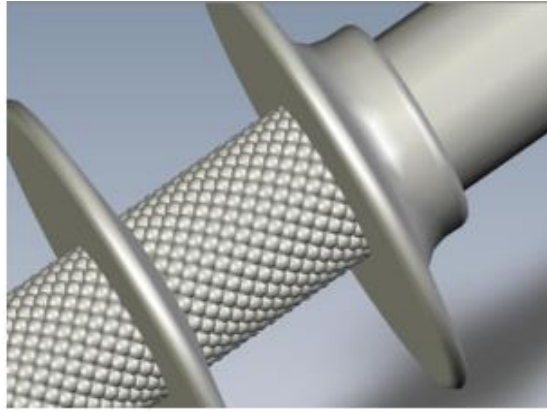


Figure 3-2: 4 mm textured trunk design (TT4) [2-81].

3.3.2. Textured Trunk and Shed (TTS) profiles

In this case, both insulator trunk and shed surfaces were moulded with square-intersection hemispherical protuberances. An additional double spiral pattern of semi-cylindrical ridges under the shed area was used to enhance the creepage distance, as illustrated in Figure 3-3. The total creepage distance for the TTS profile was 503 mm, 32 mm increased in comparison with TT profile.

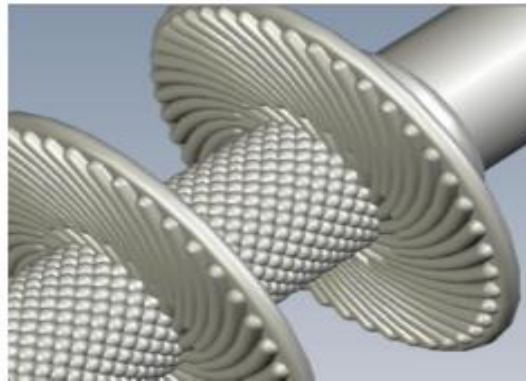


Figure 3-3: 6 mm textured trunk shed design (TTS6) [2-81].

3.4. The Rotating Wheel Dip Test (RWDT)

The reliability and the safe operation of the power transmission lines and distribution networks are greatly affected by the performance of the outdoor insulation [3-5]. For this reason, it is crucial to study the influence of outdoor insulators on high voltage systems. The rotating wheel dip test (RWDT) is one of the most commonly used methods of investigating the performance of high

voltage insulators. Based on the standard IEC 62730, RWDT has been considered as a screening test in order to identify any material or design unsuitable for use in overhead transmission lines. The standard also specifies the principal operation and test conditions required to examine four-shed polymeric insulators under the rotating wheel dip test.

3.4.1. Test insulators

Two different 4-shed insulator designs were used in this study, which were manufactured in-house using room-temperature vulcanised (RTV-2) two-component silicone rubber (600A/B) by casting over a glass-fibre core with aluminium end fittings crimped on each end. The mechanical and electrical properties of the 600A/B component are given in Table 3-1 [3-6].

Table 3-1: Characteristics of 600A/B silicone rubber material

Property	Inspection method	600A/B
Permittivity	IEC 60250	2.9
Dielectric strength [kV/mm]	IEC 60243	23
Tracking resistance	IEC 60587	1A 3.5
Dissipation factor	IEC 60250	3×10^{-4}
Tensile strength [N/mm ²]	ISO 37	6.50
Hardness Shore	ISO 868	30
Tear strength [N/mm]	ASTM D 624 B	20
Elongation at break [%]	ISO 37	500
Volume resistivity [Ω cm]	IEC 60093	10^{15}

The pigtail and pin aluminium fittings were attached directly to the fibreglass core, as illustrated in Figure 3-4. A superior adhering primer was used to enhance the adherence of the silicone rubber to the metal surfaces of the pin and the pigtail. A strong bonding between them was achieved.

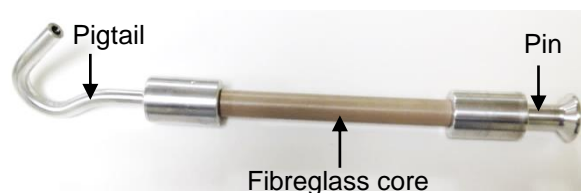


Figure 3-4: Pigtail and pin aluminium end fitting design.

The insulator profile adopted was based on a conventional design (CONV), as shown in Figure 3-5a. The same basic profile was used for the textured insulators, with the textured surface moulded on the insulator trunk (TT6) (Figure 3-5b). The dimensions of both insulator designs are summarized in Table 3-2.

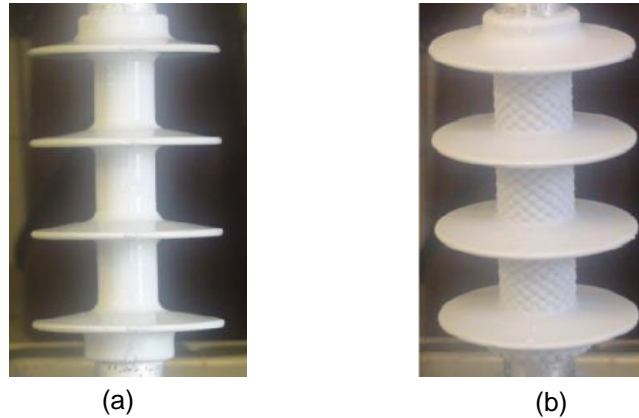


Figure 3-5: Test samples for conventional (a) and textured trunk (b) insulators.

Table 3-2: Dimensions of tested insulators

Parameter	Conventional (CONV) (mm)	Textured trunk (TT6) (mm)
Creepage distance	375	471
End fitting separation	175	175
Shed diameter	90	90
Shed separation	46	46
Trunk diameter	28	28
Inner core diameter	18	18
Form factor	2.76	2.76

3.4.2. Insulator preparation

Two types of silicone rubber (SiR) insulators were fabricated in the High Voltage Laboratory at Cardiff University. The conventional insulator was manufactured as a standard commercial insulator available in the market while the TT6 insulator was designed based on the same basic profile of a standard insulator with textured surface enhancement of the insulator trunk. The RTV-2 silicones were prepared by mixing two components of the base resin (600A) and the curative (600B) with a ratio of 9:1 using an MCP 5/01 vacuum casting machine

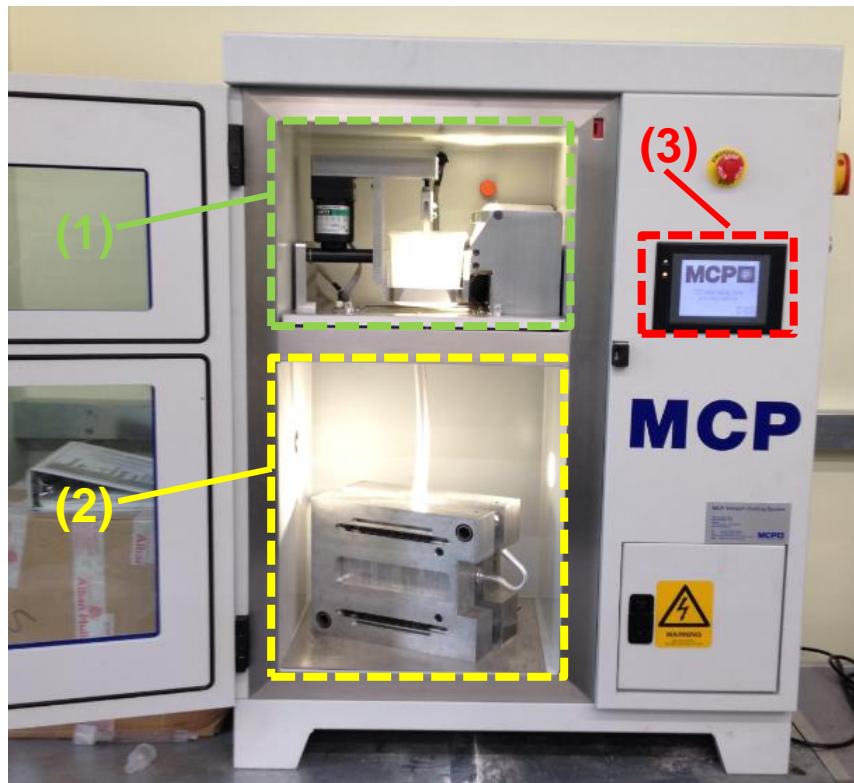
(Figure 3-6a). During the casting process, the mixed components were injected into the mould.

As can be seen in Figure 3-6a, the main components of the casting machine are (1) the top mixing chamber, (2) the lower injection chamber, and (3) the touch control panel. The mixed components of SiR (600A/B) are placed in the top chamber while the mould is placed in the lower chamber.

At the beginning of the casting operation, trapped air is removed from the mixed components by degassing the top chamber for a few minutes. After about 12 minutes of degassing and mixing, the SiR component is ready to be injected into the lower part of the casting machine where the mould is located. During the injection process and due to the complex geometry of the mould, a variable pressure is applied to force the mixture to fill the mould cavity.

When the material starts to emerge from the venting channels, the mould cavity becomes full. The vacuum casting machine is then switched off and the mould placed in the oven (Figure 3-6b) for curing at 50° Celsius for eight hours. Next, the mould is left to cool for one hour, before the mould is separated to reveal the cast (Figures 3-6c and 3-6d).

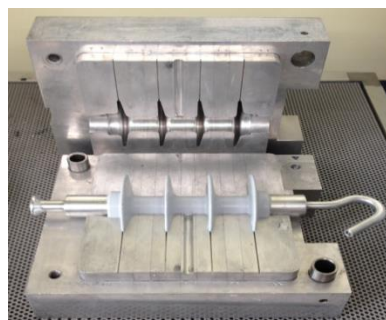
The insulator is then removed from the mould and inspected for any clear defects or voids. If no imperfection appears, it is left for an extra 24 hours at room temperature to ensure that the cross-linking of the polymer has been completed.



(a)



(b)



(c) Conventional (CONV)



(d) Textured (TT6)

Figure 3-6: (a) the vacuum casting machine: (1) the top mixing chamber (2) the lower injection chamber (3) touch control panel; (b) oven; (c) conventional insulator; and (d) textured insulator

3.4.3. Rotating wheel dip test set-up and facilities

A Rotating Wheel Dip Tester was designed and constructed in [3-11] in accordance with IEC 62730 standards [3-1]. The apparatus was designed to be able to accept AC and DC voltages. Figures 3-7 and 3-8 show the circuit diagram and the arrangement setup of the RWDT test.

The Ferranti high voltage 7.5 kVA, 100 kV step-up transformer was fed from the 220V mains supply voltage through a voltage controller, an isolating transformer, and a low-pass LC filter. For DC tests, the Glassman WX15P70 Series DC source was utilised to provide 1 kW of output power with a voltage up to 15 kV and a current of 70 mA. A 2 rpm DC permanent magnet motor with a Single Pole Single Throw Normally Open (SPSTNO) relay was used to attain the rotational movement of the test insulators. The tank used for the salt solution was made of a glass reinforced plastic (GRP) material with dimensions of (1.6 m x 0.25 m x 0.75 m). The voltage and current transducers consisted respectively of a voltage divider with a ratio of 3750:1 and a 200 Ω shunt resistor for current measurement. The voltage and current signals were acquired using a computerized data acquisition system. For this purpose, a data acquisition (DAQ) card (MIO-16E series) was used, and its input was protected using a three-stage overvoltage protection system.

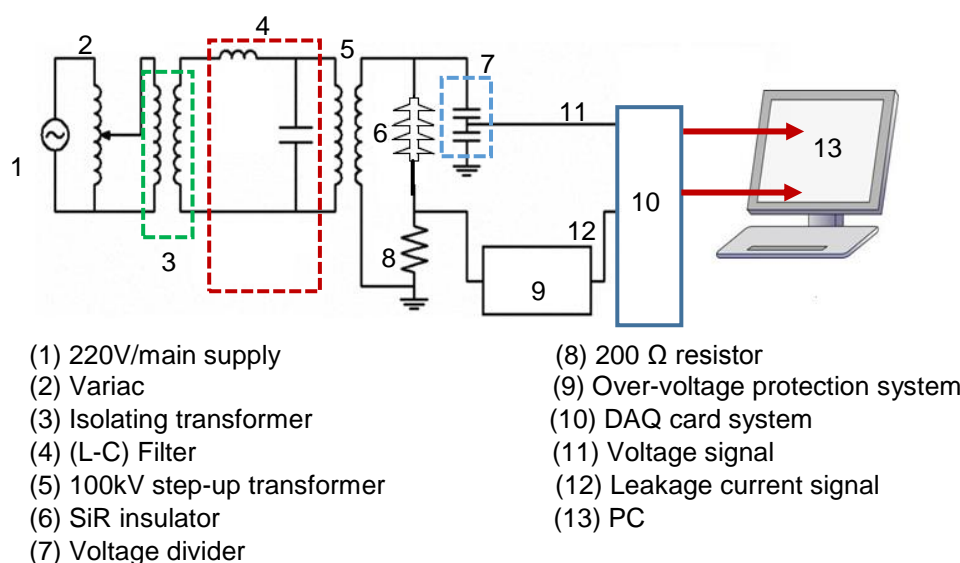


Figure 3-7: Circuit diagram of RWDT.

this resistor is acquired by the DAQ card through a coaxial cable (RG58). The signal is then saved into a personal computer using a LabVIEW code. The operating voltage signal is acquired directly to the DAQ system through a voltage divider and a BNC attenuator with a total ratio of 3750:1. For the motor control system, the speed regulator and a box in which the relay is situated are placed in the other side of the frame. The relay receives the control signal from a digital output pulse generated by a DAQ card. The complete cell is firmly fixed with a metal frame equipped with wheels, which allow it to be easily moved.

3.4.5. Motor control program and data acquisition system

In order to move the wheel where the insulator is mounted, a DC permanent magnet motor was used. Choosing such a kind of motor provides simple speed control and offers a fast response to starting and stopping [3-12]. The requirement to have a simple speed control is due to the different weights of insulators; each type of insulator requires different torques to achieve the same movement time (8 s) from two different positions. Because the torque/speed characteristic of a DC motor is quite linear, the speed can be simply controlled by changing the current [3-11].

(a) Motor control program

Using the LabVIEW graphic programming language, an appropriate code was written to control the motor of the RWDT [3-7]. The program was developed to control the motor speed and to rotate the motor in the desired position. To generate the input signal to stop the motor, it was decided to use the value of the instantaneous power as a threshold condition [3-12]. Thus, when the insulator touches the high voltage electrode, the instantaneous power value reaches the threshold level. At this same time, the DAQ card generates a digital output signal to stop the motor. Using the graphical LabVIEW program shown in Figure 3-9, the user can follow the number of cycles that are run during the test and

determine the optimal threshold value required to stop the motor. Figure 3-10 shows clearly the flow chart of the motor control program and how it communicates with the main data acquisition system.

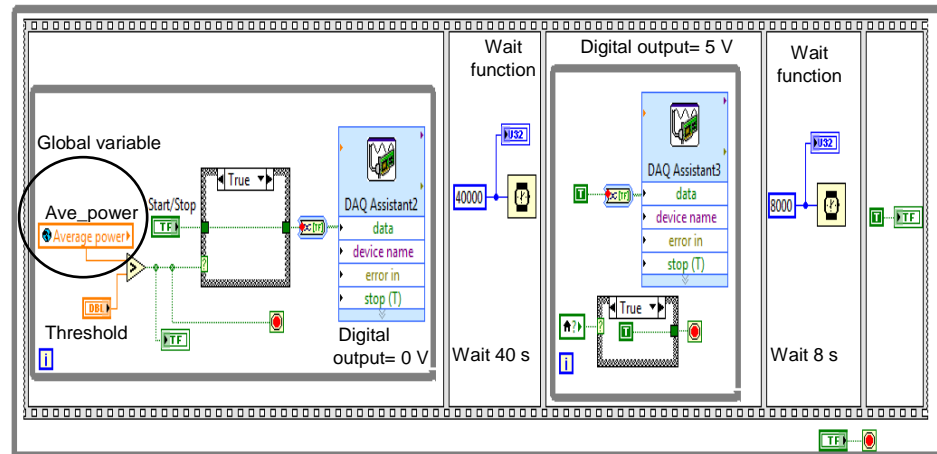


Figure 3-9: The graphical LabVIEW program of the motor control of RWDT.

The data acquisition and the motor control programs were linked together to detect the number of cycles completed during the test. The program stages to achieve this interfacing are described as follows:

- a) The global variable value of the instantaneous power is created to interface both programs, and through this value, it is possible to check whether the motor has to be stopped.
- b) When the insulator rotates between the two positions, the program outputs a digital pulse of 5 V, and the average power value is under the threshold level.
- c) While the insulator is in a perpendicular position, where it is energised, the average power value exceeds the threshold level and the digital output of the program is carried down at 0 V, thus driving the motor to stop.
- d) Once the motor has stopped, the global variable of the average power is set to true, thus allowing the DAQ system to run. After 40 s, a pulse of 5 V is sent again to activate the motor and rotate the insulator to the next position.

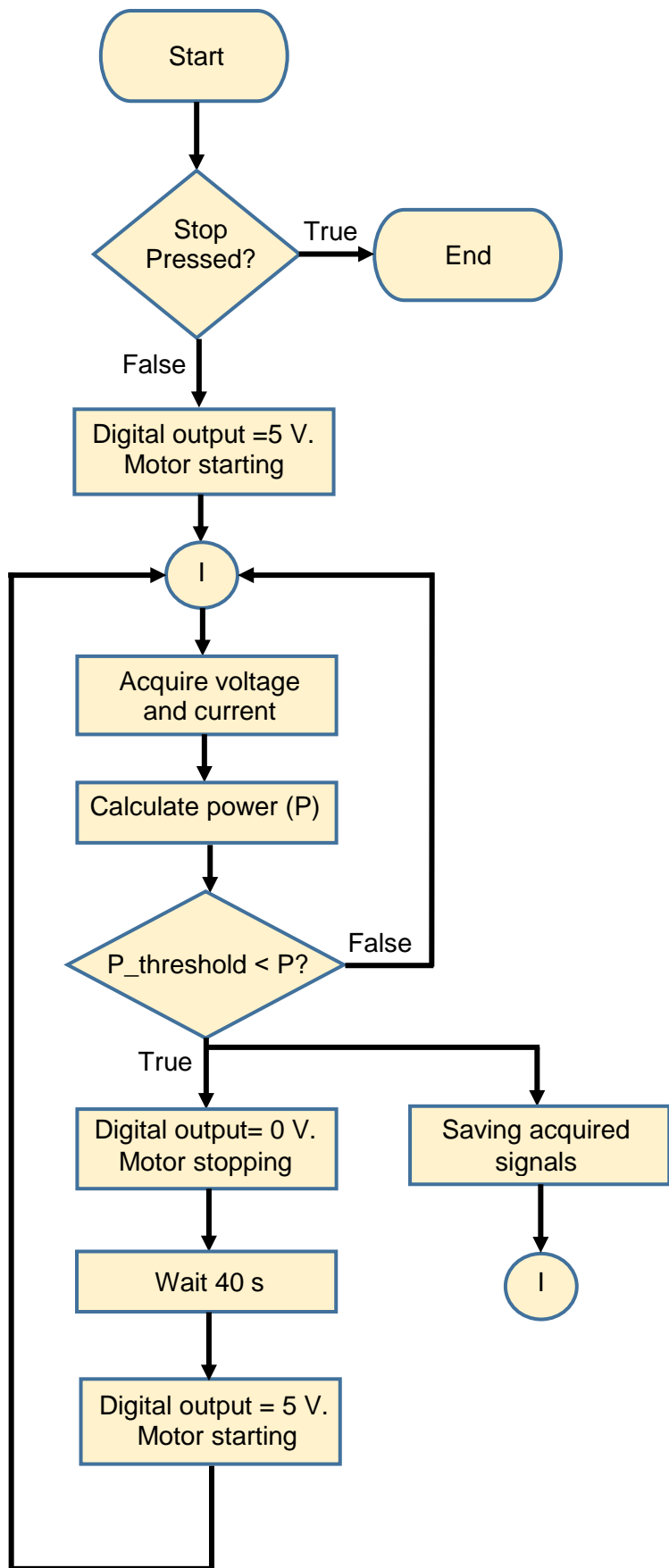


Figure 3-10: Flow chart of the motor control program.

(b) The data acquisition system

The E-series MIO-16E National Instruments board was used to acquire the leakage current and the voltage signals during the test. The maximum input range varied between -10 V/+10 V. The data acquisition board can acquire either 32 single-ended analogue inputs or 16 differential analogue inputs. The physical connection between the board and the RWDT control unit was attained by an SCB-68 connector block. The connection between the connector and the DAQ board was made with an SHC68-68-EPM shielded cable.

The data acquisition (DAQ) program of the RWDT was also built in LabVIEW (Figure 3-11). The program was designed to acquire, monitor, and store the waveforms of leakage current and applied voltage signals. The interface of the DAQ program with the motor control system is illustrated in Figure 3-11.

The DAQ software starts acquiring/saving data when the insulator makes contacts with the HV electrode. The sample rate of the data acquisition board is 10^4 samples per second for each of the two analogue channels of the voltage and current signals. The leakage current and voltage traces were stored in a Technical Data Management Streaming (TDMS) file format [3-8].

Data were saved in sets of 200 samples, which represent one cycle of the 50 Hz voltage and current waveforms. The acquisition of samples was repeated until all 4×10^5 samples had been processed and, then, the next file was accessed. Each acquired file represented the saving data of one wheel revolution.

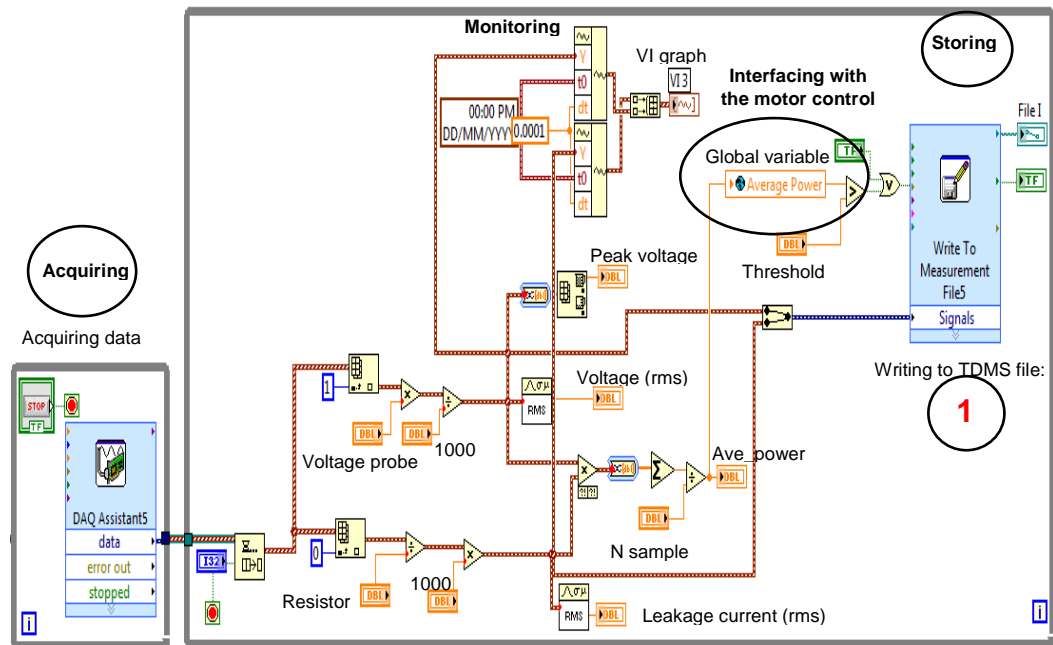


Figure 3-11: The LabVIEW block diagram code for acquiring, monitoring and saving the leakage current and applied voltage signals.

(c) The post-processing data program

The post-processing LabVIEW program was developed to read and analyse the data acquired from the RWDTs and the fog chamber tests. The block diagram of the software user is shown in Figure 3-12. The program allows the user to choose the path from which to read the saved files and determines a specific path for the calculated parameters. The code is also responsible for specifying the electrical characteristics to be analysed. The electrical parameters, such as the peak and root mean square (rms) leakage current of the applied voltage, average power dissipation, total harmonic distortion (THD), power factor angle, and absorbed energy are calculated. Studying the behaviour of these parameters helps to evaluate the performance of SiR insulators and material degradation under test conditions.

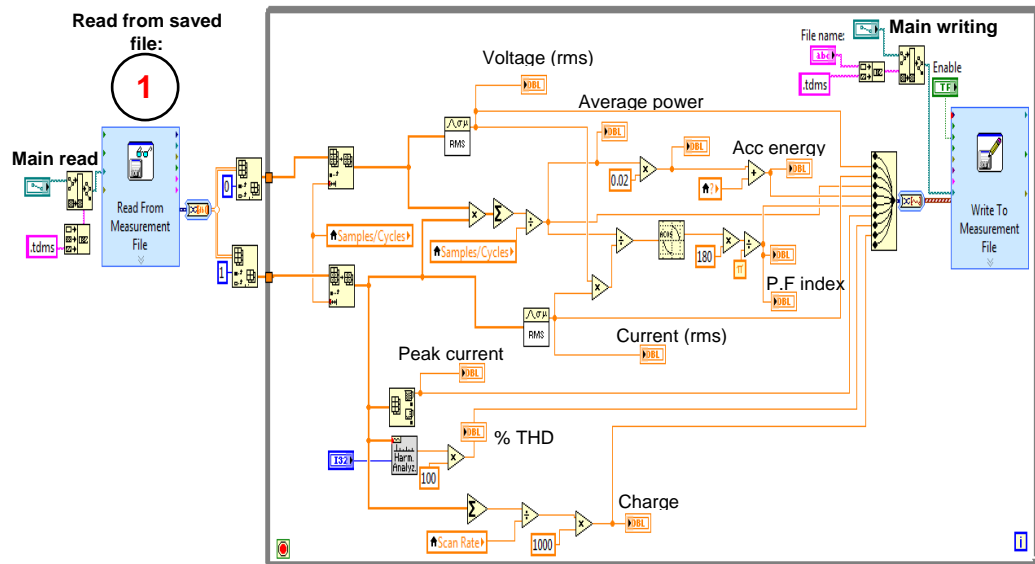


Figure 3-12: The post-processing LabVIEW programming code: analysing and storing functions of the electrical properties.

The rms leakage current magnitude was used to evaluate the behaviour of discharge activities that occurred on the insulator surface. These discharges may lead to surface drying and, ultimately, the formation of dry bands on the surface. The average power dissipation was used to measure the heat dissipated on the surface of the insulator since it is one of the major causes of material degradation. The cumulative dissipated energy was used to calculate the total power losses on the insulator surface, and based on these losses, the degradation level on the surface can be predicted.

The power factor index calculates the phase shift angle between the voltage and the leakage current, which can be used to distinguish the features of the resistive surface conduction and surface discharge activity. The electrical parameters used in this work are calculated on the post-processing program code as follows:

- 1- The root mean square (rms) value of the voltage (V_{rms}) and current (I_{rms}) signals for one cycle is calculated according to the following equations:

$$V_{rms} = \sqrt{\frac{1}{N} \cdot \sum_{n=1}^N V_n^2} \dots\dots\dots (3-5)$$

$$I_{rms} = \sqrt{\frac{1}{N} \cdot \sum_{n=1}^N i_n^2} \dots\dots\dots (3-6)$$

where N corresponds to the number of samples per cycle (200 samples for this work).

2- The absolute peak value of the both voltage ($|V_{Peak}|$) and current ($|I_{Peak}|$) signals over one cycle is calculated by identifying the greatest value.

3- The average power dissipation for one cycle is computed by multiplying each instantaneous value of the voltage (v_n) by its corresponding value of leakage current (i_n). Then, the sum values of the instantaneous power are divided by the number of data points in that cycle according to Equation (3-7):

$$P_{av} = \frac{1}{N} \sum_{n=1}^N v_n \cdot i_n \dots\dots\dots (3-7)$$

Consequently, multiplying the average power dissipation with the cycle period ($T= 0.02s$) will produce the energy dissipated per cycle:

$$E_{av} = P_{av} \cdot T \dots\dots\dots (3-8)$$

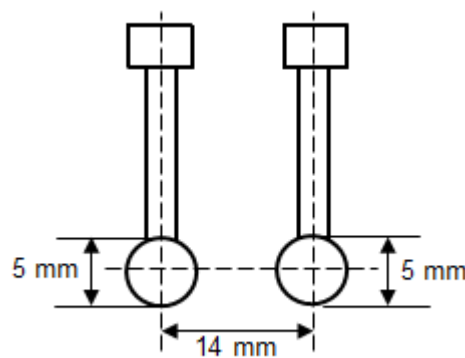
4- The cumulative dissipated energy is calculated by summing the energy of each cycle to the all former calculated energy cycles as described in Equation (3.9).

$$E_{acc} = \sum_{n=1}^n E_{avn} \dots\dots\dots (3-9)$$

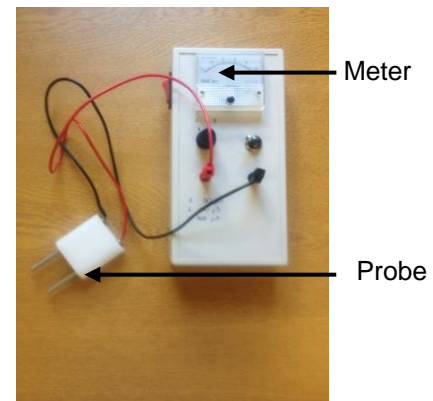
3.5. Surface conductance measurement tests

3.5.1. Surface conductance meter

The device was built in [3-13] according to IEC 60507 standards to evaluate the local surface conductance of the pollution layer and to check its uniformity on the insulator surface [3-9]. The possible arrangement of this device is described by a conductance meter with two spherical electrodes built as illustrated in Figure 3-13. The electrodes were made of stainless steel pins 5 mm in diameter with a distance of 14 mm between their centres. The pins were spring-loaded so they could be pushed by hand against the insulator surface. The spring force at full compression was approximately 9 N.



(a) Spherical electrodes [3.9]



(b) Conductance meter

Figure 3-13: The arrangement of surface conductance meter.

The voltage source with a Zener-diode at 6.8 V supplied the current through a probe between the electrodes. The measuring meter offered different full-scale deflection at values of 50 μA , 100 μA , and 500 μA . The selector switch was used to determine the scale deflection suitable for the measurement ranges. The measurements of the pollution layer were carried out at different places on the insulator surfaces as specified in [3.9]. The uniformity of the surface layer is achieved when the difference between each measured value and their average, as a percentage, is limited to $\pm 30\%$.

3.6. Measurement of insulator pollution level

According to IEC 60815, ESDD is the standard technique used for measuring pollution levels on insulator surfaces [3-2]. The levels of ESDD at the top and the bottom surfaces of insulators are usually different. The method used to evaluate the ESDD level in the laboratory, which is expressed in mg/cm², is called the rag-wipe technique [3-10]. The ESDD measurements can be calculated from the conductivity and the temperature of the solution obtained from washing a particular area of the insulator surface using deionized water. The conductivity (σ_T) of the solution is then measured by a HANNA conductivity meter at temperature T (°C). The volume conductivity (σ_{20}) at 20°C is then calculated by the following equation:

$$\sigma_{20} = \sigma_T [1 - b(T - 20)] \dots \dots \dots (3-10)$$

where: T = the solution temperature (°C).

σ_T = volume conductivity at T°C (S/m).

σ_{20} = volume conductivity at 20°C (S/m).

b = the coefficient depending on the temperature of T, as obtained by the equation (3-7).

$$b = -3.2 \times 10^{-8}T^3 + 1.032 \times 10^{-5}T^2 - 8,272 \times 10^{-4}T + 3.54 \times 10^{-2} \dots \dots (3-11)$$

The salinity (S_a) (kg/m³) and the ESDD (mg/cm²) is then obtained using the following equations:

$$S_a = (5,7\sigma_{20})^{1,03} \dots \dots \dots (3-12)$$

$$ESDD = S_a \times V/A \dots \dots \dots (3-13)$$

where: V = the volume of the deionised water (cm³).

A = the area of the insulator surface for collecting pollutants (cm²).

Next, the pollutant solution was filtered using a funnel with vacuum aspiration; this was then pre-dried, and the filter paper (GF/A 1.6 μm) was weighed using a high precision scale.

The NSDD can then be calculated as follows:

$$\text{NSDD} = 1000(W_f - W_i)/A \quad \dots \dots \dots (3-14)$$

where: W_f = the weight of the filter paper containing residuum after drying (g).

W_i = the initial weight of the filter paper under dry conditions (g).

A = the area of the insulator surface for collecting pollutants (cm^2).

NSDD = the non-soluble deposit density (mg/cm^2).

3.7. Fog chamber test

3.7.1. Test samples

Different 4-shed insulator designs with a smooth conventional surface and with textured patterns were used in this study. The insulators were manufactured in the high voltage laboratory at Cardiff University, as described in section 3.4.2. The insulator profiles adopted are the same insulators as those used for RWDT in addition to the textured trunk and shed (TTS) design. The insulator dimensions were also detailed in section 3.4.1.

3.7.2. The preparation of pollution suspension

The pollution suspension of polymeric insulators was prepared according to a modified version of IEC 60507 solid layer methods [3-9]. The contaminating suspension consisted of kaolin (40g), tap water (1l), wetting agent (1g), and a suitable amount of sodium chloride (NaCl) to achieve a volume conductivity range from 2.9 to 20.0 S/m. The pollution slurry with volume conductivities of 4 S/m, 11.2 S/m, and 20 S/m were prepared, and the performance of the different pollution levels for the insulators was evaluated.

3.7.3. The fog chamber

The insulators were tested in the clean fog chamber of Cardiff University high voltage laboratory (Figure 3-14). The chamber wall is made of polypropylene, and its dimensions are 2 m x 2 m x 3 m. An earthed aluminium mesh is present on the chamber floor. Visual inspection of the test sample inside the fog chamber is possible through a transparent door, which has a rectangular opening at approximately the height of the tested insulator to allow recording during the test using visual and infrared cameras.

Three pairs of water spray nozzles supply the chamber with a uniform fog: two pairs of nozzles are placed in opposite corners of the chamber, and a third pair is located on the chamber floor. The fog supply is provided by a control panel located outside the chamber's high voltage cage. This panel can be used to adjust the water flow rate and air pressure, which allows the wetting rate of the polluted insulator to be controlled. The high voltage is supplied to the chamber through a vertical aluminium tube with grading rings at both ends to limit corona discharges. Using a suitable mounting extension, different types of insulators can be mounted in the chamber. The test insulator is grounded by connecting the lower electrode to the earthed floor.



Figure 3-14: Test set-up of fog chamber tester (Cardiff University High Voltage Laboratory).

3.7.4. The test circuit diagram

The test circuit diagram of the fog chamber is presented in Figure 3-15. A Hipotronics AC Dielectrics test set provides the test voltage through a 150 kVA, 50 Hz transformer that can supply a 2 A load at a maximum output voltage of 75 kV. A control panel can be used to adjust the voltage supply by changing the (0-960 V) primary voltage via a Peschel Variable Transformer. The voltage can be controlled manually or by using a program to follow a predetermined voltage pattern. The circuit breaker will interrupt the supply in the case of a flashover event. The RMS voltage is viewed on a digital display control panel, and the voltage waveform is recorded through an RC divider with a voltage ratio of 10000:1.

The current measurement and protection consists of a leakage current measurement resistor (selected from values of 4700 Ω , 1140 Ω or 94 Ω) with shunt branches of back-to-back high power Zener, Schottky diodes and gas discharge tube, which together suppress any overvoltage that might occur and protect the data acquisition card (DAQ). The data acquisition system monitors and records the voltage and leakage current waveforms using a developed LabVIEW program on a personal computer.

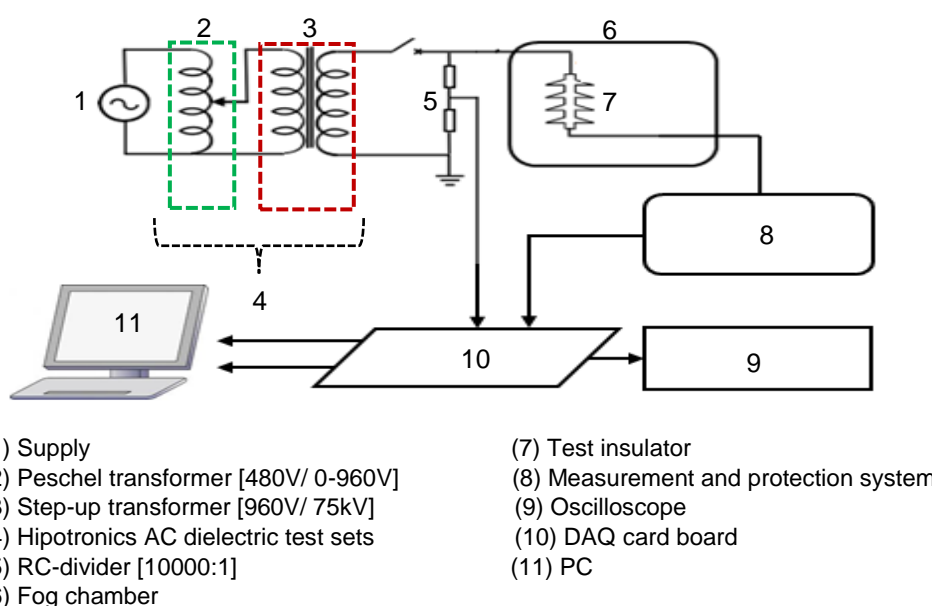


Figure 3-15: The test circuit diagram of fog chamber.

3.7.5. The data acquisition system

A data acquisition (DAQ) system program that acquires, monitors, and stores the waveforms of leakage current and voltage applied signals was built based on the NI-LabVIEW platform. The program received the digitised data by an NI-PCI-6251 data acquisition board with the assistance of an SCB-68 connector block, as illustrated in Figure 3-16. The DAQ board was fixed to a personal computer (PC). The connection between the SCB-68 connector and the DAQ board was achieved using an SHC-68-68-EPM shielded cable. The selected sampling rate was 10^4 for both DAQ card channels, which acquired leakage current and voltage signals. The signals were then saved in sets, as each cycle of 50 Hz consisted of 200 samples. The acquisition of samples was repeated until all 6×10^4 samples had been stored; then, the next file was opened. As these stored samples were segments of leakage current and voltage waveforms, an appropriate post-processing software program was used to analyse and assess the data recorded during the test. The program features and the electrical parameters calculated were clearly described in section 3.4.5c.

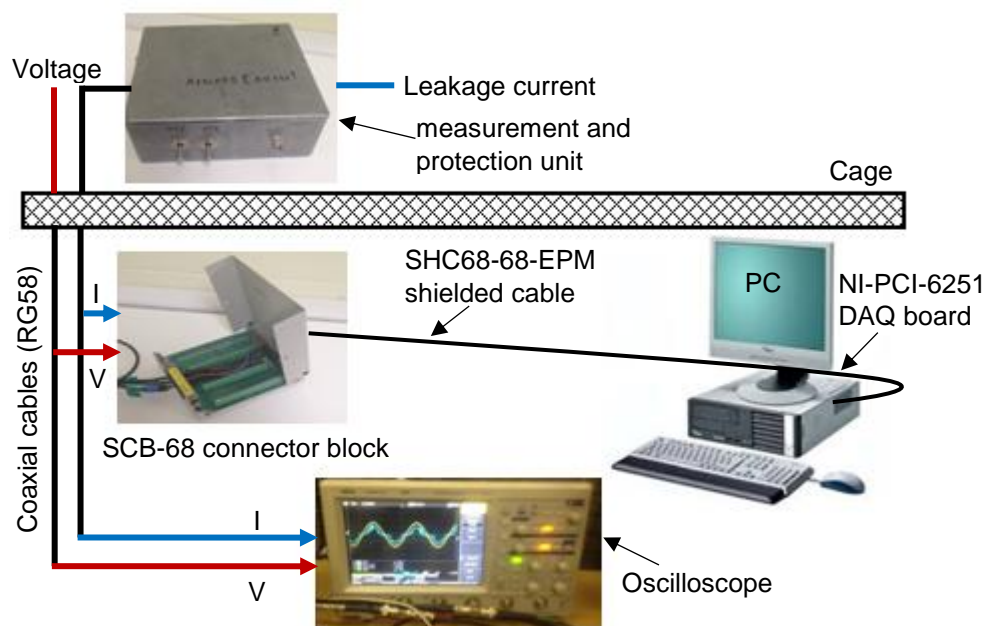


Figure 3-16: Arrangement of data acquisition system.

3.7.6. Thermal and visual cameras records

The observing and recording of discharge activities and dry band formation on the surface of tested insulators during the fog chamber and wheel tests were performed using FLIR A325 infrared (IR) thermal camera and a high-resolution video camcorder. The FLIR A325 was used to check the surface heating and thermal stress along the insulator profile and to reveal any dry band formation and/or discharge activity that may occur during the test, while the video camera was used to capture any discharge activity.

The FLIR ThermaCAM Researcher software controlled all the operations of the camera, and it saved the infrared records files into a personal computer. The IR camera has a spectrum range from 7.5 to 13 μm with an IR resolution of 320x240 pixels and an image frequency of 60 Hz.

Both the IR thermal and video cameras were fixed on a tripod and placed outside the fog chamber and/or tracking wheel tester. During a fog test, unclear recordings may be observed due to the condensation process. For this reason, a suitable fan was directed at both IR and video cameras.

3.8. Summary

Several test methods were conducted to study the performance of outdoor polluted insulators. There are currently no specific international standards for using an artificial pollution test on polymeric insulators. For this reason, significant effort has been dedicated to finding techniques for testing polymeric insulators to investigate their performance under different test conditions.

Different 4-shed silicone rubber insulator designs with the conventional smooth surface, based on a standard commercial insulator and with textured patterns, were fabricated in-house using an MCP 5/01 vacuum casting machine.

The RWDT based on the standard IEC 62730 was used to detect the material and/or the design of SiR insulators inappropriate for use on overhead transmission lines under AC and positive DC excitations. The designs used for this test evaluation were conventional (CONV) and 6 mm textured trunk (TT6) SiR insulators.

The surface conductance evaluation tests were also performed on tested samples using a conductance meter built based on IEC 60507 standards. The tests were used to evaluate the variation trends of the local surface conductance on each insulator surface. The technique used for assessing the ESDD and NSDD pollution levels according to IEC 60815 was also achieved.

In this chapter, an artificial pollution test method has been presented. The test procedure was based on the IEC-60507 solid layer method with modification of the pollution suspension by the addition of a non-ionic wetting agent. The insulator was then contaminated with a pollution layer and was tested in the chamber.

During the RWDTs and clean fog tests, the waveforms of leakage current and voltage applied signals were acquired and saved using a data acquisition system program built based on the NI LabVIEW software. The stored data were then analysed using another post-processing program to calculate the essential electrical parameters used for performance evaluation.

Thermal and visual observations were obtained by using an FLIR A325 infrared camera and a high-resolution video camcorder to investigate any indications of aging on the surface of the tested insulators.

CHAPTER 4: COMPARATIVE PERFORMANCE OF SILICONE RUBBER POLYMERIC INSULATORS UNDER HVAC AND HVDC ENERGISATIONS USING THE ROTATING WHEEL DIP TEST

4.1. Introduction

The increased use of polymeric insulators on the overhead power transmission and distribution systems has led to the development of various designs of insulators with different profiles and materials. In addition, recent growth in renewable energy systems has seen a parallel increase in HVDC systems. Insulator performance has not always been excellent, especially in polluted and wet environments, where degradation has been the main reason [4-1]. Outdoor insulation is continuously exposed to environmental factors such as salt fog, high humidity, acids and, consequently, performance is severely affected [4-2]. Discharge activities and dry band arcing due to surface contamination cause tracking, loss of hydrophobicity and erosion of the silicone rubber insulator surface [4-3]. Therefore, new anti-dry band designs using textured surfaces have been proposed to achieve better performance under polluted conditions [3-11]. In the recent IEC 62730:2012 standard [3-1], the RWDT has been used as a screening test in order to reject materials or designs unsuitable for use on overhead transmission lines. This chapter presents experimental studies carried out using a RWDT on two 11kV silicone rubber polymeric insulators with different profiles. The main purpose of this study is to compare the aging performance of polymeric insulators under AC and positive DC excitations. The procedures of the Standards were adopted to perform AC and positive DC tests on different insulator designs. A conventional polymeric insulator design was selected and compared with insulators with textured surfaces. The textured surfaces were developed by Cardiff University to increase the creepage distance and to enhance tracking/erosion performance. The results of long-term testing are reported; both voltage and leakage current signals were measured and digitized through a computerised data acquisition system. The signals were then

processed to calculate other significant parameters of the test results, as described in section 3.4.5c. In particular, the magnitude and shape of the leakage current waveform, the RMS leakage current, power dissipation, the power factor angle, and the cumulative dissipated energy on the insulator surface were observed to characterize each test. Use of these parameters makes possible a direct comparison between different insulator designs under alternating and positive direct voltage applications. Continuous monitoring of the shed surface and insulator trunk using an infrared camera were undertaken to assess the temperature distribution along the insulator profile. Hydrophobicity tests were performed before and after termination of the test to evaluate the degradation level of the insulator surface and its material. In addition, localized surface conductance measurements were evaluated using a conductance meter with probes fabricated as detailed in section 3.5.1. This evaluation helps to identify and explain the variation in conductance and its distribution across the surface of each insulator.

Computer simulation based on Finite Element Method (FEM) was used to calculate the potential and the electric field distributions along the leakage distance of the insulator. The insulator model was developed and simulated using COMSOL Multiphysics software under dry clean and wet polluted conditions with the assumption of the uniform pollution layer on the entire surface. These simulation results help to identify the intensive regions of the high electric field that is susceptible to the formation of the dry bands.

4.2. Experimental conditions

Based on the IEC 62730:2012 standard, the total applied voltage during the test under alternating and positive direct excitations was 35 V/mm multiplied by the leakage distance. The leakage distance of the tested insulator was calculated as 375 mm. Therefore, a voltage of 13kV was selected. The salinity of the solution in the test tank, consisting of salt (NaCl) and deionized water,

was 1.4 g/l. The requirements, measurements and acceptance criteria for RWDT are summarized as follows:

a. The content of salt (NaCl) dissolved in 300 litres of deionized water is:

$$1.4 \text{ grams/litre} \times 300 \text{ litres} = 420 \text{ grams}$$

b. The salt solution in the tank shall be replaced weekly.

c. Each revolution of rotation should have four test positions consisting of energisation, de-energisation, dipping, and dripping positions.

d. Test samples of the same design shall be evaluated together. Pairs of test samples of a different design shall be assessed separately.

e. The tracking wheel test is considered to have been passed if on both test insulators:

- erosion does not reach the glass fibre core, and in any case, the erosion depth is less than 3 mm
- no tracking occurs on the tested samples
- no shed or housing is punctured

4.3. Experimental procedure

Two different silicone rubber insulators were used in this study, which were manufactured as described in section 3.4.2. Before starting the test, the insulators were cleaned with deionized water and then mounted on the wheel test ring, as shown in Figure 4-1. The silicone rubber insulators were tested continuously under AC and positive DC energisations for 190 wheel revolutions, for a total test time of 10 hours. In this test, each revolution takes 192 s with 4 test positions consisting of energisation, cooling, dipping, and dripping. For each position, the test sample remains stationary for about 40 s, and it takes 8 s to rotate through 90° from one position to the next. In the first period of the test cycle, the insulator is dipped into the salt water. The second period of the cycle allows the excess saline solution to drip off from the sample, ensuring the

formation of a thin wet layer on the surface. In the third period, the sample is exposed to the high voltage stress. In the last period of the test revolution, the surface of the tested insulator, which had been heated by discharges activities and dry band arcing in the previous period, is allowed to cool [3-1].

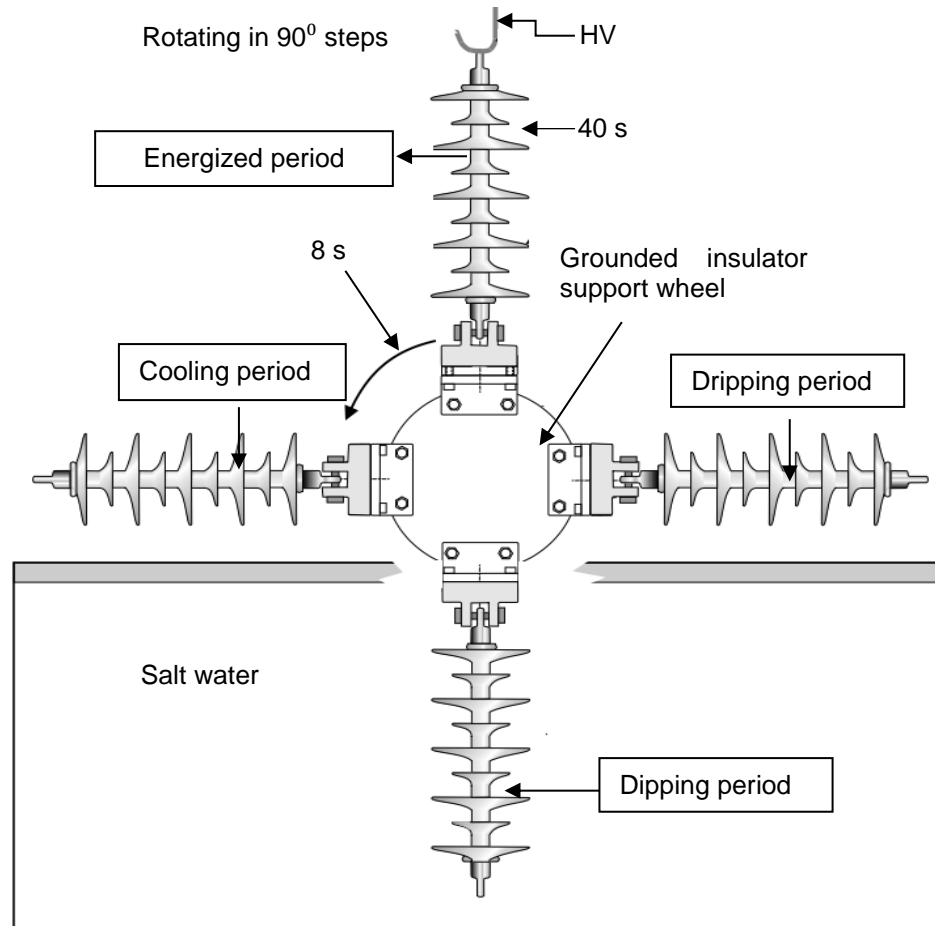


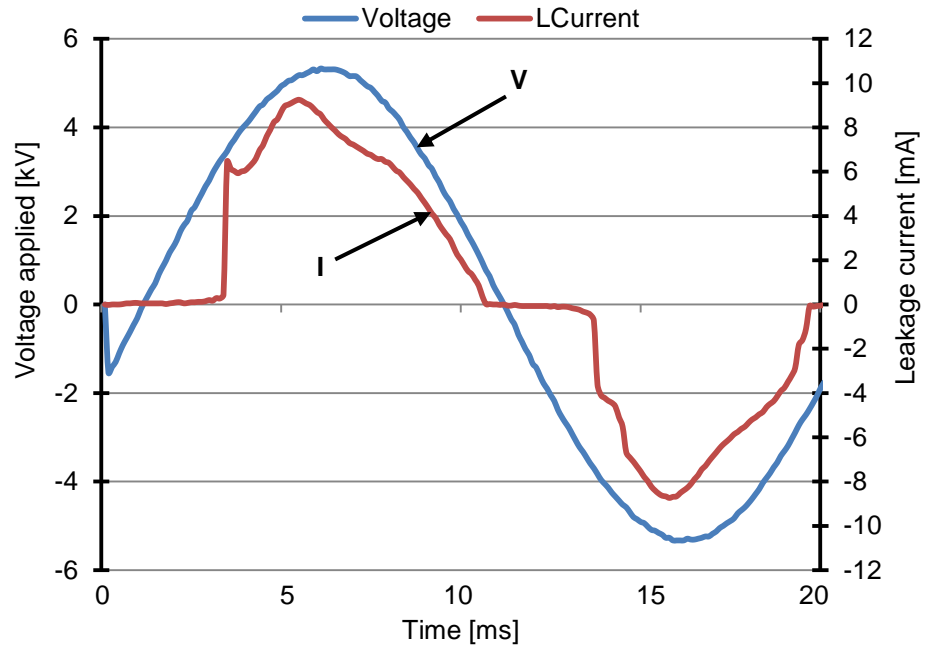
Figure 4-1: Schematic diagram of rotating wheel dip test [3-1].

4.4. Rotating wheel dip tests under AC excitation

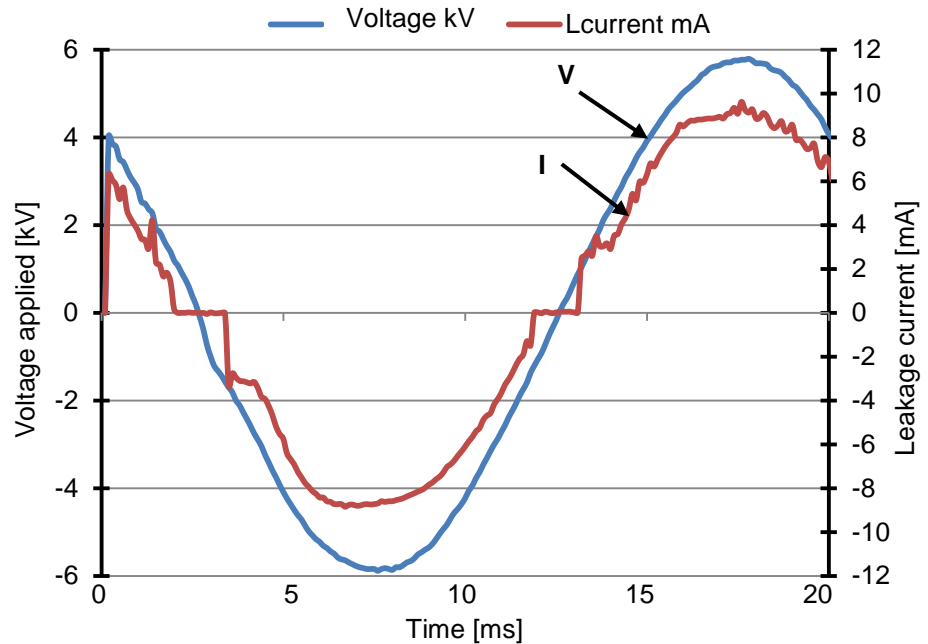
4.4.1. Leakage current

Figure 4-2 shows typical waveforms of applied voltage and leakage current for the conventional and textured insulators, measured during the 15th test cycle, 24 s after the start of the third period. It is clear from the two plots that discharge activity occurred on both surfaces. However, it was more severe on the conventional surface. The high resistive leakage current behaviour observed at initial energization leads to drying of the surface and the formation of dry bands.

When the formation of dry band arcing occurs, this can be seen in the current waveform of the conventional insulator by the steps at 3.5 ms. This waveform is similar to that observed in [3-11, 4-4]. In the case of a textured surface, the discharge activity is much lower, and a mostly conductive behaviour is observed.



(a) Conventional insulator

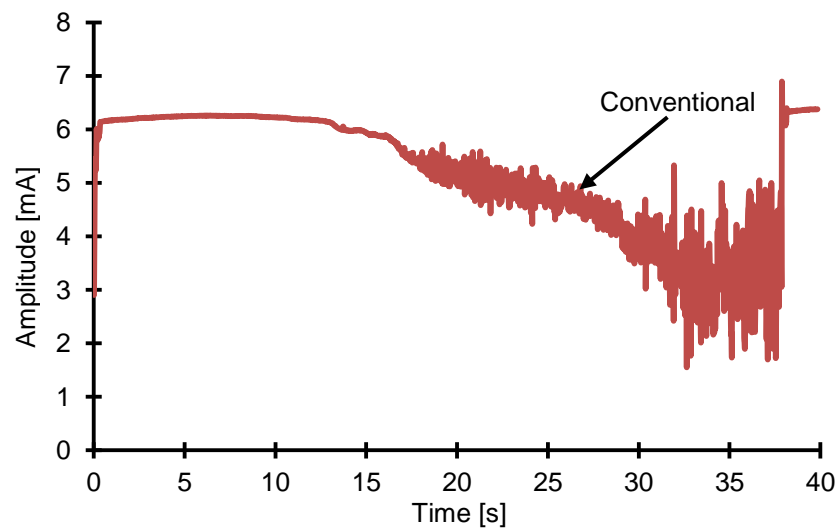


(b) Textured insulator

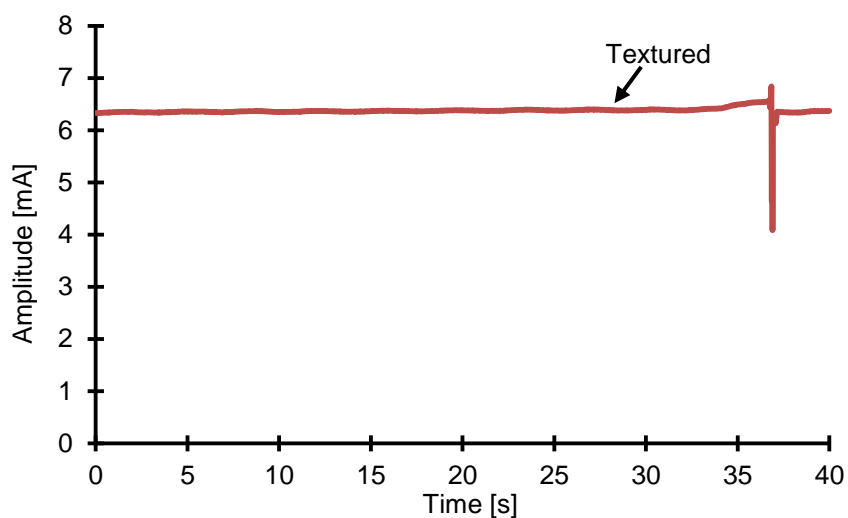
Figure 4-2: Leakage current and voltage applied waveforms during the 15th wheel revolution.

4.4.2. RMS leakage current

Figure 4-3 shows the typical shapes of RMS leakage current measured for the tested insulators. As described earlier, each insulator was energised for a period of 40 s. For the conventional insulator, the wet surface dried over time due to the dripping of water and Joule heating. Non-uniform discharge activity caused heavy arcing and further drying. This drying progression was accompanied by a fall in the leakage current magnitude reaching to 3 mA at the end of the energisation period. For the textured insulator, a continuous thin conducting layer was maintained. Discharge activity was limited on the surface, and the magnitude of leakage current was slightly reduced.



(a) Conventional insulator

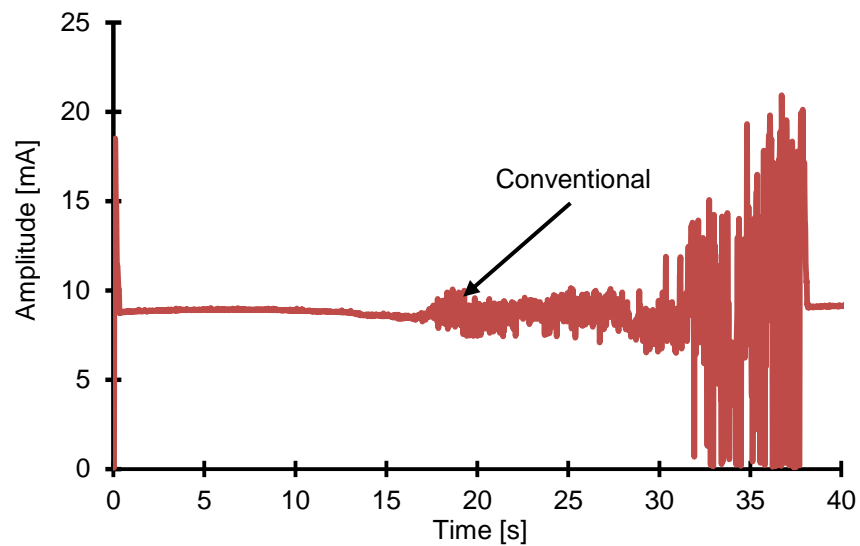


(b) Textured insulator

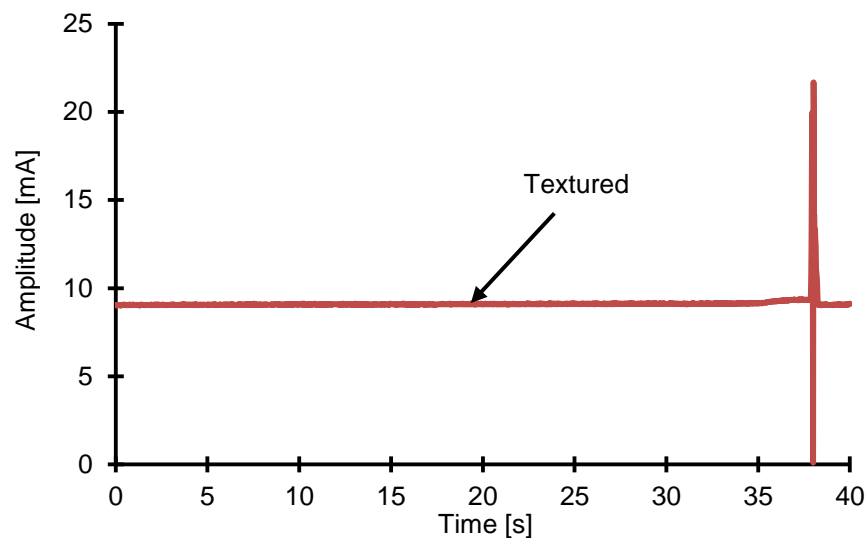
Figure 4-3: Typical RMS leakage current for conventional and textured insulators.

4.4.3. Peak current magnitude

As can be seen in Figure 4-4, the typical variation of the absolute peak magnitude of leakage current was measured for the two insulators. The average peak current magnitude for both insulators was approximately 8 mA. It is obvious that on a conventional insulator, there are significant variations in current magnitude due to intermittent discharge activity reaches up to 18 mA at the termination of a 40 s period. In contrast, the textured insulator exhibits very little evidence of discharge activity.



(a) Conventional insulator



(b) Textured insulator

Figure 4-4: Typical variation of the absolute peak magnitude of leakage current.

4.4.4. Power dissipation

Figure 4-5 illustrates the average power dissipated on the surface of the test insulators during the 15th wheel revolution. It can be seen that the power dissipation for the conventional profile increases significantly until it reaches the initial peak value of 40 W after 20 s. However, with a textured profile, the trend of the shape is mostly constant with a lower value of power dissipation about 20 W. After the initial peak of the conventional surface, the dissipated power decreases gradually and significant distortion is observed during this period. This distortion is caused by the increasing discharge activity occurring on the insulator surface.

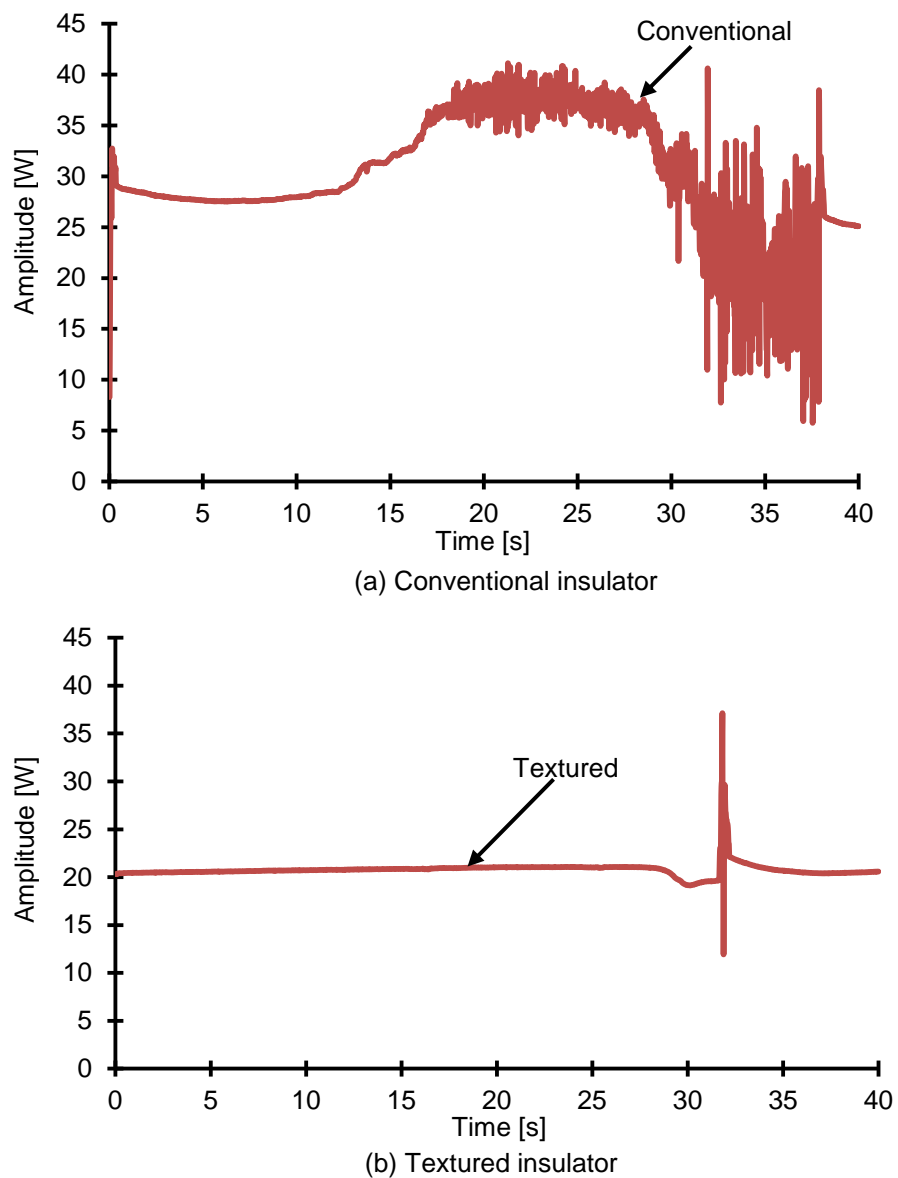
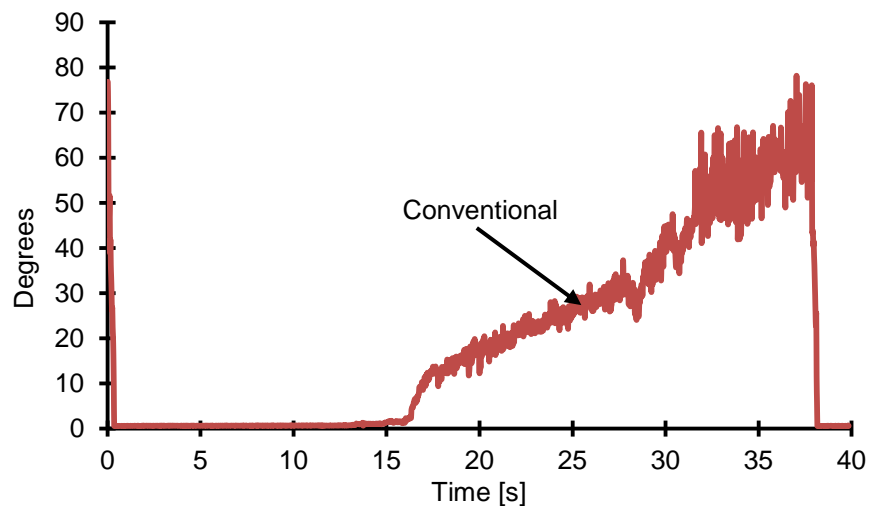


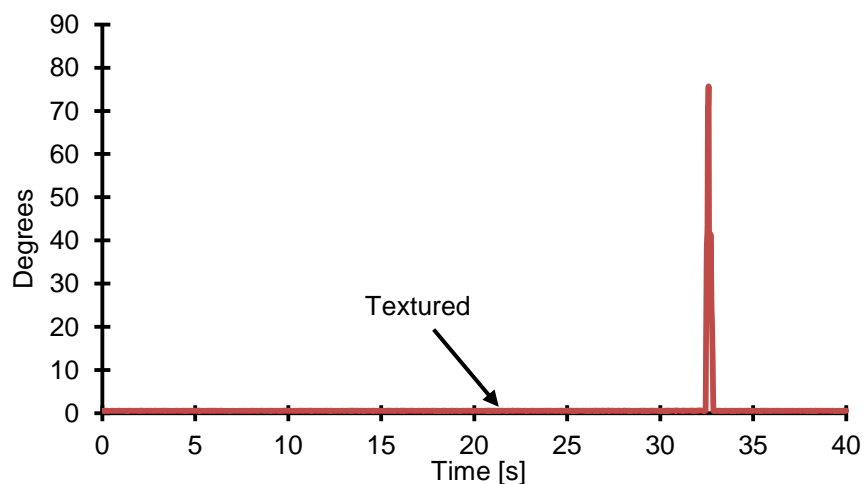
Figure 4-5: Average power dissipated by conventional and textured insulators.

4.4.5. Power factor angle

The distinguishing features of resistive surface conduction and discharge surface activities during one energisation period of 40 s can be observed in Figure 4-6 showing the calculated power factor angle for conventional and textured insulators respectively. It is clear from the graph that the conventional surface begins to exhibit localised drying from 17 s into the energised period. The power factor angle deviates from zero, reaching a measurement of 75° after 38 s. For the textured profile, resistive surface conduction dominates during the energization cycle (the power factor angle remains close to zero). This behaviour is observed for all cycles during the 10-hour test period.



(a) Conventional insulator



(b) Textured insulator

Figure 4-6: Power factor angle for conventional (a) and textured (b) insulators.

4.4.6. Cumulative dissipated energy

Figure 4-7 shows the total cumulative dissipated energy for both insulators under AC excitation within a 10-hour test. The trends for both insulators are similar, reaching 160 kJ at the termination of the test. However, the discharge by partial arcing is likely to be more damaging than the ohmic power for the textured insulator.

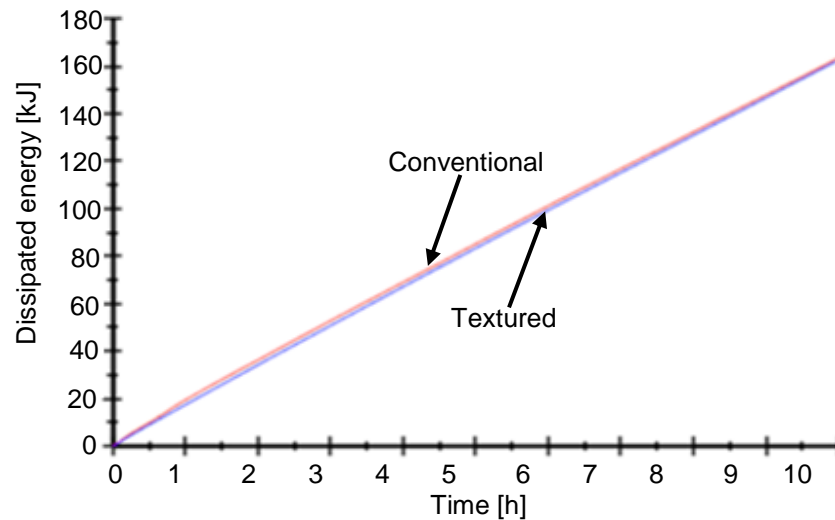
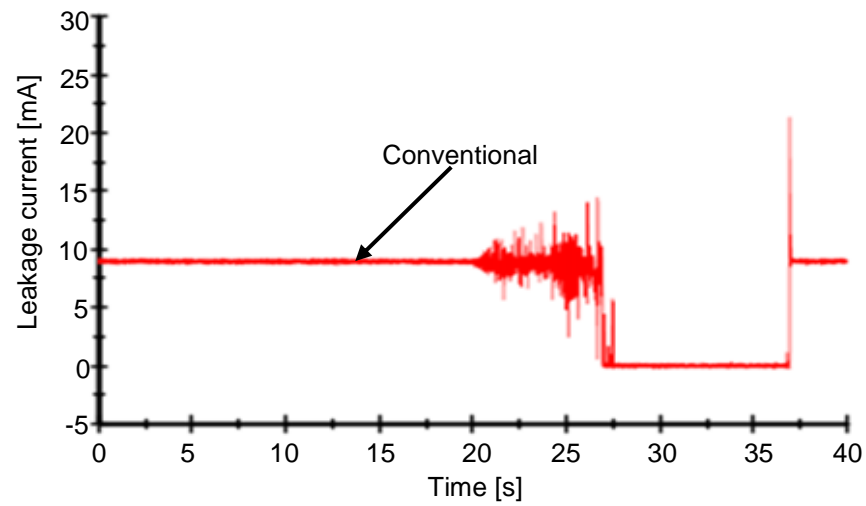


Figure 4-7: Total cumulative dissipated energy during 190 wheel revolutions under AC excitation (10 hours).

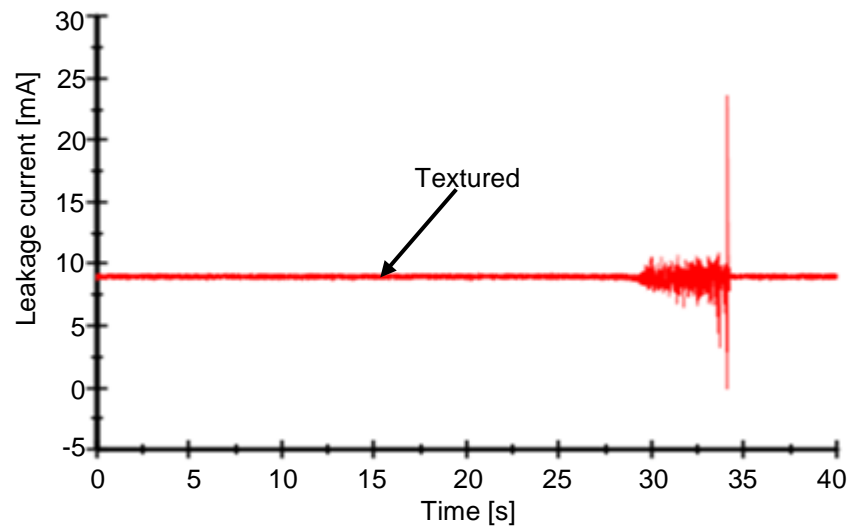
4.5. Rotating wheel dip tests under positive polarity DC excitation

4.5.1. Leakage current

Typical leakage current traces measured for the two insulator designs are shown in Figure 4-8. Both insulators exhibit a significant current at the beginning of the period reaches to about 9 mA. For the conventional insulator, the leakage current is frequently observed to be interrupted. The interruption period was observed between 27 s and 34 s. This is thought to be caused by a significant partial arcing, not observed in AC testing. In contrast, the textured insulator shows limited discharge activity and no current interruption periods. This behaviour is attributed to the lack of significant dry band formation.



(a) Conventional insulator



(b) Textured insulator

Figure 4-8: Typical variation of leakage current for both insulators under DC excitation.

4.5.2. Cumulative dissipated energy

Figure 4-9 illustrates the total cumulative dissipated energy for tested insulators under DC excitation for a 10-hour test. The trends for both designs are similar, reaching 650 kJ at the end of the complete 190-revolution test. This result confirms the severity of the DC excitation on both insulator surfaces compared with the AC excitation.

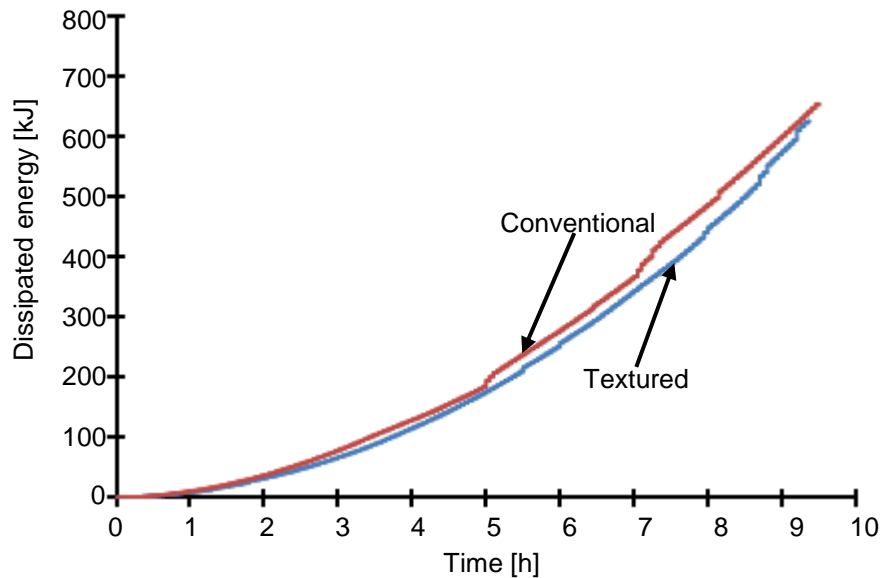


Figure 4-9: Total cumulative dissipated energy during 190 cycles test under DC excitation (10 hours).

4.6. Visual and infrared (IR) observations of aging

4.6.1. Visual and infrared (IR) observations

During the tracking wheel tests, thermal and visual video records were obtained in order to investigate indications of aging on the insulator surfaces. The purpose of the IR imaging is to reveal any surface heating due to discharge activity and to detect dry band formation when a 13.12 kV voltage is applied to the insulator. The calibration of IR camera was performed using an insulator with known temperature. The calibration performance by the manufacturer in recent service also confirms the precision of the device within ± 0.2 °C from the target temperature. Using the FLIR ThermaCAM Research software allowed the camera saved the infrared records as .SEQ files. This file format can be dynamically post processed restoring the real-time data. Figure 4-10 shows infrared records and temperature distributions along the axis LI1 on the surface profile of conventional and textured insulators. The temperature distributions caused by discharge activity at the 20th, 90th and 150th cycles are shown in Figure 4-10 (a), (b), (c) respectively.

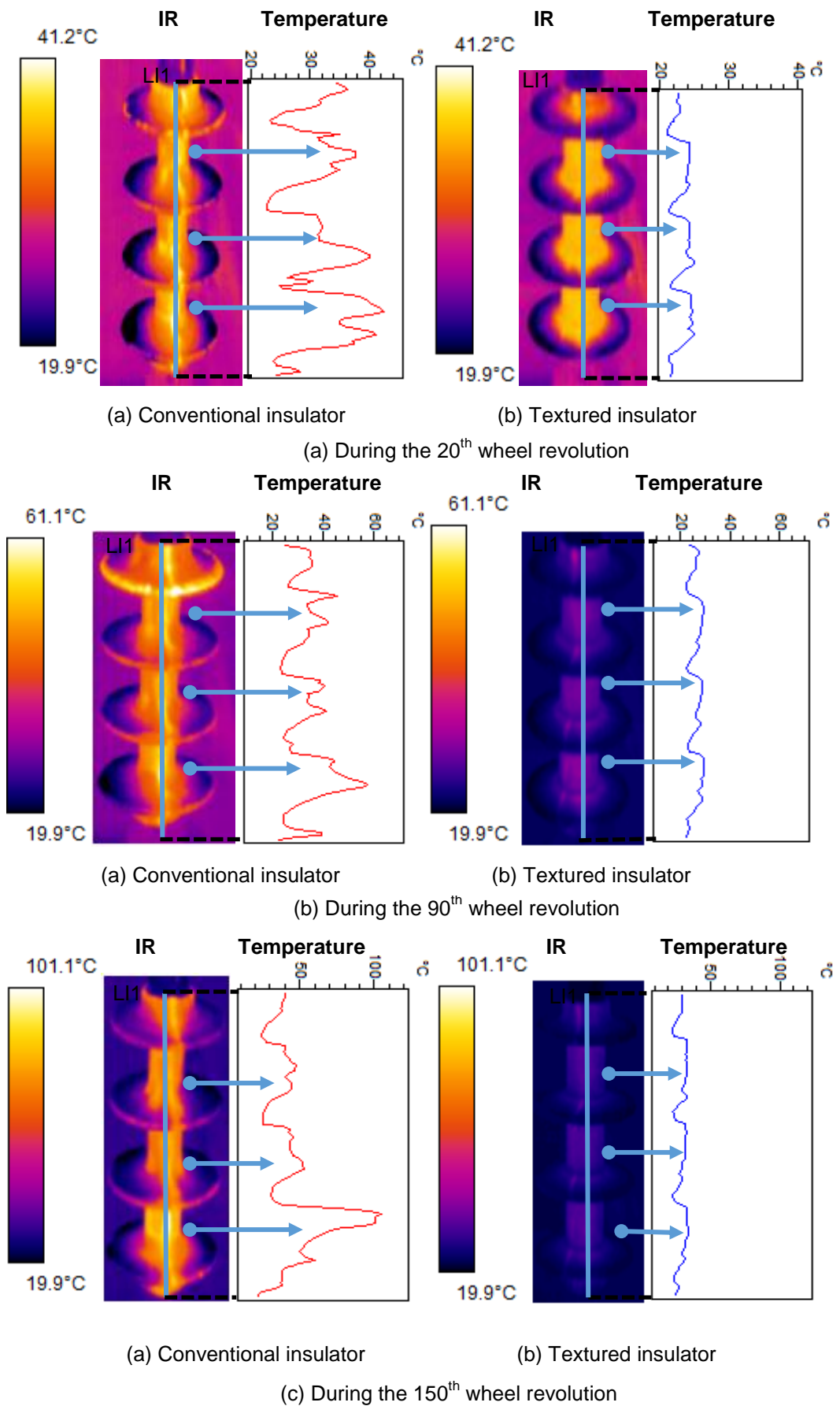


Figure 4-10: Infrared record and temperature distribution along the surface profile of tested insulators during rotating wheel dip tests, of different instants.

It is clear from the IR captures that the higher temperature value was recorded on the conventional non-textured insulator. This correlates to the higher discharge activity and dry band arcing occurring on this surface, which was not observed in the textured insulator.

During the test, dry band arcing occurred and it was clearly observable on the trunk surface of the conventional insulator during energization periods. The visual captures recorded by the HD digital camera reveal visible discharge activity and dry band arcing on the trunk surface of the conventional insulator. As shown in Figure 4-11, the yellow light of dry band arcing was observed. Such arcing leads to tracking on the polymeric surface [4-4, 4-5, 4-6].

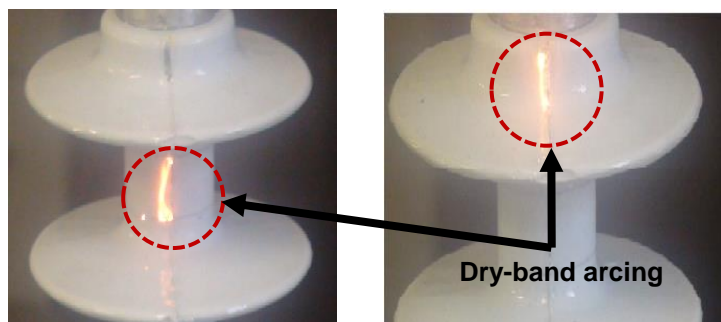


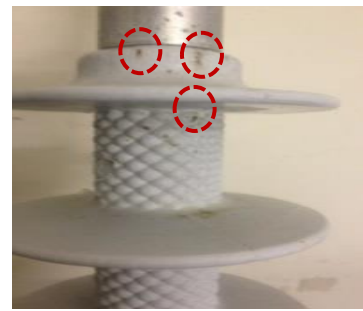
Figure 4-11: Visible discharges activities during rotating wheel dip test.

After each 10-hour test, visible changes to the tested sample surfaces were observed. Surface degradation by tracking and erosion was detected. As shown in Figure 4-12, a black mark was observed on both shed and trunk surfaces of the tested insulators, principally on the trunk surface near both the energized and the ground ends.

The occurrence of such tracking may have been caused by high electric field stress. In addition, surface tracking on the moulding seam of the insulator trunk was seen for both samples. The tracking on the moulding line can cause significant damage to polymeric insulators under severe conditions. The result shows both insulator designs were affected by AC and positive DC excitations, the latter being more severe [4-7].



(i) Tracking and erosion

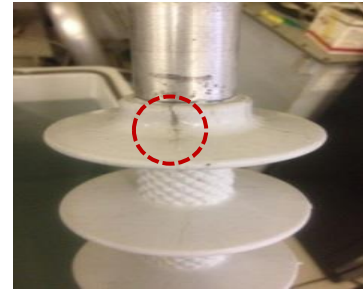


(ii) Black dirt mark

(a) AC test



(i) Severe erosion



(ii) Tracking on moulding seam

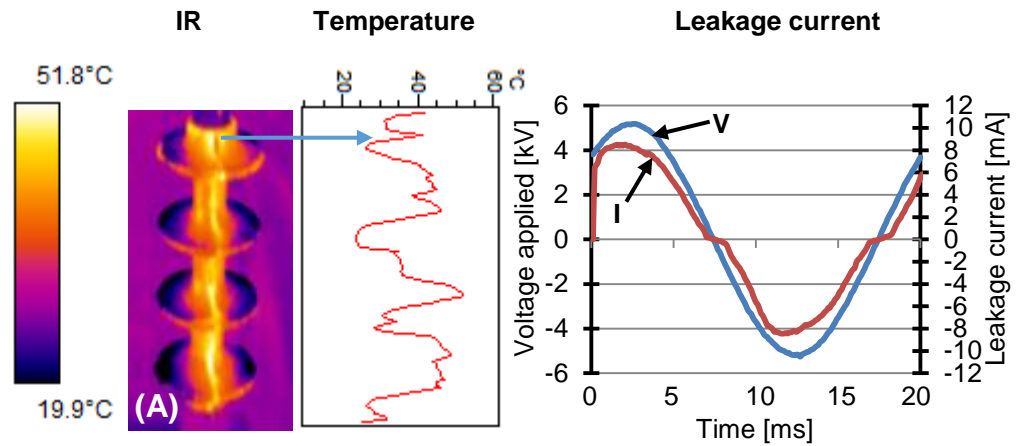
(b) DC test

Figure 4-12: The visual appearance of tested samples at the end of the test.

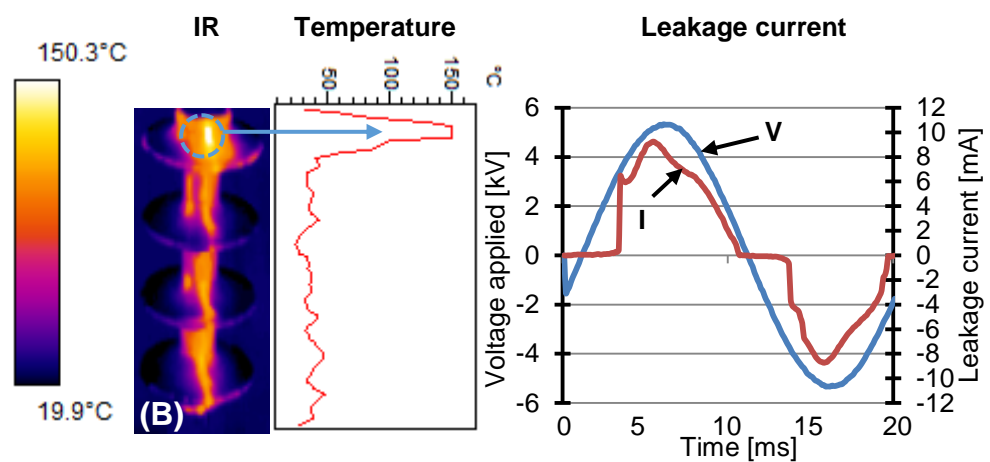
4.6.2. Electrical discharge activities and temperature distribution

Using the IR camera, images of the temperature distribution along the surface profile were taken each second during the tracking wheel test. Figure 4-13 shows two instant thermal images, A and B, which were captured at 16 s and 23 s during the 15th cycle test.

It is clear from the instant thermal image A that the partial arcing started to form after 16 s of the energization period. This can be also identified from the leakage current waveform that corresponded to thermal image A. In the subsequent thermal image B, when a hot spot developed due to partial arcing, the surface temperature was increased significantly. Partial arcing increased the local temperature along the surface profile, with the material near the top electrode reaching 150°C. With this increasing of the temperature, the non-linear relationship between leakage current and applied voltage were illustrated in Figure 4-13 b. The thermal images and the leakage current waveform obtained are similar to those observed in [4-8].



(a) Thermal image A recorded after 16 s of energisation period.



(b) Thermal image B recorded after 23 s of energisation period.

Figure 4-13: Temperature distribution and leakage current waveforms of the conventional insulator when (1) partial arcing was formed and (2) a hot spot due to partial arcing developed.

4.7. Hydrophobicity tests

Surface hydrophobicity is one of the most used criteria to evaluate the performance of composite insulators. The hydrophobicity of a silicone rubber surface changes with time due to the effects of discharge activities and outdoor environmental conditions. In this study, the hydrophobicity evaluation of tested samples was carried out using the water spray method, as described in the Swedish Transmission Research Institute (STRI) guide [2-92]. A suitable spray bottle was used to provide a fine mist from a distance of 25 cm. The wetting process was continued for 20-30 seconds until the whole surface was completely wetted. The hydrophobicity classification (HC) was evaluated within 10 seconds

after the completion of the test. Hydrophobicity tests were performed before and after the test to check the degradation level of the insulator material, as shown in Figure 4-14.

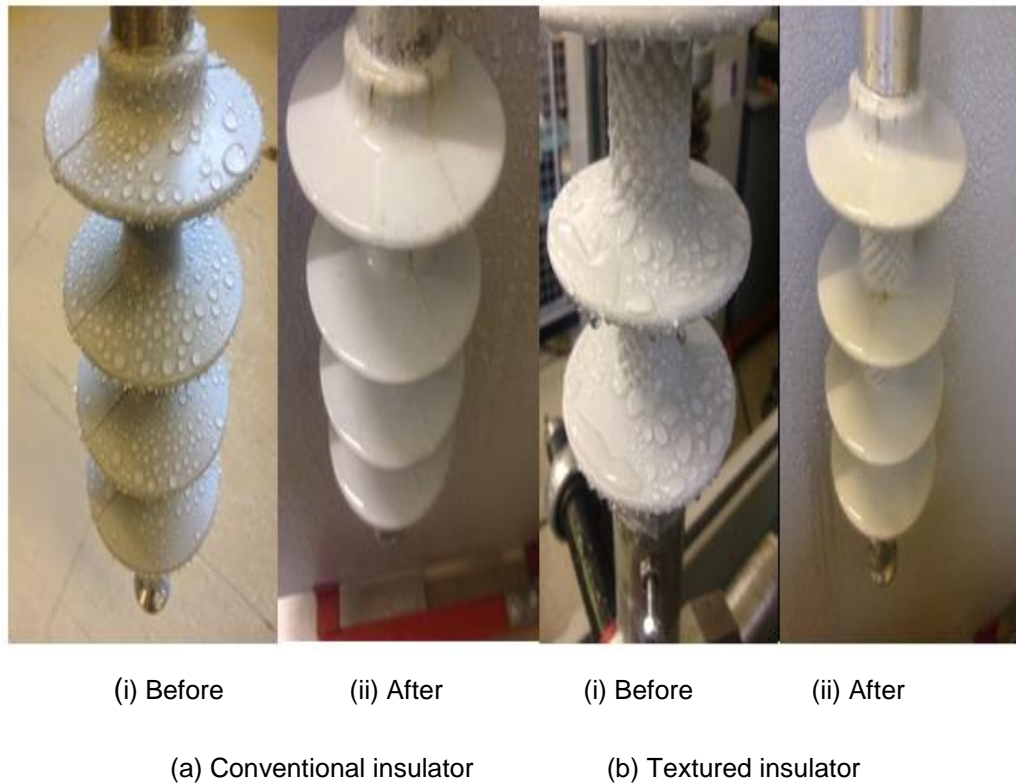
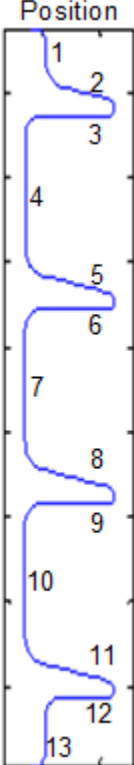


Figure 4-14: Hydrophobicity comparisons between tested insulators.

After the 10-hour test, a reduction in hydrophobicity for the tested samples was observed under AC and positive DC excitations. The HC levels were defined for each insulator, and the obtained results are shown in Table 4-1. The loss of hydrophobicity on the tested insulators may have been caused by the higher electric stress and discharge activities on the surface during the test. The higher temperature value recorded along the conventional profile attributed to the higher discharge activity occurs on this surface. This might be also correlated with the HC level results obtained at different positions along its surface where in the case of textured design may be better performed. The silicone rubber insulator material was found to recover its surface hydrophobicity after a recovery period of 24 hours.

Table 4-1: Evaluated hydrophobicity level of samples after 10-hour test.



Position	Insulator profile			
	Before		After	
	Conventional	Textured	Conventional	Textured
1	HC 1	HC 1	HC 6	HC 6
2	HC 2	HC 2	HC 5	HC 5
3	HC 2	HC 2	HC 6	HC 5
4	HC 1	HC 1	HC 6	HC 5
5	HC 2	HC 1	HC 5	HC 5
6	HC 2	HC 2	HC 5	HC 6
7	HC 1	HC 2	HC 6	HC 5
8	HC 1	HC 2	HC 6	HC 6
9	HC 2	HC 2	HC 5	HC 6
10	HC 1	HC 1	HC 5	HC 5
11	HC 1	HC 2	HC 6	HC 6
12	HC 2	HC 1	HC 5	HC 5
13	HC 1	HC 1	HC 6	HC 5

4.8. Localised surface conductance evaluation tests

During a test using the RWDT, local surface conductance measurements were evaluated using a conductance meter with two spherical probes built as described in section 3.5.1. The probe was used to measure the conductance values on the insulator trunk, and top and bottom shed surfaces. The measurement was carried out for both insulator designs. The localised measurements were evaluated at selected times after the start of the test. This evaluation helped to identify and explain the trends of the conductance and its distribution on each insulator surface. The average conductance measurements of the top and bottom sheds of the tested samples are reported in Figure 4-15 and Figure 4-16 respectively. It is clear from the graphs that the textured profile had a lower increase during the test. The average surface conductance values of the upper shed surfaces for textured insulator were significantly decreased by

22 % in comparison with the conventional. This can be clearly observed in the bottom shed curve (Figure 4-16) where the increase of surface conductance values was marginal for the textured design and 46 % decrease of surface conductance measurements attained compared with the conventional. A similar variation trend was also observed on the insulator trunk and 42 % reduction of surface conductance values was obtained, as can be clearly seen in Figure 4-17. This tendency suggests that the textured design reduces the hydrophobic characteristics, and therefore, it can promote an increase in the insulator's life expectancy and improve overall performance.

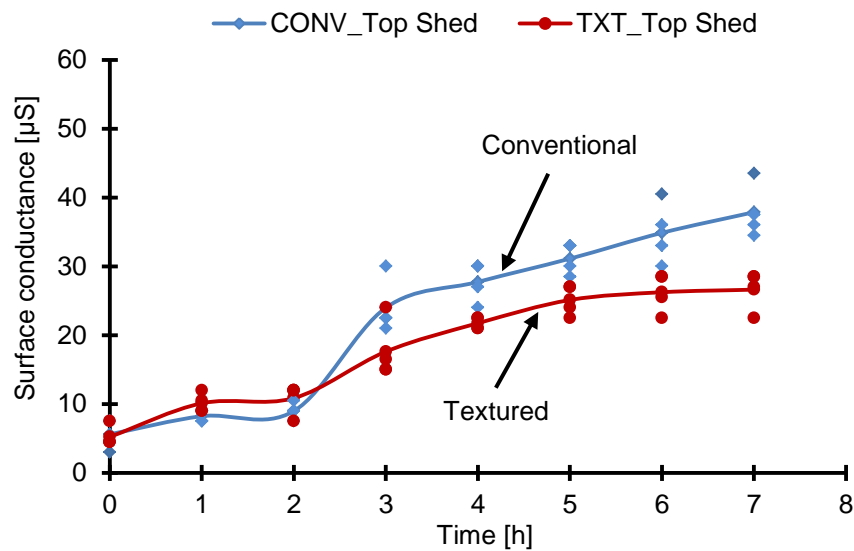


Figure 4-15: Average surface conductance measurements for the top sheds of tested insulators.

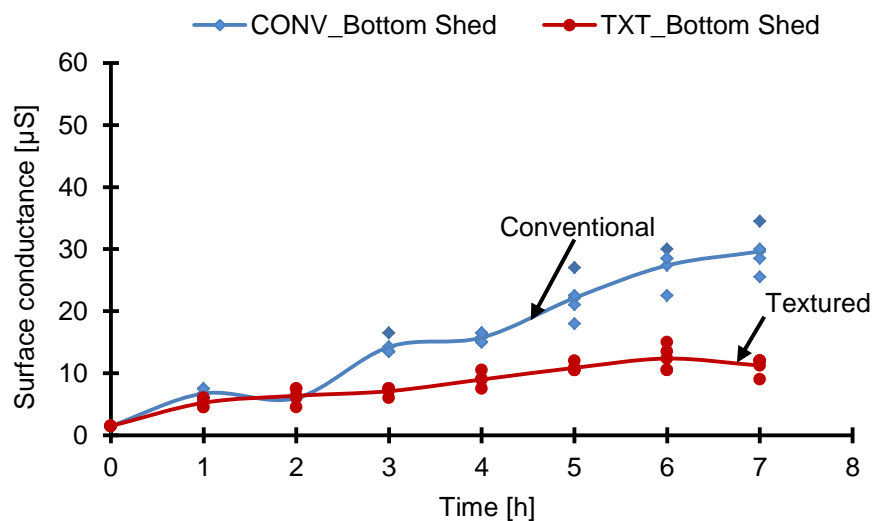


Figure 4-16: Average surface conductance measurements for the bottom sheds of tested insulators.

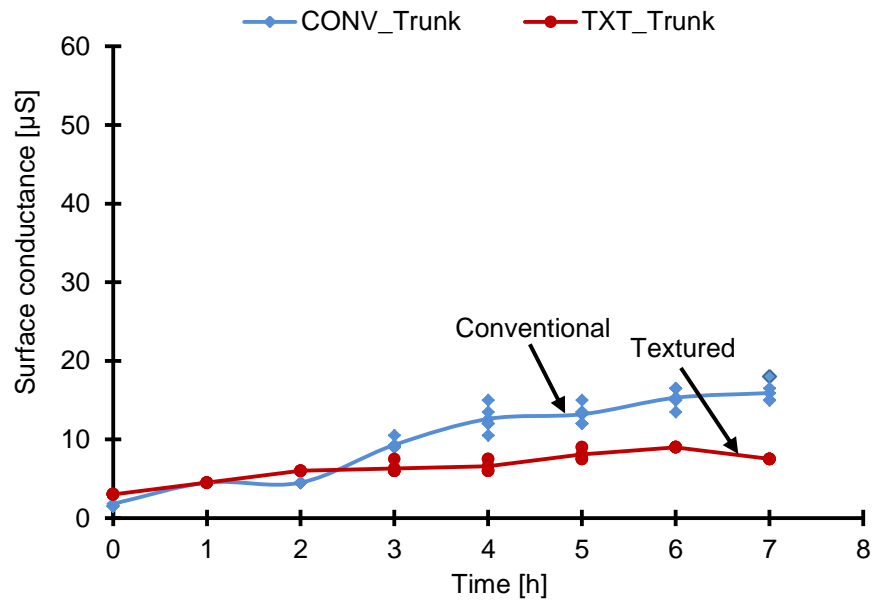


Figure 4-17: Average surface conductance measurements for the trunk of tested insulators.

4.9. Computation of electric field distribution over the polluted surface of silicone rubber insulator

A clear understanding of problems such as electric discharge and the dry band can only be attained through precise determination of electric field distribution along the insulator surface under various ranges of environmental conditions. Simulation of the electric field over the surface of the insulator is proposed to determine the high electric stress regions on the surface, thereby identifying the most vulnerable areas on the insulator. Commercial software based on the Finite Element Method [FEM] is used for insulator modelling to calculate the electric potential and electric field distribution along the leakage distance of the insulator.

The insulator model is developed for dry clean and wet polluted conditions with the assumption of uniform pollution layer for the entirely surface. It should be highlighted that, under normal conditions, silicone rubber insulators would not be often subjected to a uniformly wetted surface situation owing to their outstanding hydrophobic surface properties. In spite of that, the following simulation results help to recognize the high field region that could be vulnerable to the dry band formation.

4.9.1. Insulator geometry and material properties

The insulator investigated in this study is the same standard 11 kV SiR insulator used for the rotating wheel dip test. The dimensions and geometry of the insulator are shown in Figure 4-18.

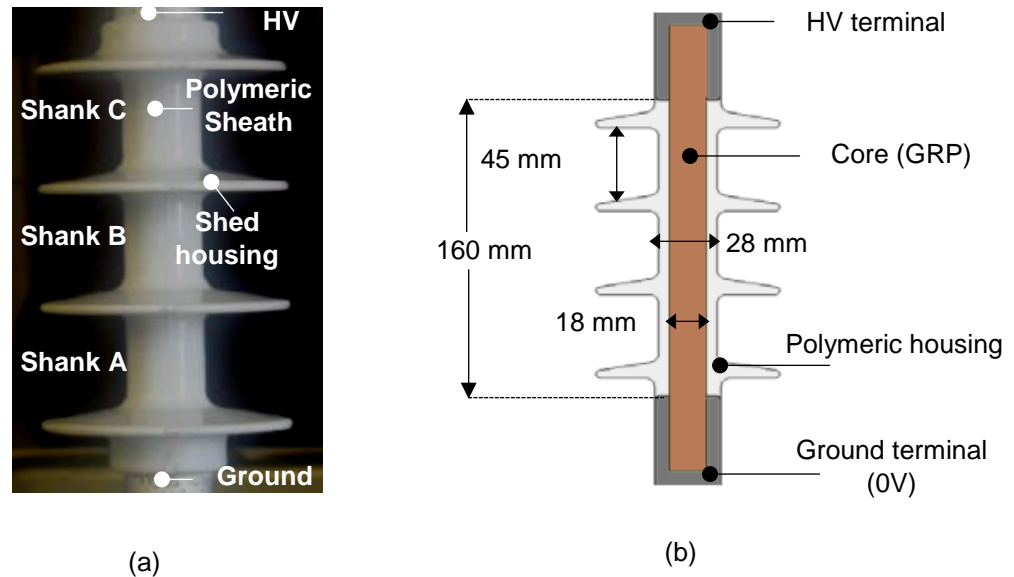


Figure 4-18: An 11 kV silicone rubber insulator: (a) insulator geometry (b) cross-sectional profile and dimensions

As it mentioned in section 3.4.1, SiR insulator comprises of three main parts; insulator housing, metal end fitting and the fibreglass core. The insulating housing is made of SiR material with a relative permittivity of $\epsilon_r = 2.9$. The metal fittings used for the high voltage energisation and ground terminals are made of the aluminium. These end fittings are attached to an 18 mm diameter fibre rod at a separation distance of 160 mm. The rod with a relative permittivity of $\epsilon_r = 7.1$ is crimped in the middle as a core to enhance the mechanical strength.

The insulator has 4-sheds with a diameter of 90 mm of each shed and spacing distance of 45 mm along the insulator unit. The measured creepage distance along the insulator surface is about 375 mm. Both SiR material and fibreglass core in this simulation were assumed to be perfect insulator with conductivity of 1.0×10^{-13} S/m. The pollution layer over the insulator surface is assumed to be uniform with 0.5 mm thickness [4-9]. The conductivity of the pollution layer was

adopted from the laboratory measurements with a value of 1.0×10^{-6} S/m. Detailed electrical properties used for insulator modelling are given in Table 4-2.

Table 4-2: Material properties for the used insulator

Materials	Relative Permittivity, ϵ_r	Conductivity, σ (S/m)
Aluminium end fittings	1.0	26.31×10^6
Silicone Rubber	2.9	1.0×10^{-13}
GRP core	7.1	1.0×10^{-13}
Pollution layer	81	1.0×10^{-6}
Air background	1.0	1.0×10^{-13}

4.9.2. Boundary conditions

An AC voltage of 18 kV at 50 Hz is energised to the top high voltage terminal while the bottom terminal is connected to the ground (0 V). The energisation voltage corresponds to the peak value of the potential that applied to the insulator during the rotating wheel dip test. The voltage was applied for 40 sec to simulate the energisation time subjected to the insulator during one wheel revolution. The air space surrounding the insulator is simulated adequately large to reduce its effect on the distribution of potential along the insulator profile and close to the electrodes. The outer edges of air region were assigned with a boundary of zero external current and electromagnetic sources, therefore representing a physical system that is an isolated open space. The axial symmetry line of the insulator as shown in Figure 4-19 was set as the symmetric axis on the r-z plane. The voltage profiles along the insulator surface for clean and wet polluted insulators were computed. The equipotential lines of the SiR insulator model under dry clean and polluted conditions were also calculated. For wet polluted insulator, the tangential electric field along the leakage path of the insulator was calculated. The surface power dissipation in the pollution layer along insulator surface was calculated.

4.9.3. Simulated model

The silicone rubber insulator described in section 4.9.1 was drawing using AutoCAD software tools and saved in an extension file of dxf format. The insulator was then imported to the COMSOL Multiphysics software, and the boundary conditions were applied. In this model, as the insulator structure is cylindrical in shape, therefore, the modelling can be simplified into a two dimension (2D) symmetric model in preference to a full three dimension (3D) model that uses much of computer memory. This simplification saves the considerable size of memory and processing time without affecting the accuracy of the simulation results. In addition, using symmetric model, only half of the insulator structure was created, as shown in Figure 4-19.

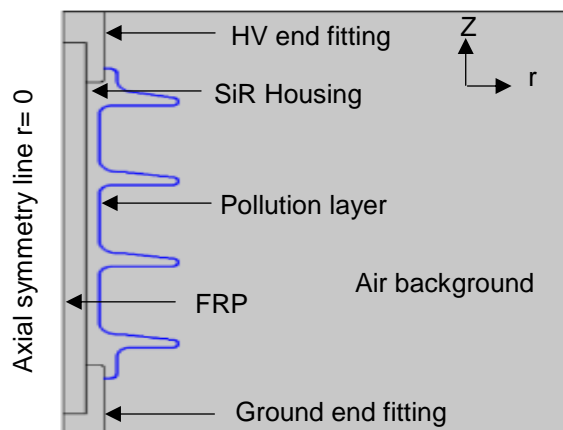


Figure 4-19: Two dimension (2D) axis symmetric model for a polluted insulator

After completing the stages of the model structure, specifying material properties and boundary conditions, the entire geometry regions except the end fitting parts were divided into small non-overlapping, non-separated triangular elements. This process is called meshing process. To improve and enhance the accuracy of the simulation results, the number of meshing element was increased in the region along the insulator surface where the electric field intensity is found to be higher. The insulator model was carried out in the FEM analysis using Static Electric mode, which assumes that electromagnetic fields and currents varying slowly [4-10].

4.9.4. Simulation results and discussion

(a) Equipotential and voltage distribution along the insulator surfaces

The equipotential lines of the SiR insulator model under clean and wet polluted conditions are illustrated in Figure 4-20 (a) and Figure 4-20 (b) respectively. The lines are simulated at 5% voltage interval, so a total of 20 equipotential line levels are plotted in the simulation results. As can be seen from both Figures, the contours are usually concentrated close to metal fitting electrodes. This indicating to the high electric field concentrated in these regions. Under wet polluted conditions, the equipotential lines are found to be more uniformly spread compared with those obtained from the dry clean surface. This behaviour occurs due to the presence of the resistive pollution layer which helps to redistribute the concentrated lines widespread along the surface profile.

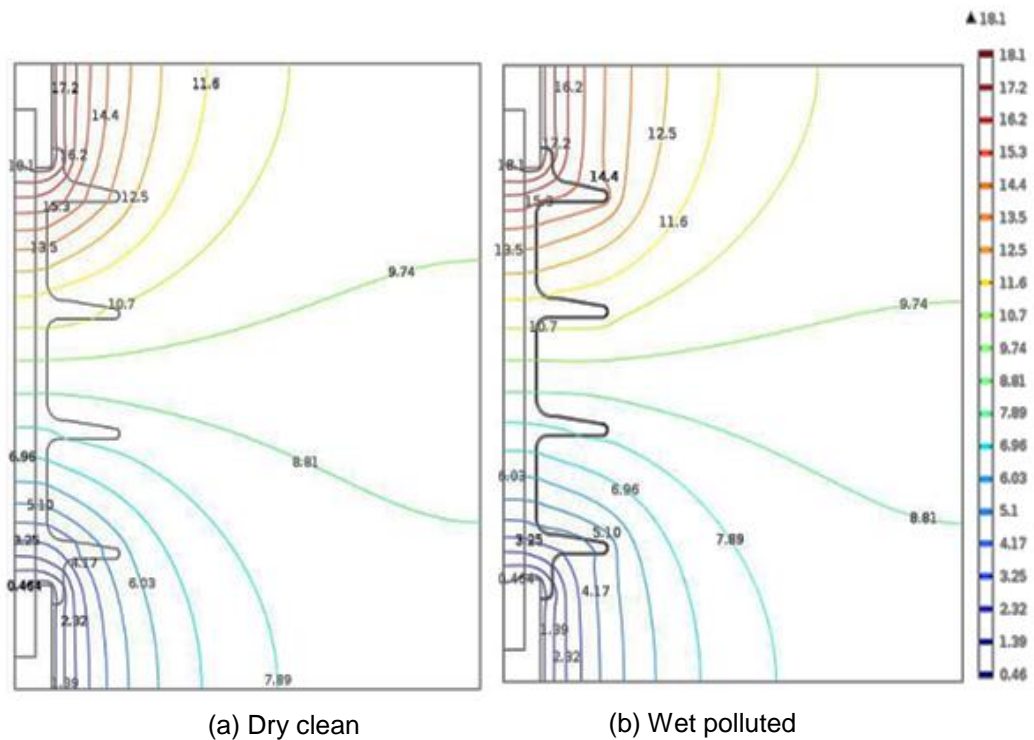


Figure 4-20: Equipotential lines along the surface profile of the clean dry and wet polluted SiR insulator

The calculated voltage distributions along the leakage profile of the insulator under both surface conditions are shown in Figure 4-21. The creepage distance is measured along the SiR surface, starting from the ground and ending at the

high voltage terminal (375 mm). An increment trend is observed for both curves when shifting toward the energisation end. The voltage profile along dry clean surface shows a high potential gradient at both ends, demonstrating high field regions on the insulator surface. This can be correlated with the equipotential lines obtained in Figure 4-20 (a) where the line concentration is close to the insulator terminals. For the wet polluted surface, the voltage profile seems to be more uniform and smoother than the profile for the clean insulator. This attributed to the equally spread distribution of the equipotential lines shown in Figure 4.20 (b).

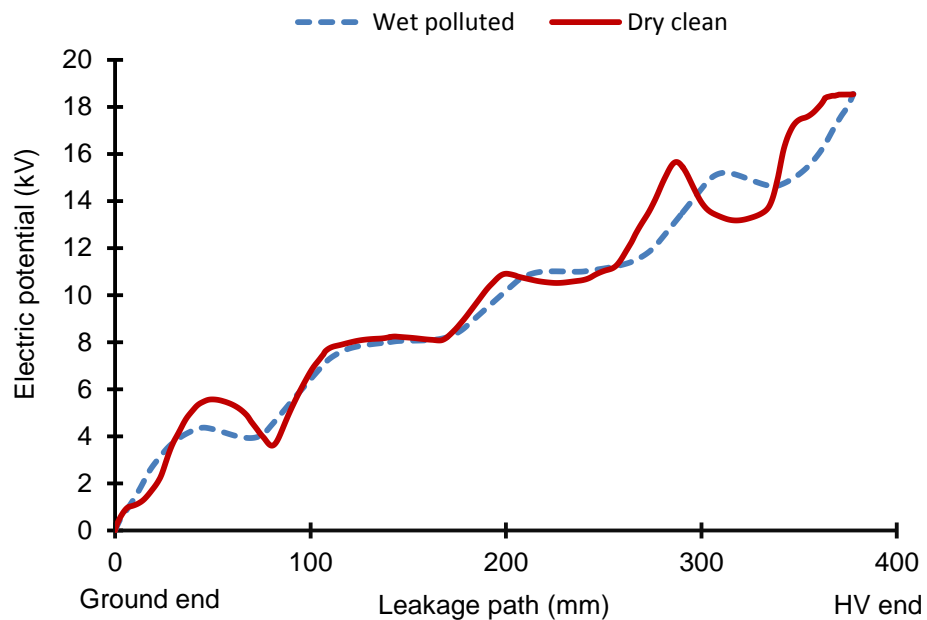


Figure 4-21: Voltage profile along the SiR insulator surface

The dry clean surface also shows curve undulations mainly at the region close to the insulator terminal ends. These undulations are caused by the equipotential lines that cross the insulator surface at more than one point as illustrated in Figure 4-20 (a). The same voltage level appears at different locations along the leakage distance causing a non- smooth voltage profile. The undulations are not observed on the potential profile under the polluted condition. This can be explained by the equipotential line only crosses the surface at one single point, as seen in Figure 4-20 (b).

(b) Electric field distribution along the wet polluted insulator

Figure 4-22 shows the plot results of electric field distribution along the leakage distance of the insulator under wet polluted surface condition. The simulated electric field was computed for 40 sec representing the tangential electric field along the insulator surface. The graph, in general, demonstrates a similar trend of electric field distribution between the ground and HV ends. The highest tangential field obtained on the surface is that near to the metal fitting electrodes with magnitude value of 1.9 kV/cm. Peaks of tangential field can be also seen in the shank regions where is the field magnitude reaching about 1 kV/cm. These peaks show a good correlation with the equipotential results and voltage profile concerning in the previous section. From the equipotential lines illustrated in Figure 4-20 (b), it is recognised that the electric field in the shanks areas tends to pass tangentially to the insulator surface, therefore enhancing to increase the electric field at the surface regions between 69 mm and 120 mm (shank A), 159 mm and 220 mm (shank B) and 240 mm and 312 mm (shank C) along the leakage distance.

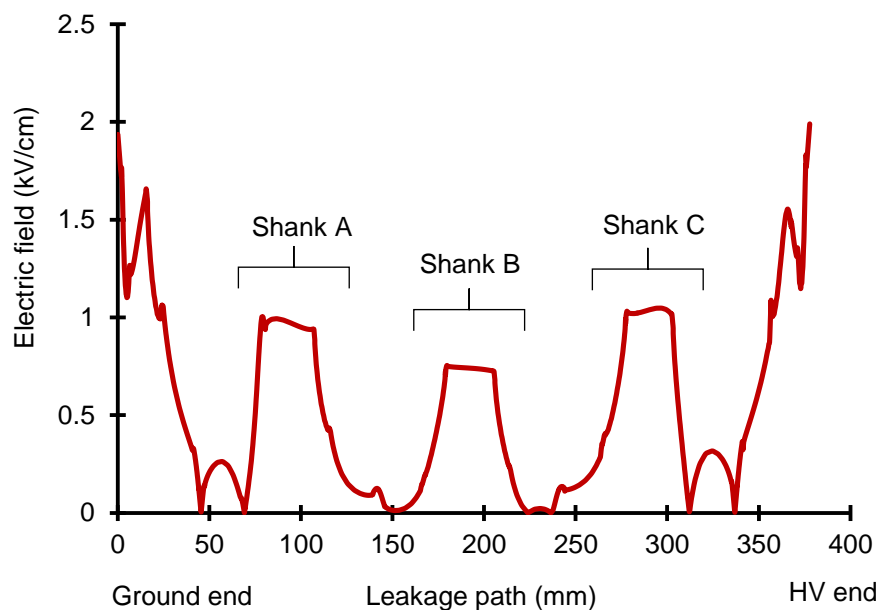


Figure 4-22: Tangential electric field along the leakage path for insulator under wet polluted surface condition

The electric field in the regions of the upper shed surface near to the ground electrode (between 44 mm and 69 mm) and the bottom shed surface at high voltage end (between 312 mm and 335 mm) are significantly low. This is because the tangential field component is run in the opposite direction of the leakage current along the SiR surface.

(c) Power dissipation in the pollution layer along insulator surface

Discharge activities and dry band formation on the surface of the SiR insulator are relatively correlated with the high electric field. With the presence of the wet pollution layer on the surface, the flow of the leakage current is mainly driven by the electric field, in particular, the tangential component. This current will cause power dissipation leading to resistive heating in the pollution layer which, consequently, will dry out the water and thus leading to the formation of dry bands on the insulator surface. The surface power dissipation in the pollution layer per unit surface area along the leakage path was calculated in [4-9]:

$$P_{\Omega} = \sigma E_t^2 \times t_p \dots\dots\dots (4 -1)$$

Where

E_t : is the tangential electric field (V/mm).

t_p : is the thickness of the pollution layer along the leakage path (mm).

σ : is the conductivity of the pollution layer along the leakage path (S/m).

The surface power dissipation in the pollution layer along the leakage path is shown in Figure 4-23 and computed using the equation (4-1) and the tangential electric field results obtained from the Figure 4-22. The thickness and the conductivity of the pollution layer used are the same values given in the section 4.9.1 and Table 4-2. The calculation of power dissipation was carried out through programming the equation in the COMSOL software.

Figure 4-23 shows two power peaks close to the end terminals in the same regions where the highest tangential electric field observed. The highest dissipated power value observed is about 18 W/m^2 . Peaks of the dissipated power can be also seen the shanks regions along the insulator surface as expected with magnitude value of 5 W/m^2 . This result gives a good correlation with the visual and infrared observations obtained in the section 4.6.1. It can be predicted that electric discharges and the formation of dry bands are probably to occur near the end terminals and shanks regions where the highly tangential field and long heating effects. Continuous heating on the SiR surface could destroy its hydrophobicity and, therefore, leads to degradation of the insulator on the long term.

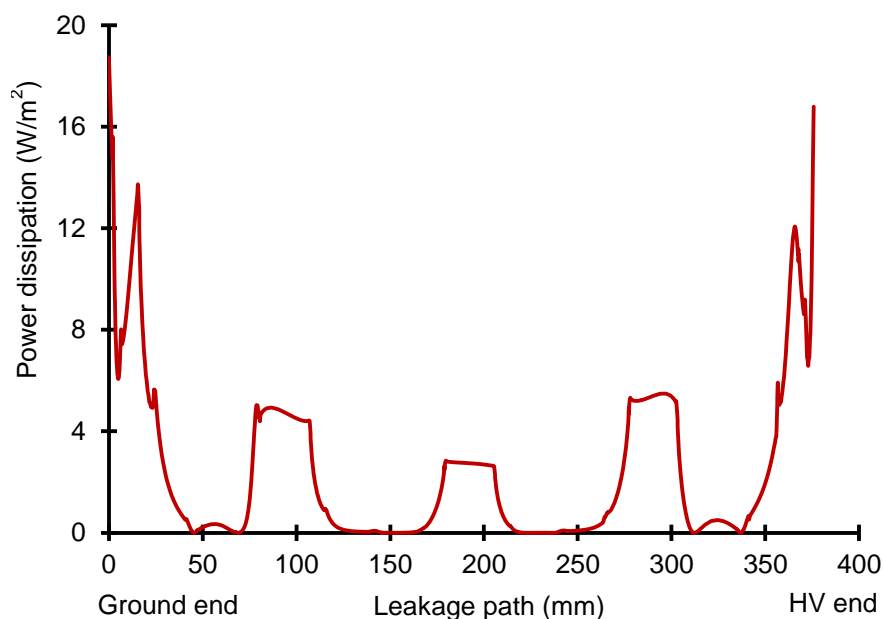


Figure 4-23: Surface power dissipation in pollution layer along polluted insulator surface

4.10. Conclusion

In this chapter, extensive tests were carried out describing the performance of silicone rubber polymeric insulators using the RWDT based on IEC 62730:2012. The procedures were adopted based on the 10 hours tests to perform AC and positive DC tests on conventional and textured insulator designs.

Several parameters, such as RMS and peak magnitudes, cumulative dissipated energy, power dissipation and power factor angle were measured to characterise the differences in performance for each design. Significant differences were observed in the leakage current waveforms for conventional and textured insulators. Surface tracking and erosion defects were observed on both insulator designs at the end of the test. Dry band arcing discharges were also visible on the trunk surface of the conventional profile. In addition, observations using a thermal camera were made on the shed surfaces and the insulator trunk, and a higher temperature was observed on the conventional surface. A decrease of hydrophobicity was measured on tested surfaces, and the time-variation trends of the conductance were defined on each insulator surface.

The potential and electric field distributions along the surface profile of silicone rubber insulator have been studied using the COMSOL Multiphysics finite element software. An ideal model has been adopted for an easily simulation the laboratory test conditions. The simulation results under dry and polluted surface conditions reveal the highly electric field region on the insulator surface as expected. In particular, near the end terminals and shanks regions. This favourable finding gives a good correlation between the two methods of simulation analysis and laboratory work through the rotating wheel dip test.

The power dissipation on the surface of the wet polluted insulator is relatively proportional to the electric field strength, particularly, the tangential field. This field has an effect on the developments of the surface leakage current leads to resistive heating in the pollution layer, thereby, the formation of dry bands. These simulation results provide useful information about surface heating that might be used to predict the formation of the dry band along the creepage path.

The conclusions of this chapter may be drawn as follows:

- For AC tests, the leakage current measurements showed that drying and discharge activity is greater for a conventional SiR insulator compared with a textured insulator.
- The power dissipated by partial arcing in conventional insulators is expected to be more damaging than the ohmic power loss for textured insulators.
- Using the calculated power factor angle for both insulator designs have distinguished the discharge surface activities during the energisation period, which was not always observed for the textured design as in the conventional.
- For both conventional and textured insulators, the cumulative dissipated energy is approximately four times greater for 13 kV positive DC than for 13 kV rms AC excitation.
- Under DC excitation, the conventional design showed regular dry band formation, associated with a frequent current interruption periods which was not observed for the textured design.
- When dry band arcing occurred, both insulator designs were affected, and more severe degradation could appear on positive DC tests than on AC tests.
- Tracking and erosion were quantified by visual recorded and were more severe in the case of the conventional design. The eroded area was also less, negligible for textured and significant for the conventional.
- The surface conductance of the polluted layer was 46 % lower for the bottom shed surface of the textured insulator than that for the conventional insulator. This tendency was also observed for the trunk and the upper shed surfaces in which the reductions were respectively 42 % and 22 % compared with the conventional.

- Electric stress on the SiR insulators was investigated and analysed by using the computer simulations. Good correlation was achieved between simulated results and practical observations on the discharge activity.

This study confirms that textured insulator profiles can improve the performance of polymeric insulators against the tracking and erosion under AC and positive DC excitations.

CHAPTER 5: ARTIFICIAL POLLUTION LAYER CHARACTERISATION ON CONVENTIONAL AND TEXTURED SILICONE RUBBER INSULATORS

5.1. Introduction

Composite insulators are increasingly deployed in new AC and DC high voltage transmission systems due to their excellent performance in polluted environments [5-1, 5-2, 5-3]. Many authors have previously suggested many empirical equations to predict the flashover voltage, FOV, levels under pollution based on a strong influence of the ESDD on the FOV [5-4]. However, it is worth noting that FOV performances are only one of the key points in the design of new polymeric insulators. In fact, the design targets in the selection of ceramic and composite insulators are different [5-5].

Ceramic insulators are not significantly affected by continuous partial discharge activity, and their anti-pollution design mainly deals with pre-arcing leakage current values. Meanwhile, composite insulators offer high hydrophobic properties even under heavy pollution. Sustained partial discharges can affect this hydrophobicity property following an increase of leakage current to tens of mA. This degradation can cause tracking events and can damage the insulator surface, increasing the probability of a flashover and permanent insulator failure [5-5]. Therefore, it is very important to limit the leakage current under certain levels for the insulators service lifetime, especially under polluted wet conditions.

Clean fog testing of artificially polluted insulators is an important tool in the design process of high voltage outdoor insulators. A voltage ramp test in the clean fog chamber, which was recently proposed in [5-6], makes possible the differentiation of insulation materials and the assessment of insulators with and without textured surfaces using the mean FOV test results of four sequential ramps. The surface layer conductance is one of the key parameters that influences the flashover level for a selected design and insulating material.

This chapter describes how ESDD, NSDD, leakage conductance, and surface conductance were investigated on 11kV silicone rubber insulators adopting conventional plain and textured surfaces. All these techniques have been applied for the first time on the novel design with texture surfaces. Each insulator was artificially polluted using the solid layer method and then tested within 24 hours of the pollutant being applied. The conductance measurements were performed by measuring the voltage at the terminals of a shunt resistor in series with the insulator subjected to a low magnitude AC voltage. The tests were repeated under different fog conditions and for a wide range of artificial pollution levels, with high voltage and fog applied simultaneously. The selection of voltage level below 300 V made possible the recording of the pollution layer conductance without the presence of dry-band or arcing. In addition, localised conductance measurements were performed using a conductance meter with a probe built as described in section 3.5.1. Localized measurements were performed alongside the layer conductance measurements at selected times after the start of the test. In conjunction with the full layer conductance measurements, the readings help to characterize fully the variation trends of conductance and its distribution on the insulator surface. This contributes to a better understanding of the FOV performance of a textured design when compared with conventional insulators.

5.2. Equivalent Salt Deposit Density (ESDD) and Non-Soluble Deposit Density (NSDD) evaluation

Measuring the ESDD and NSDD on insulator surfaces is very important to determine the degree of pollution severity. In addition, these measurements can provide useful information to identify the required creepage distance for the insulator to be selected. For this reason, it is important to consider the procedure and technique for measuring the ESDD and NSDD parameters on different polymeric insulator designs.

5.2.1. The requirements to measure the pollution severity degree

Based on the IEC standard 60815 [3-2], the following equipment is essential for measuring ESDD and NSDD parameters using a swab technique method:

- distilled water
- vinyl gloves
- cling film
- thermometer
- conductivity meter
- filter paper (GF/A 1.6 μm)
- funnel
- cotton/brush/ sponge
- weight scale
- labelled container
- washing bowl
- drying oven
- cylinder

5.2.2. Application and removal of pollution layer

Silicone rubber rectangular samples as specified in IEC 60587 and 4-shed insulators with both smooth conventional surfaces and textured patterns were polluted as described in section 3.7.2 [4-3]. The contaminating suspension consisted of kaolin (40 g), tap water (1 l), Triton X-100 wetting agent (1g), and a suitable amount of sodium chloride to attain the required volume-conductivity values (2.9, 4, 8, 11.2 and 20 S/m) [5-6]. The ESDD and NSDD parameters were evaluated according to the procedure detailed in section 3.6. The ESDD values were calculated from the volume conductivity of the solution resulting from washing the insulator with demineralized water, as shown in Figure 5-1. The solution temperature was recorded using a thermometer with a precision of 0.1 °C. Each solution, resulting from the cleaning process, was then filtered using a funnel with vacuum aspiration and pre-dried; then the filter paper (GF/A 1.6 μm) was weighed. A precision scale with an error of less than 0.2 mg was used; the process stages for measuring NSDD are illustrated in Figure 5-2.

The pollution layer was removed using a clean brush and a selected amount of demineralised water (100-300 cm³). Since metal fittings were present, they were covered with cling film before the removal of the pollution layer and were not taken into account in the evaluation area. Vinyl gloves were used to avoid contamination and were cleaned with distilled water at the end of any operation on each sample.

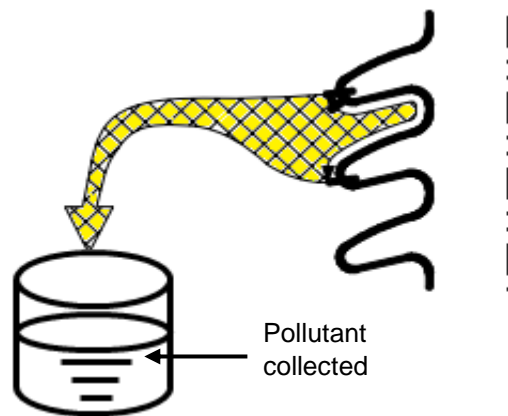


Figure 5-1: Swabbing of the pollutant on insulator surface [3-2].

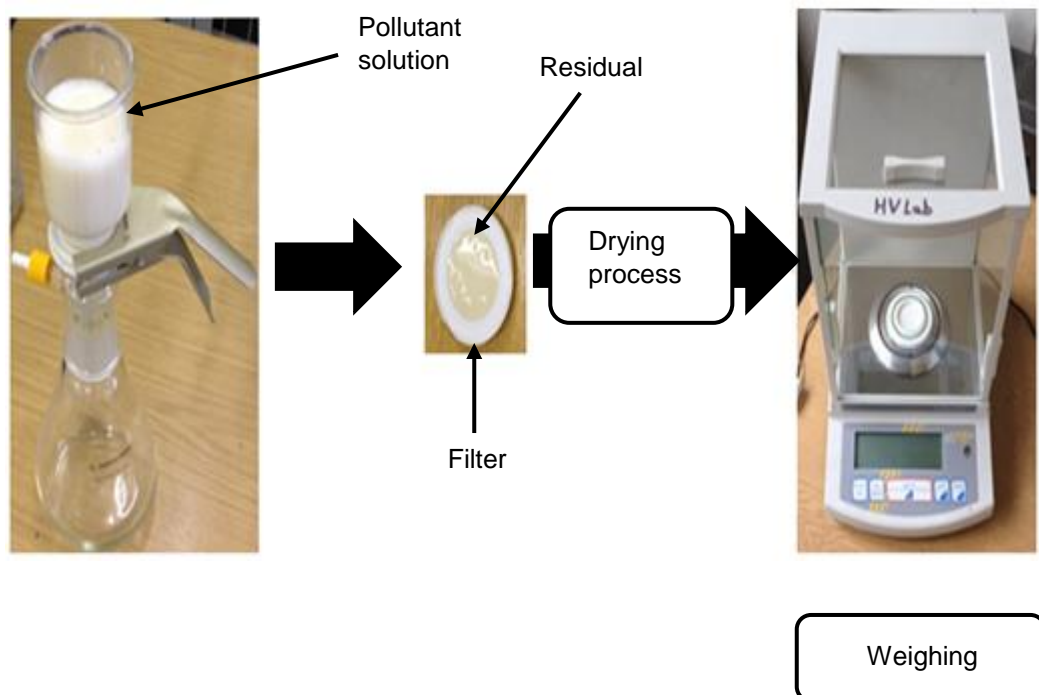


Figure 5-2: Procedure for measuring non- soluble deposit density (NSDD).

5.2.3. Equivalent Salt Deposit Density (ESDD) on rectangular plain samples

Ten rectangular samples (120 mm × 50 mm × 6 mm) with smooth (CONV) and textured (TXT) surfaces were tested, as shown in Figure 5-3. All the samples were moulded using an in-house facility, consisting of a vacuum casting machine and metal moulds. Two different commercial room temperature vulcanized (RTV) silicone rubbers (type A and type B) were adopted for the sample moulding. Seven of them had textured surfaces, with either a 2, 4 or 6 mm square pattern (TXT2, TXT4 and TXT 6 respectively) [3-5].



Figure 5-3: Rectangular samples with flat (left) and textured (right) surfaces.

The samples were polluted using the dipping technique into slurry preparations with volume conductivity equal to 4, 8 and 11.2 S/m. Each sample was dipped horizontally five times and then carefully placed to dry horizontally in order to maintain the maximum amount of pollutant solution on the surface; only the ESDD values of the top surfaces were evaluated. Figure 5-4 shows the correspondence between suspension pollution conductivity and ESDD for the rectangular samples.

It is worth noting that the conventional samples and samples with small dimple sizes (TXT2 and TXT4) showed an ESDD higher than that of the TXT6 samples. The ESDD value of the CONV sample is approximately three times higher than that of the TXT6 sample at volume conductivities of 4 S/m, 8 S/m and 11.2 S/m. The ESDD value of the CONV surface at 4 S/m is about 1.6 mg/cm² while with the TXT6 design is only 0.5 mg/cm². For TXT2 and TXT4 samples, the ESDD values measured at 8 S/m are respectively 1.3 mg/cm² and 1.2 mg/cm² while with the TXT6 design, the ESDD measurement is 0.85 mg/cm². The same trend of those measurements is also observed at the volume conductivity of 11.2 S/m. The deposition values shown in Figure 5-4 suggest a reduced deposition with the increase in dimple radius by 6 mm. The pollution slurry was found to deposit more readily in the grooves than on the rests of the dimples, with the pollutant film layer breaking and running away from the surface into the grooves. In fact, on the smooth-surface conventional samples, the thickness of the film liquid was visibly higher than on textured samples and, therefore, a higher quantity of salt was deposited. This observation could explain the reduced pollution deposition on the textured samples with texture [5-12].

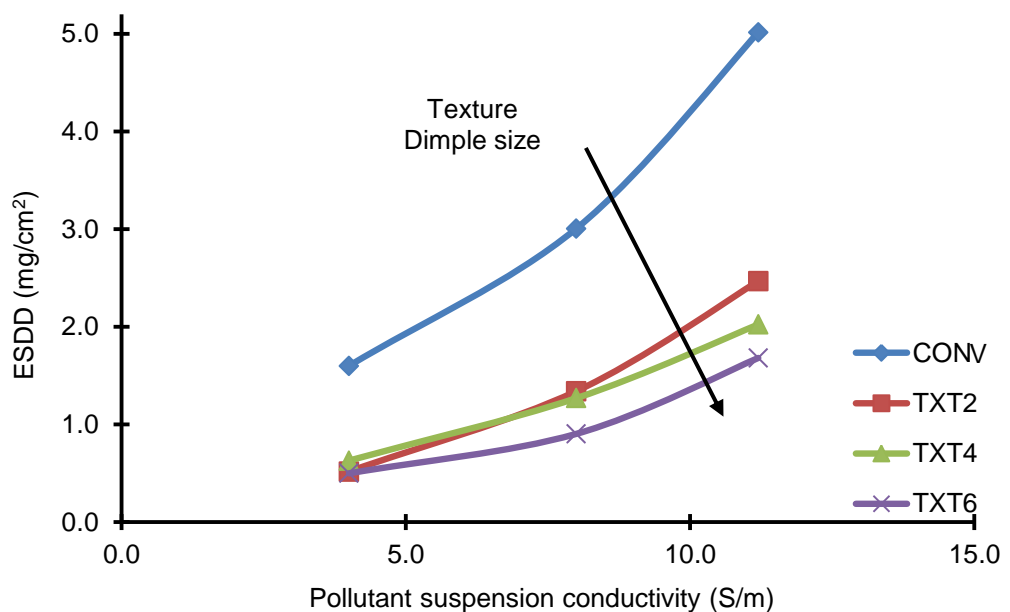


Figure 5-4: ESDD on rectangular samples versus pollutant suspension conductivity.

5.2.4. Equivalent Salt Deposit Density (ESDD) on 4-shed insulators

A modified version of the IEC 60507 solid layer method was applied to several 4-shed insulators with smooth conventional surfaces (CONV) and with textured patterns either on the trunk (TT) or on the trunk and shed surfaces (TTS), as described in section 3.3. Table 5-1 shows the specifications of the insulator design; two different commercial RTV silicone rubbers, type A and type B, were selected for the insulator moulding. Initial hydrophobicity analysis showed that material A presented a lower degree of hydrophobicity than did material B.

Table 5-1: SiR insulator specifications

Design	Creepage distance (mm)	No of sheds	Trunk diameter (mm)
CONV	375	4	28
TT	471		
TTS	503		

Four conventional insulators were moulded using both materials. After a few days, the insulators were washed with hot water and polluted with a suspension made with kaolin (40 g), wetting agent (1 g), and selected amounts of NaCl as shown in Table 5-2 in order to obtain volume conductivity values equal to 2.9, 4.0, 8.2, 11.2 and 20 S/m.

Table 5-2: The amount of NaCl requires for pollutant suspension conductivity

Sodium chloride (NaCl) (mg)	Volume conductivity (S/m)
48	2.9
126	4
252	8.2
366	11.2
684	20

The salt deposit densities resulting from the average of several tests for a conventional design are shown in Figure 5-5. The two materials presented very close ESDD values, e.g. the ESDD value of the material A and B at volume conductivity 8.2 S/m is respectively around 0.42 and 0.418, thus confirming that the use of the wetting agent is sufficient to remove completely, but it only affects temporarily the hydrophobic properties of the materials. The trend is not linear, with the maximum conductivity value occurring close to the saturation point for NaCl solubility [5-12].

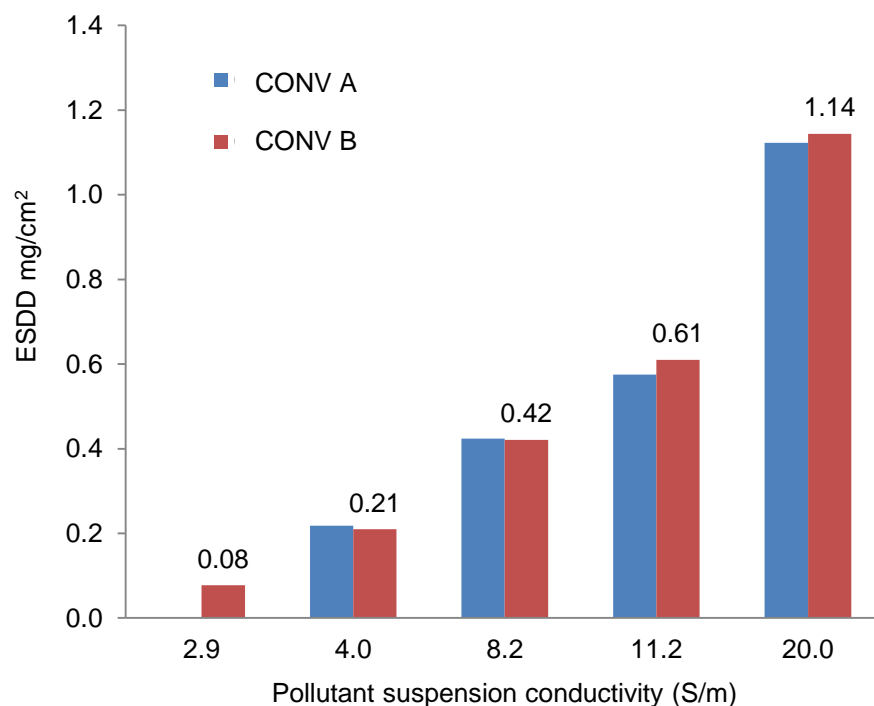


Figure 5-5: ESDD values for conventional insulators of material A (in blue) and material B (in red) versus conductivity of the pollutant suspension applied.

The comparative ESDD evaluation was extended to all the insulator designs as this study required a considerable number of evaluations in order to achieve good statistical margins. All the textured insulators showed very similar ESDD values to those of the conventional design, as shown in Figure 5-6. Only for the severe pollution level (20 S/m) was a small ESDD increase recorded for all the textured insulators.

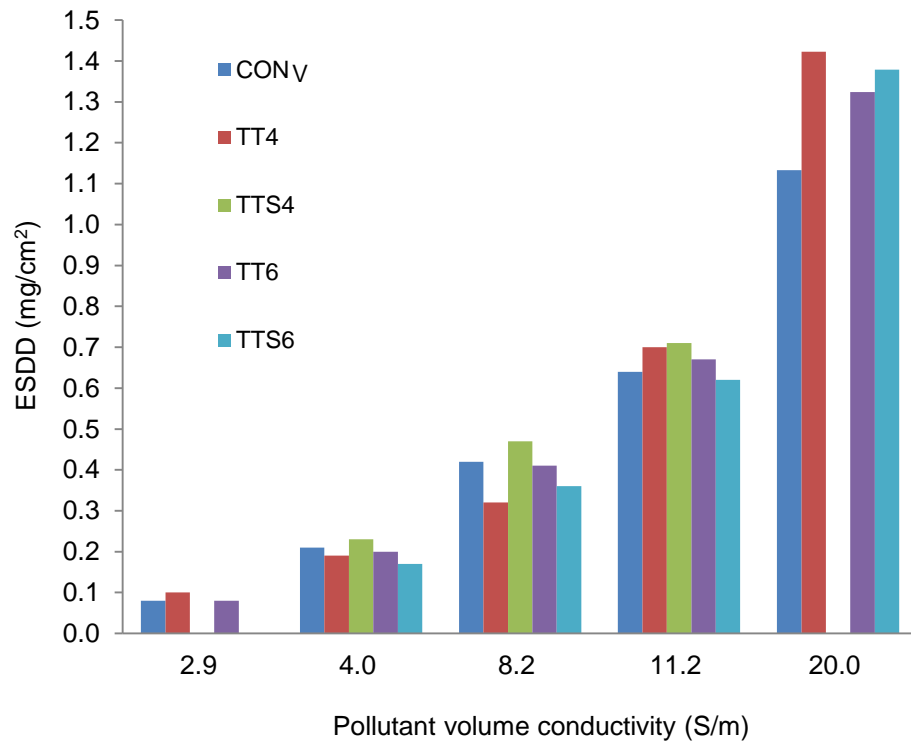


Figure 5-6: ESDD values for all insulator designs versus pollutant suspension conductivity applied.

It is interesting to note that the TTS4 (in green) showed a consistently higher value than the other designs, e.g. the ESDD value for TTS4, CONV and TTS6 designs at the volume conductivity of 8.2 S/m are 0.46 mg/cm², 0.41 mg/cm² and 0.35 mg/cm² respectively. The same trend of those results is also obtained at the volume conductivities of 4 S/m and 11.2 S/m. Water film retention varies according to texture size, and this plays a significant role in reducing the pollutant accumulation on rectangular samples. For this reason, TT6 and TTS6 insulators showed a consistently lower value in comparison with TT4 and the conventional designs.

The NSDD evaluation showed a value equal to ± 0.20 mg/cm² for all the designs, showing that texturing the insulator surfaces had no effect on inert material accumulation.

5.3. Leakage conductance evaluation tests under AC and DC voltages

In service, insulators are exposed to several types of contaminants that can cause the formation of a significant pollution layer. This layer is involved in significant leakage current when exposed to wet weather conditions. In particular, it can experience fog density in the range of 0.01 to 0.3 g/m³ under normal operation. The fog chamber in the high voltage laboratory processes fog densities that are significantly higher (usually 1-3 g/m³) [5-7]. Therefore, the wetting process in a fog chamber is faster than in actual service.

The leakage layer conductance was evaluated using AC and DC low voltage sources on conventional and textured insulators that were artificially polluted. The leakage conductance was evaluated under different fog conditions and artificial pollution levels in order to identify any impact of texturing.

5.3.1. Fog density

A uniform fog was produced inside a polypropylene chamber (2m x 2m x 3m) using two pairs of cold-water spray nozzles, located at opposite corners, as described in paragraph 3.7.3. The fog generation was controlled by the selection of controlled air pressure and water flow rate. The air pressure selected for these tests was 40-45 psi, and the water flow rate was in the range 3 to 8 l/h. The water tank was pre-filled with tap water and was allowed to reach thermal equilibrium with the laboratory environment. The injected water was at the same temperature as the air, and no external heating was provided during the test; therefore, the fog formation could be assumed to be adiabatic. The amount of water that needed to be injected into the chamber to establish fog is a function of the initial state of the air inside the chamber given by Equation (5-1):

$$m_w = \text{Vol}_{\text{Chamber}} \cdot \rho \cdot (x_{\text{ss}} - x_{\text{lab}}) \dots \dots (5-1)$$

where

m_w is the amount of water (kg);

Vol_{Ch} is the volume of the fog chamber (m^3);

ρ is the dry air density;

x_{ss} is a specific humidity of air at the oversaturation condition (kg/kg);

x_{lab} is a specific humidity of air at the initial laboratory conditions (kg/kg).

The laboratory conditions, with the ambient temperature of 20 °C and relative humidity (RH) 70%, gave a specific humidity equal to 0.010 kg/kg in the psychrometric chart; the corresponding oversaturated condition (x_{ss}) was equal to 0.0114 kg/kg. Therefore, the fog density achieved was equal to 1.5 g/m^3 . It is possible to predict the temperature drop due to the fog formation to 17 °C inside the chamber, and this was confirmed by infrared temperature measurements during the tests.

5.3.2. Wetting process

In fog tests, the wetting accumulation is due to condensation, adsorption, and the collisions of water droplets encroaching on the insulator surface. In these cold-fog tests, there is no contribution by condensation since the fog temperature is never higher than that of the insulator surface. Therefore, the wetting is only by the adsorption and collision contributions.

The adsorption of water by NaCl in the pollution layer from the humid air can start when the relative humidity (RH) is equal to or over 75% [5-8]. However, this is a slow process, and as soon as the selected fog density is reached, the wetting is mainly due to the water drops colliding with the insulator. From the visual video records, it is possible to identify the time when the maximum fog density is reached. These show 4 min 30 s and 1 min 40 s for 3 and 8 l/h water flow respectively.

It was found that the pollution layer presents an initially high hydrophobicity due to the low molecular weight (LMW) silicone chains [5-9, 5-10, 5-11]. Then, when the fog starts, the water accumulates on the surface as individual droplets, without forming a continuous water film, but is sufficient to increase the layer conductance. Additional wetting during the test will create continuous water film areas, mainly on the shed, as shown in Figure 5-7.

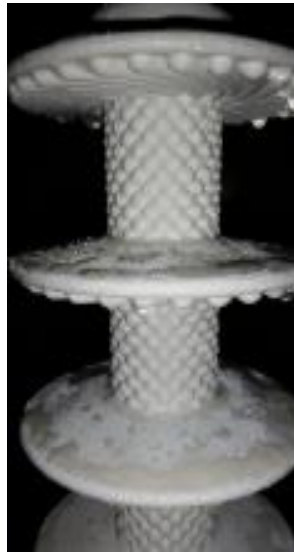


Figure 5-7: Wetting on TTS6 insulators.

Quantities of NaCl will dissolve in the surface water film areas, leading to an even higher conductance value. After reaching the maximum conductance value, the additional wetting will start to wash away some salt. The excess water accumulated on the surface will flow off the insulator, washing away some salt and, hence, lowering the conductance value over time.

For the tests performed in the fog chamber facility, four plastic containers (12 cm diameter) were placed on the floor close to the insulator at four locations, as illustrated in Figure 5-8. These measurements permit monitoring of the amount of water collected and verify the fog uniformity.

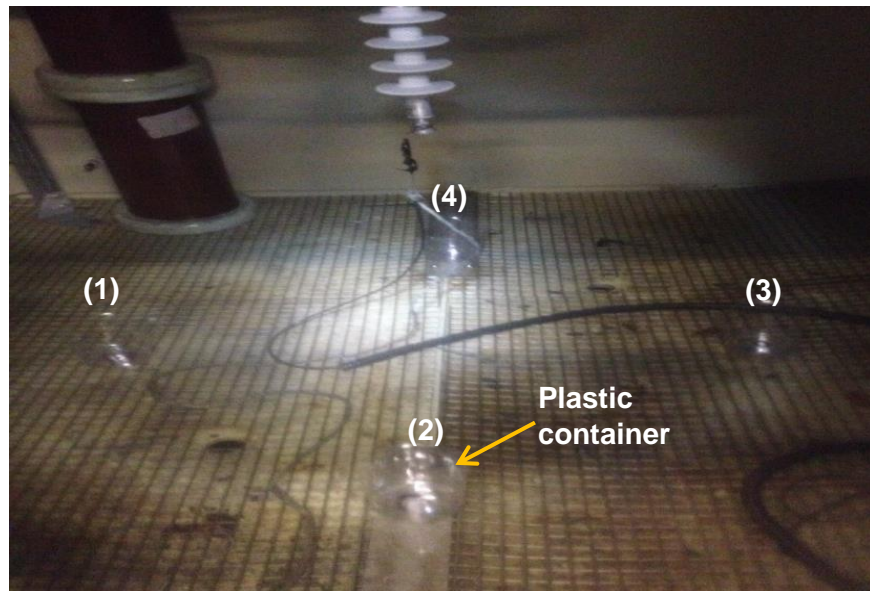


Figure 5-8: Verifying the fog uniformity in the fog chamber tests.

The water accumulation rate per unit area is 54 mg/s/m^2 for a water flow rate of 3 l/h. Each container produced a similar weight of collected water, confirming the good uniformity within the insulator location.

5.3.3. AC and DC leakage conductance evolutions

Leakage conductance variation was monitored using a shunt resistor placed between the insulator ground terminal and the laboratory earth point. The applied voltage and leakage current waveforms were recorded using a computerised data acquisition system (DAQ).

In the first series of tests, the leakage current of a conventional insulator was recorded during the application of a low voltage AC source (200 V) and fog generation simultaneously. Figure 5-9 shows the temporal variation of the leakage current flowing in the wet pollution layer (ESDD 0.21 mg/cm^2) for a water flow rate of 3 l/h and 8 l/h. The maximum conductance value was around $0.7 \text{ }\mu\text{S}$ for both flow rates. The graph shows that the leakage current variation is a function of the water flow rate settings. Higher flow rates will increase the speed of wetting, and the conductance layer will reach the maximum value quicker.

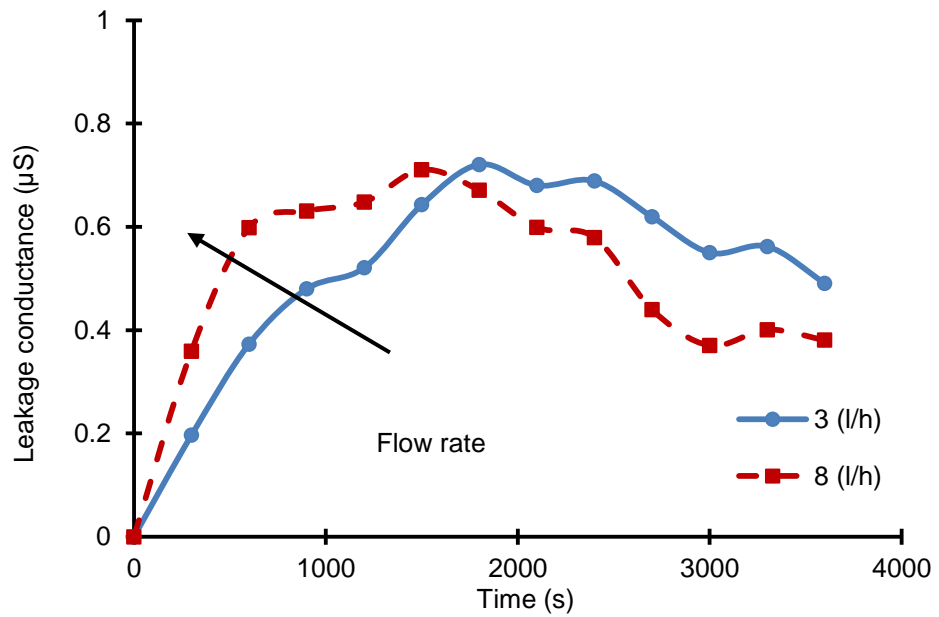


Figure 5-9: AC leakage current of a conventional insulator versus applied fog time; ESDD 0.21 mg/cm².

The second series of AC tests recorded the changes in leakage conductance with the times for plain and textured surfaces. Figure 5-10 shows the conductance change for insulators with ESDD 0.21 mg/cm² and a flow rate of 4 l/h. The maximum conductance was approximately 1 μS for both designs and reached with the same exposure time to fog.

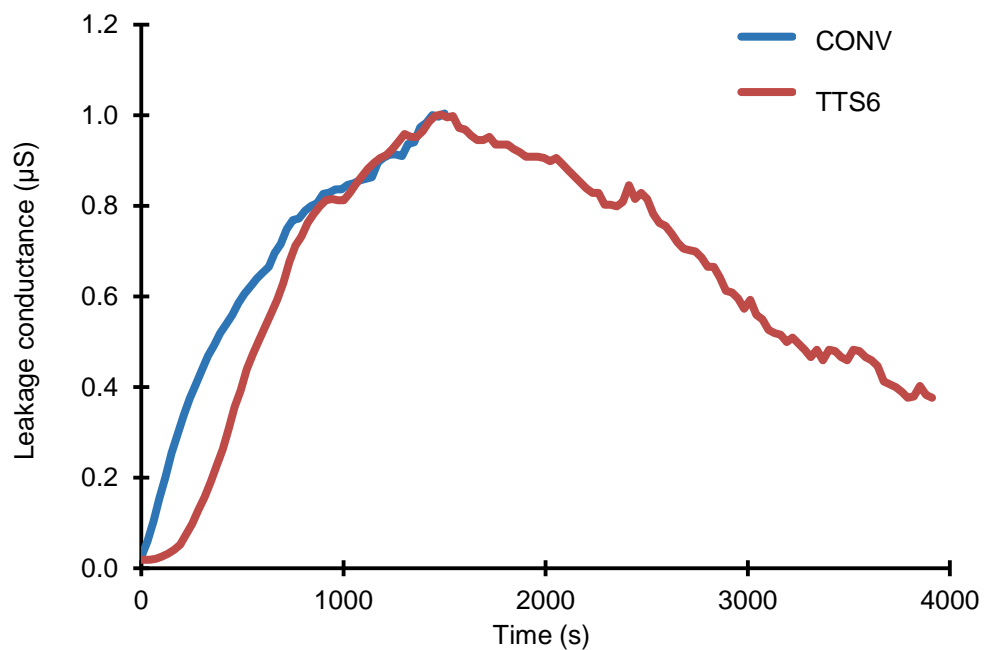


Figure 5-10: AC leakage current for ESDD 0.21 mg/cm²: conventional (CONV) and texture (TTS6).

The initial trend suggests that the layer conductance is a function of the wetting rate and depends on the type of surface. In fact, as was observed in the rectangular sample tests, the water film tends to flow away from the top of the dimples towards the grooves. In this particular case, the trunk surface is vertical. Therefore, any excess of water flows over the film, formed by the mix of LMW silicone chains and the wet pollution layer, towards the top surface of the shed below. The accumulated NaCl and kaolin in the groove takes a longer time to become fully wet compared with the conventional surface.

If a very high ESDD value (1.20 mg/cm^2) is present on the insulator surface, different conductance trends for conventional and textured designs are observed, as shown in Figure 5-11.

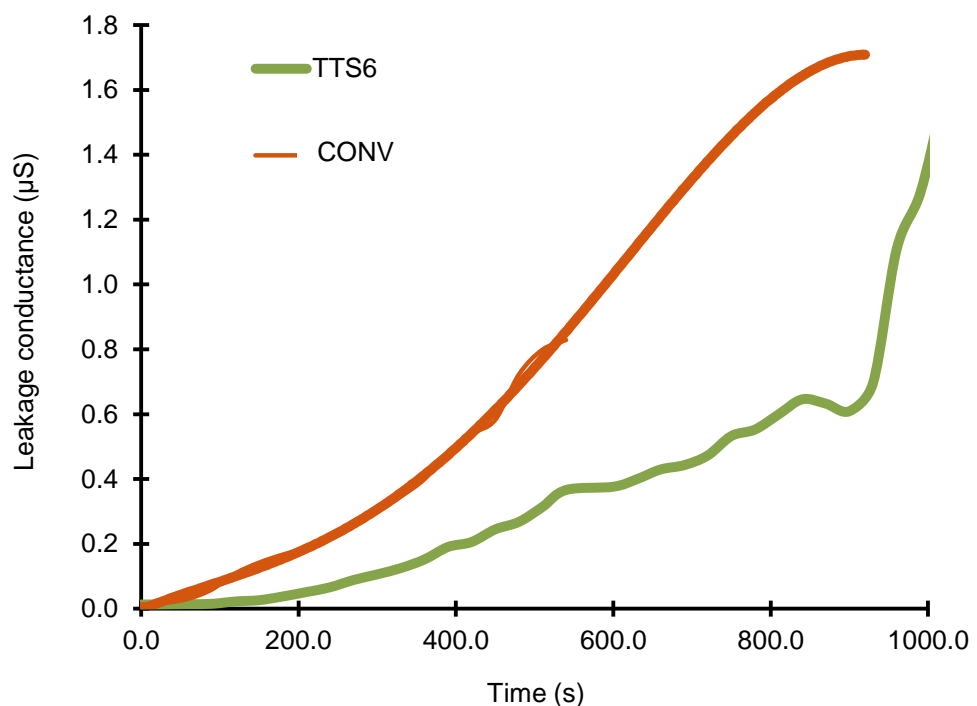


Figure 5- 11: AC leakage current for ESDD 1.20 mg/cm^2 : conventional (CONV) and texture (TTS6).

Figures 5-10 and 5-11 show the wetting delay on textured insulators is clearly enhanced in comparison with conventional surfaces. In addition, the wetting of the textured surface is more delayed when the pollution is higher. This effect is very convenient, offering a higher margin in the real service.

The DC test series, using a voltage of 320 V, confirmed the slower response time of a textured insulator compared with a conventional one, as illustrated in Figure 5-12. The leakage conductance variation is very similar to the test performed using the low voltage AC source.

Once the full wetting is achieved, the maximum conductance value was reached. After the peak, water droplets with a larger radius started to form and to slide on the surface falling off the insulator, gradually washing the pollution layer from the surface. The two designs were subjected to the same rate of washing. This confirms the importance of the correct selection of the wetting rate and the limited time window for the flashover tests.

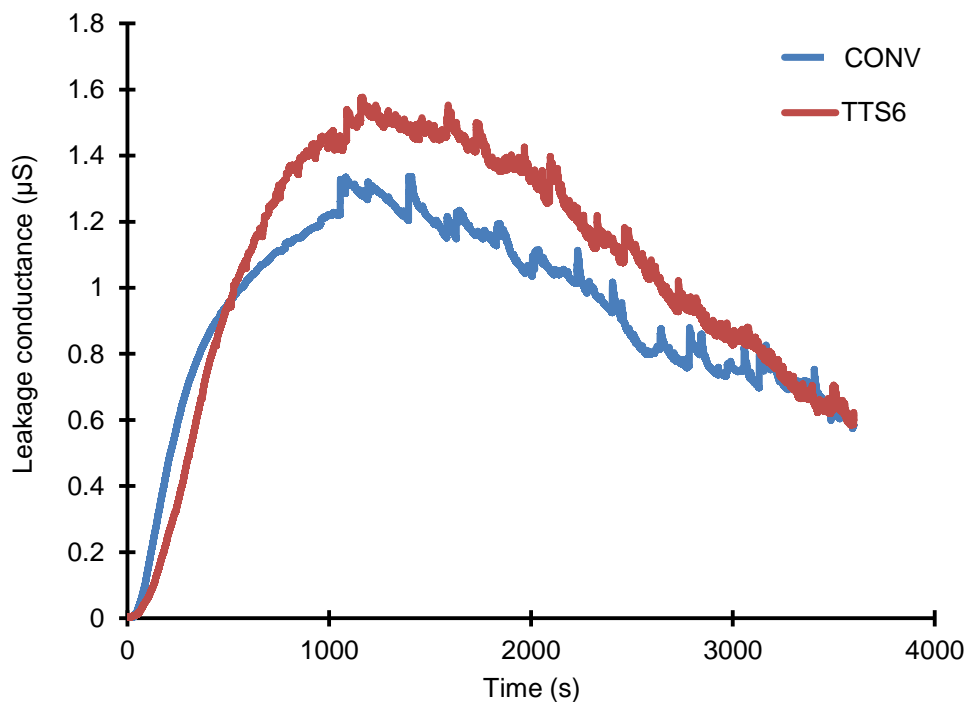


Figure 5-12: DC leakage current for ESDD 0.21 mg/cm²: conventional (CONV) and texture (TTS6).

5.4. Surface conductance evaluation tests

5.4.1. Test procedure

During the artificial pollution test, the pollution layer is often assumed to be uniform over the entire surface of the insulator. In order to verify this assumption,

the surface conductance of different areas of the insulator surface was measured. The measurement was extended to all the designs. A low voltage AC of 200 V was applied during the test in order to avoid any temperature increase of the pollution layer and any dry band formation. The test was used suspension of salinity with volume conductivity 4 S/m and a fog rate of 3 l/h.

The localized conductance measurements were evaluated using a conductance meter with two spherical probes built as described in section 3.5.1. Several locations on the insulator surface were analysed. The localized measurements were evaluated at selected times after the start of the test. This evaluation helps to explain and identify possible trends of the conductance during fog exposure and its distribution on each insulator surface.

5.4.2. Test results and discussion

Figures 5-13 and 5-14 show the surface conductance values on the shed and trunk areas of conventional and textured insulators. The values shown are an average of several measurements recorded (i) at peak time and (ii) after one hour of fog exposure on the upper shed surface (USS), lower-shed surface (LSS), and trunk (Tr). In the graphs, the washing effect has been made more visible, highlighted as red areas, and calculated as the differences between the maximum conductance values, which were obtained within a period of 20 minutes to 25 minutes and the measurements at the end of the full period (one hour) tests. The washing effects of textured and conventional insulators were quite similar, thus confirming the leakage conductance trends following the peak values, as described previously in Section 5.3.3. An average variation of 10-20 μS was recorded for both designs on the upper shed surface (USS). As expected, the washing effect was reduced on the lower shed surface (LSS), with average reduction of 5-10 μS .

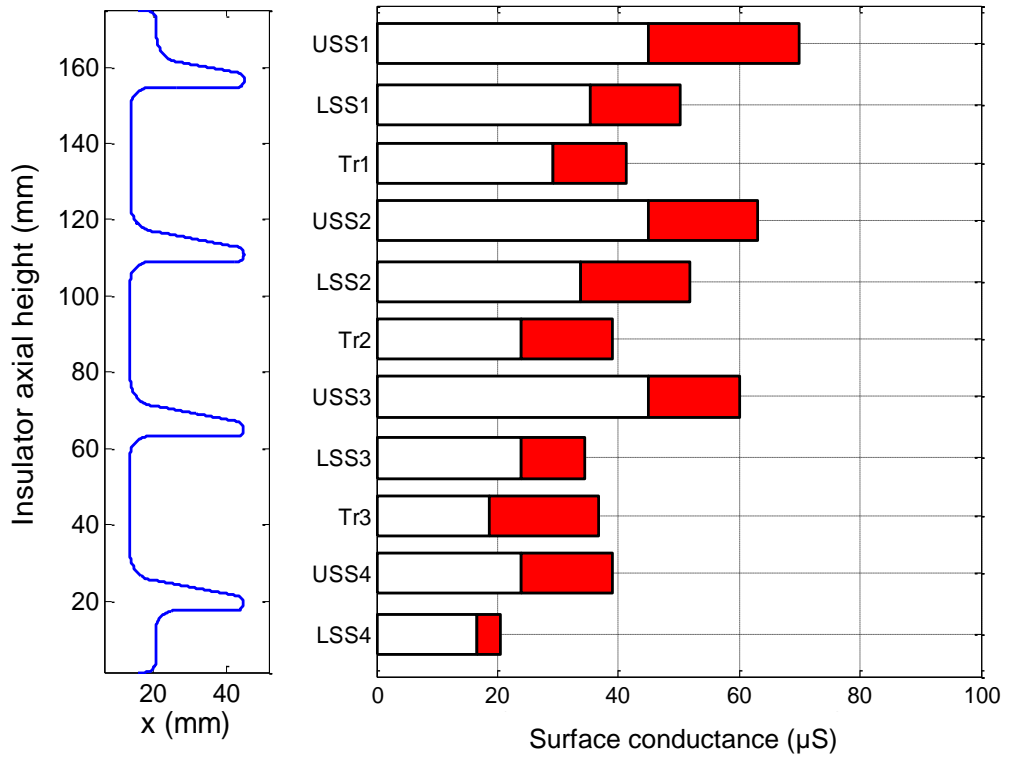


Figure 5-13: Surface conductance measurements on sheds and trunk of conventional insulators at peak time (red) and after 1 hour-test (white).

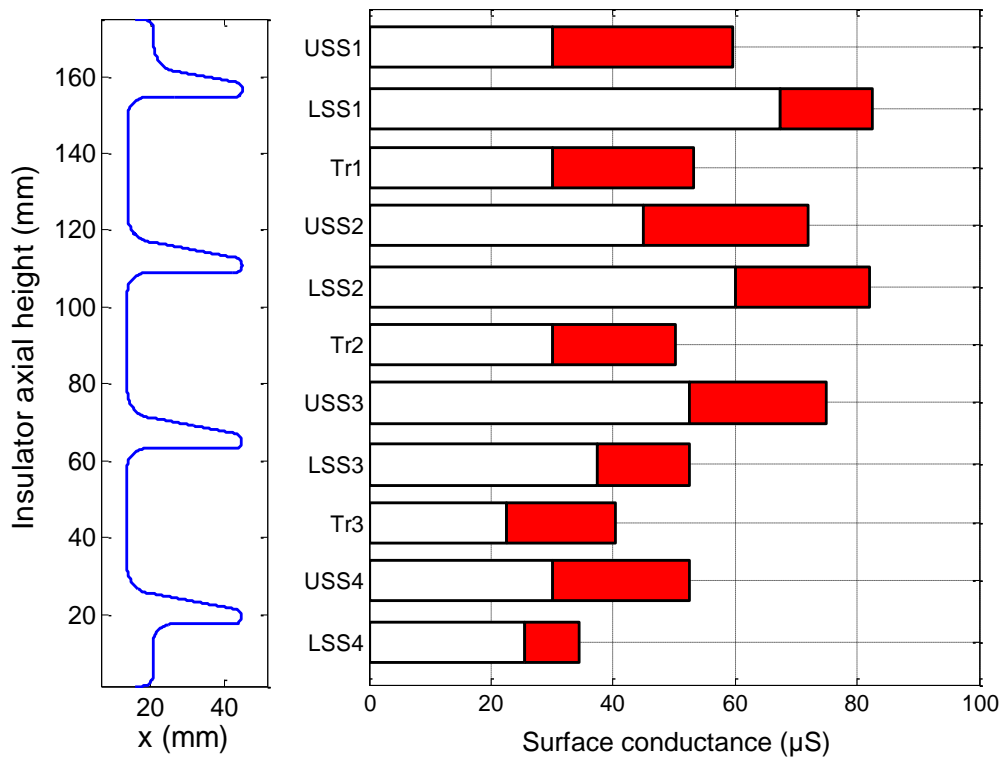


Figure 5-14: Surface conductance measurements on sheds and trunk of textured insulators at peak time (red) and after 1 hour-test (white).

It is quite clear on both graphs that the washing is not uniformly distributed along the insulator surface. The surface conductance values on the trunk surface (Tr) after one hour test are in both designs in the range of 20-30 μS . For this reason, a textured insulator in service will experience effective washing as on conventional design.

5.5. Conclusion

An investigation of the artificial pollution layer characterisation on conventional insulators and for the first time on the textured silicone rubber insulators has been described in this chapter. Based on the clean fog testing method, several tests were carried out to evaluate the changing behaviour of the insulator surfaces under different conditions. ESDD and NSDD parameters were quantified for different materials, and each design was evaluated. For leakage conductance measurements, the variation trend for each insulator profile was determined and the distribution trends of surface conductance were characterised.

The conclusion of this chapter may be summarized as follows:

- For ESDD evaluation on rectangular samples, textured surfaces do not significantly increase the accumulation of pollutant. This evaluation was performed with an artificial layer, and the increase in dimple size (6 mm) was shown to reduce the pollutant deposition on textured surfaces.
- The ESDD values obtained for the TXT6 rectangular sample were three times lower than that values measured for the CONV sample at the volume conductivities of 4 S/m, 8 S/m and 11.2 S/m.
- For ESDD evaluation on 4-shed insulators, the two materials of silicone rubber insulation exhibited very similar ESDD values due to the Triton X-100 wetting agent temporarily removing the hydrophobicity properties.

- In 4-shed insulators, the textured design has shown comparable ESDD value with the conventional profile.
- The maximum leakage conductance of the tested insulators was measured, and an interesting trend of the layer conductance was observed with textured profiles under both AC and DC voltages. This trend showed that the wetting delay of the textured surface is enhanced and more delayed was observed when the pollution level is higher. This effect is very useful offering a greater margin in the real service.
- For textured designs, the leakage current growth is limited to a significantly slower rate than for conventional designs. In service, the wetting rate of fog is much lower than in the laboratory, and the delay in leakage current formation identified in the tests could be very valuable for textured design application.

CHAPTER 6: PERFORMANCE OF ARTIFICIALLY POLLUTED SILICONE RUBBER POLYMERIC INSULATORS USING THE CLEAN FOG CHAMBER FACILITY

6.1. Introduction

SiR outdoor insulators are an attractive option for use in HVAC and HVDC power lines [6-1]. Polymeric insulators offer superior flexibility during the design, which means they can be moulded into any size and shape [6-2]. However, polymeric insulators are known to exhibit weaknesses following heavy surface discharges and exposure to other chemicals and UV radiation, such as a loss of hydrophobicity, the formation of tracks, surface erosion during electrical discharge and degradation due to corona activities and flashover events. Therefore, their long-term endurance has been a subject of concern over the last three decades. Many studies have been conducted in laboratories and field test stations to understand the aging performance of polymeric insulators used in outdoor applications.

In this chapter, the results of clean fog tests based on the solid layer method are presented. For test purposes, different designs of SiR insulator were prepared in the laboratory using casting techniques as described in section 3.4.2 and used in these tests. The flashover performance of conventional and textured SiR insulators was investigated. The effect of the wetting rate and the pollution severity degree were also quantified. In addition, a comparative long term test of different insulator profiles when energised by alternating and positive direct voltages under artificial pollution conditions was explored.

Both voltage and leakage current measurements were recorded using the LabVIEW data acquisition system. The stored data were then processed to calculate other significant parameters of the test results. Visual and thermal cameras were also employed to monitor the test insulator during the test time and to inspect any feature of degradation on its surface.

6.2. High voltage tests

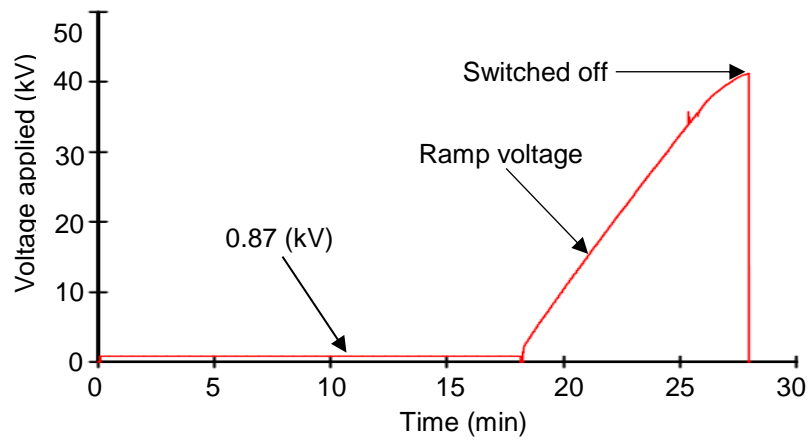
Since the performance of SiR insulators has not been fully understood, the extensive tests discussed in this chapter aimed to offer a better understanding of the performance of SiR insulators. Various designs of SiR insulators, including conventional and textured profiles, were subjected to the following tests:

- clean insulator fog test
- high voltage flashover tests with ramp control under different pollution conditions, based on tests described [2-81]
- clean-fog tests with a voltage source of 12 kV AC based on a modified version of IEC 60507 solid layer method
- clean-fog tests with a voltage source of 12 kV positive DC based on a modified version of IEC 60507 solid layer method

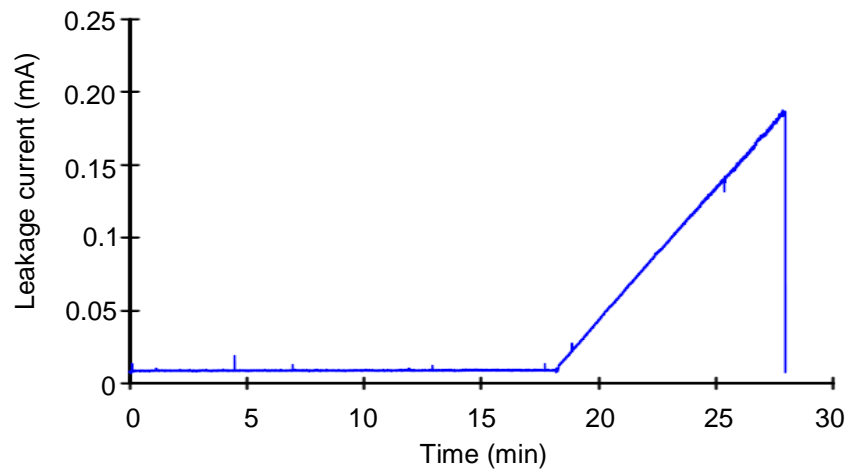
The performance of tested insulators may be well characterised if they are assessed over the same range of test conditions, such as voltage stress, pollution severity level, water conductivity and wetting rate. Several parameters were measured to provide any features of aging or surface degradation such as leakage current measurements, FOV levels, accumulated energy and visual and IR observations.

6.3. Clean insulator fog test

The main purpose of this test was to evaluate the performance of a clean SiR insulator under fog conditions and compare it with the performance of the same profile under the solid layer method. As this was a preliminary test, non-standard procedures were followed. The applied fog rate was 8 litres/hour at an air pressure of 35 psi. As shown in Figure 6.1, a voltage of 0.87 kV was applied to the insulator for 18 minutes. After that, the test voltage was increased gradually at steps of 4 kV up to 43 kV whereupon the supply voltage was switched off to avoid flashover.



(a) RMS voltage applied



(b) RMS leakage current

Figure 6-1: Voltage RMS and leakage current RMS records during a clean SiR insulator fog-test.

The insulator has shown a lower leakage current value, and no discharge activities or actual flashover events were observed below 40 kV. However, above 40 kV, significant discharge activities were noticed and revealed by visual records, as illustrated in Figure 6.2.



Figure 6-2: Visual records of a clean SiR insulator at 42 kV.

For polluted insulators, a pollution layer is deposited on the insulator surface. When the polluted surface is wetted due to fog or rain, a conducting layer is formed and the leakage current passes over the surface. After several stages, this leakage current may ultimately lead to flashover, as will be explained in the next section.

6.4. High voltage flashover tests with ramp control under different pollution conditions

The flashover phenomenon is one of the most complex problems observed in high voltage outdoor insulators. This phenomenon occurs due to several reasons, such as diverse pollution severity in different environments, non-uniform pollution distribution along the insulator surface and the difficulties of modelling the complex form of the insulator [6-3].

Under harsh environmental conditions, where the surface of the polluted insulator is affected by dew and mist deposition as well as fog and/or rain, a film of water is formed and the leakage current flows through the surface. The leakage current begins to dry the pollution layer on the insulator surface, and this leads to dry band formation. Continued wetting accompanied by dry band formation creates partial arcs. These arcs extend along the insulator profile and may eventually cause the flashover event [6-3]. In this way, the performance of a polluted insulator may be characterised by the FOV and the flashover current. In general, the progression of the pollution flashover event may be processed into five main stages:

- i. build-up of the conductive layer
- ii. dry-band formation
- iii. partial arcing
- iv. arc extension on the surface
- v. eventual arc expansion to the entire insulator followed by flashover [6-4]

In Chapter 5, the influence of the surface layer conductance on the flashover level for a selected design was determined. This was very important since the controlled of the increasing the layer conductance could be reduced significantly the flashover voltage. In this chapter, a comparative study between the flashover performance of conventional and textured SiR insulators is conducted. The effects of several factors (pollution severity, wetting rate and insulator shape) are investigated.

6.4.1. Test classification

High voltage tests were conducted to explore the flashover performance of 11kV SiR polymeric insulators. These tests were carried out on different insulator designs under various pollution conditions, as illustrated in Figure 6-3.

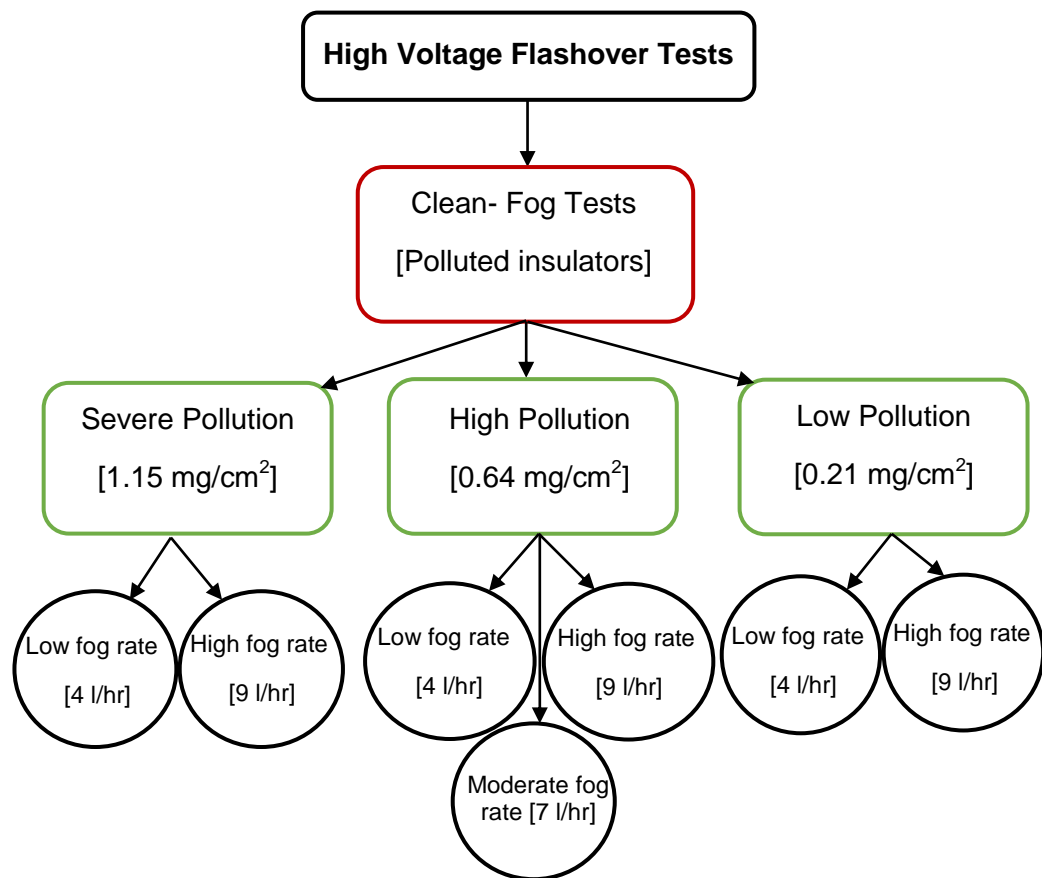


Figure 6-3: High voltage flashover tests

6.4.2. Test techniques

The technique of a high voltage ramp test was carried out as proposed by colleagues in the research group [2-81]. The rate of the increase of the actual test voltage was 4 kV/minute. This rate was sufficient to cause a flashover event within 5 to 10 minutes. The voltage supply was interrupted immediately by the circuit breaker at the instant of the flashover event (over-current protection).

The procedure of high voltage flashover ramp test can be summarized as follows:

1. Conventional and textured SiR insulators were tested in the fog chamber at the same pollution severity level.
2. At the beginning of the test, a minimum voltage of 0.87 kV was initiated using a Hipotronics AC system, after which, the voltage was controlled by a program to follow a predetermined voltage ramp of 4 kV/minute.
3. The fog generation in the chamber room was started simultaneously with the application of the test voltage and was kept running until the termination of the test.
4. At the instant of the flashover event, the circuit breaker interrupted the voltage supply.
5. The test insulator was then left to cool down for 5 minutes, after which a new ramp test was initiated until the required number of FOVs was achieved.
6. The RMS voltage was viewed on a digital display control panel and the voltage waveform was recorded through an RC-divider. The current measurement and protection consisted of a leakage current measurement (shunt resistor) within parallel branches of back-to-back high power Zener and Schottky diodes and a gas discharge tube, which together suppressed any overvoltage that could occur, and it protected the data acquisition card (DAQ).

7. The data acquisition system monitored and recorded the voltage and leakage current waveforms using a developed LabVIEW program on a personal computer.
8. During the ramp test, the infrared and video cameras were triggered to investigate any flashover actions and discharge activities on the insulator surfaces.
9. After the termination of the test, the insulator was cleaned thoroughly and left for at least for 24 hours to get full recovery of its hydrophobicity. Then, the insulator was re-polluted to be ready for the new test.

6.4.3. Flashover performance of tested insulators

For the flashover series tests, the voltage was applied at a fixed rate of increase (4kV/min) until an FOV event occurred. For each test series, the polluted insulator was subjected to a number of sequential ramps consisting of between 4 and 12 flashovers. The longer number of ramps was conducted to investigate the influence of layer wetting and pollution reduction on the FOV. Figure 6-4, shows the mean curve of 4 ramp test series for a CONV SiR insulator used suspension of salinity with volume conductivity 11.2 S/m and a fog rate of 8 l/h.

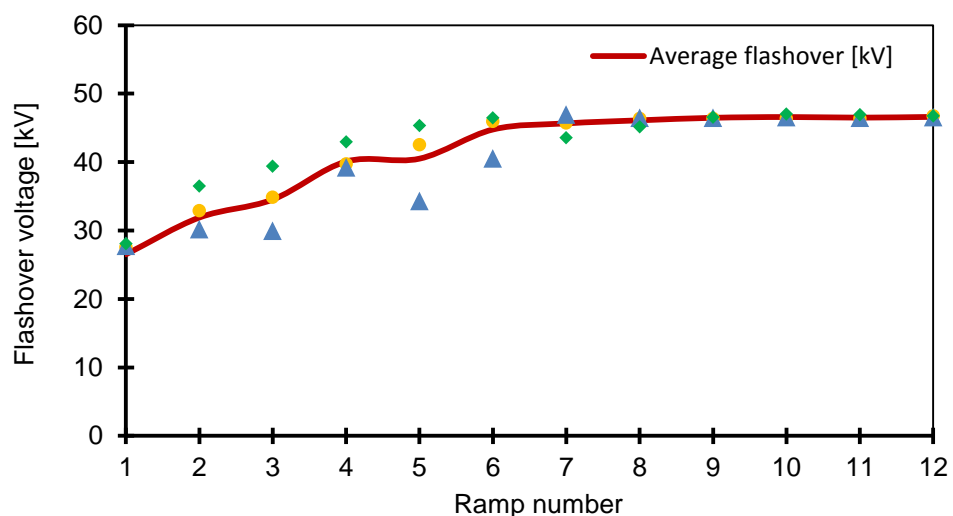


Figure 6-4: Mean FOV curve of 4 ramp voltage test series for a conventional SiR insulator. Each ramp test series consisted of 12 flashovers.

Each ramp voltage test series consisted of 12 flashovers. The flashover voltage gradually increases from 26 kV for each series test reaching to 45 kV at the 12th flashover shot. However, from the 8th flashover, the curves become more stable and the flashover voltage remained constant in the level of 45 kV.

The trend of the mean curve shows that the insulator is most susceptible at the first flashover shot where the lowest FOV is noticed, the pollution layer is entirely wet and the resistance minimum. For the following flashover shots, the flashover voltage level was steadily increased due to the washing effect on the pollution layer of the insulator surface. From the 8th until the 12th flashover shots, a considerable amount of the pollution layer was removed due to the prolonged exposure to the fog.

For this reason, only the early flashover events were considered for evaluating the flashover performance. The first four flashovers are very important as they simulate the service line conditions where a contaminated insulator is gradually wetted by an early morning fog. The FOV results reported in Table 6-1 were all obtained as the mean value from the first four flashovers.

Several difficulties were encountered when measuring the FOV on hydrophobic surfaces like SiR. These difficulties were caused by variations in the fog temperature, air density, and pollution layer status and, therefore, may have affected the test conditions.

Despite that variability, good reproducibility was achieved on the FOV results. The FOV dependency on the pollution severity level (ESDD) is quantified as will be clarified in the next section. The influence of SiR profiles and wetting rate on the mean FOV are also performed.

Table 6-1: High voltage Flashover tests results

Test conditions	Insulator profile	Number of test series	Total number of flashovers	Mean flashover voltage (kV)	Standard deviations	FOV level improvement compared with CONV
Severe pollution (1.15 mg/cm ²) lower fog rate (4 l/h)	CONV	2	8	25.8	3.2	-----
	TTS4	2	8	27.5	3.3	6 %
	TT6	1	4	27.6	2	6 %
Severe pollution (1.15 mg/cm ²) higher fog rate (9 l/h)	CONV	4	16	31.7	4.3	-----
	TTS4	4	16	34.5	4.3	8 %
High pollution (0.64 mg/cm ²) lower fog rate (4 l/h)	CONV	3	12	26.4	6.6	-----
	TT6	3	12	30.6	2.5	14 %
High pollution (0.64 mg/cm ²) moderate fog rate (7 l/h)	CONV	4	16	31.6	7	-----
	TT6	3	12	33.2	9	5 %
High pollution (0.64 mg/cm ²) higher fog rate (9 l/h)	CONV	4	16	32.4	8	-----
	TT6	4	16	34.0	9.2	5 %
Lower pollution (0.21 mg/cm ²) lower fog rate (4 l/h)	CONV	2	8	33.7	2.5	-----
	TT6	2	4	40.0	5.7	16 %
Lower pollution (0.21 mg/cm ²) higher fog rate (9 l/h)	CONV	3	12	40.4	9	-----
	TT6	1	4	40.8	2.9	1 %

For all insulators, the results showed that the textured insulator designs exhibit an increased flashover performance compared with conventional non-textured insulators. As can be seen in Table 6-1, textured insulators can offer an increased FOV performance up to 16 % in the case of the TT6 design compared with the average FOV of the conventional insulator under conditions of low pollution (0.21 mg/cm²) and low fog rate (4 l/h). The same performance of the TT6 design was also observed under higher polluted (0.64 mg/cm²) conditions with a lesser improvement of the flashover level reached to 14 %.

The performance TT6 insulator design under the conditions of the severe pollution (1.15 mg/cm²) and lower wetting rate (4 l/h) was significantly decreased compared with its performance in the cases of high and low pollution conditions. Nonetheless, it still improved the flashover voltage level by 6 % compared with the conventional design. This could be indicating to the effectiveness of the textured insulator design for improving the FOV performance even under harsh ambient conditions.

6.4.4. The influence of pollution severity level on the flashover of SiR insulators

In order to investigate the influence of the pollution severity level on the FOV, several voltage ramp test series were conducted on a CONV SiR insulator. The tests used suspensions consisted of kaolin, Triton X-100 and three different salinities with volume conductivities of 4, 11.2, and 20 S/m. The higher wetting rate of 9 l/h was selected for the tests. Each test series consisted of four consecutive flashovers, as illustrated in Figure 6-5, for 0.21, 0.64 and 1.15 mg/cm² ESDD levels.

It can be seen that the FOV trend for the 0.21 mg/cm² ESDD level is substantially higher if compared with the curves obtained by adopting 0.64 and 1.15 mg/cm² ESDD levels; all tests were conducted using the same wetting rate, which was equal to 9l/h. The average flashover voltage for the case of 0.21 mg/cm² was approximately 26 % higher than that obtained for the level of 1.15 mg/cm². This flashover voltage was also increased by 20 % compared with that attained under the case of 0.64 mg/cm². The flashover voltage was significantly decreased with the increase of the pollution layer conductance that was associated with the controlled wetting of the layer. The flashover was found to steadily recover due to the pollution layer washing.

Unlike the case of lower pollution (0.21 mg/cm²), a severely polluted layer (1.15 mg/cm²) has an influence on the FOV, and the lowest values of all test series were obtained. The average flashover voltage for the 1st flashover shot was 27.5 kV whereas, for the case of lower pollution condition, the mean FOV was 34 kV. For this case, it was more important to select an appropriate fog rate to improve the FOV performance, especially at the severely polluted conditions.

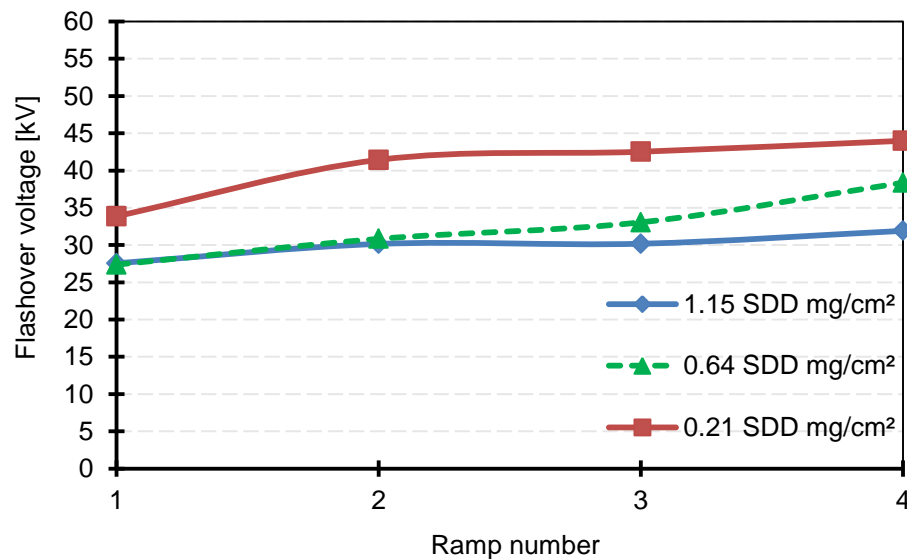


Figure 6-5: Ramp voltage test series for fog rate 9 l/h: effect of pollution severity level on FOV. Red curve ESDD 0.21 mg/cm², Green curve 0.64 mg/cm², and Blue curve 1.15 mg/cm².

6.4.5. Flashover voltage (FOV) variation with salt deposit density (ESDD)

This test was performed on two different SiR insulators with conventional non-textured design (CONV) and with textured trunk profile (TT6) at fog rates of 4 and 9 l/h. The test was carried out using ESDD values of 0.21, 0.64 and 1.15 mg/cm². As shown in Figure 6-6, the mean FOV decreases as the pollution degree increases and this was revealed in all the ramp tests and with both wetting rates. The mean flashover curve for the CONV insulator is consistently lower than that of the TT6. The average FOV for the TT6 insulator in the case of the lower pollution level (0.21 mg/cm²) and the fog rate of 4 l/h was 40 kV, a value 16 % higher than 33.7 kV found for the CONV insulator. For the case of the higher pollution condition (0.64 mg/cm²), the average flashover voltage for the TT6 insulator was 30.6 kV, 14 % higher than the CONV insulator. These results show that the improvement in FOV of the textured design is greater compared with the conventional, and this effectively raised the lowest FOV values.

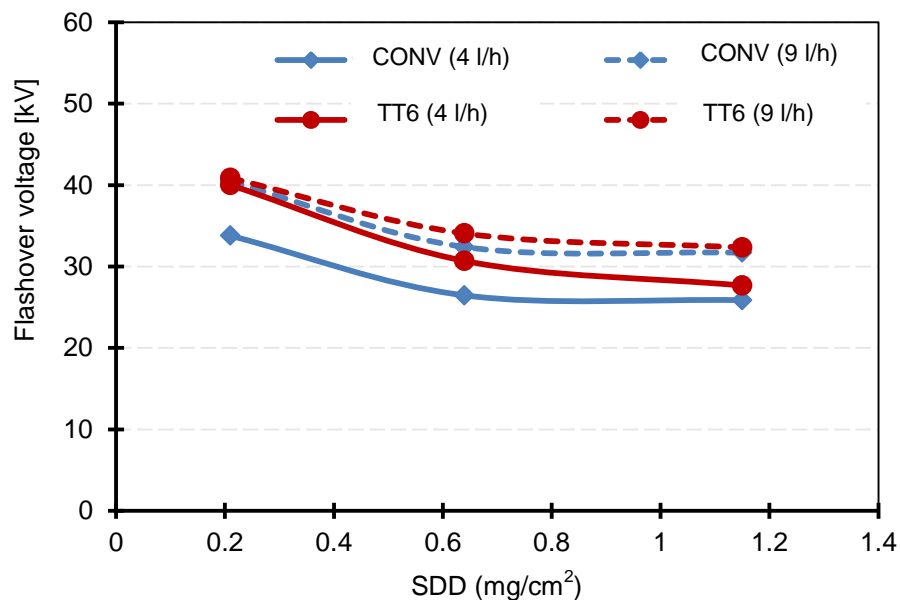


Figure 6-6: FOV variation with ESDD value at fog rates of 4 and 9 l/h using CONV and TT6 insulators.

6.4.6. The influence of the wetting rate on the flashover of SiR insulators

Two SiR insulator designs with a smooth conventional surface (CONV) and with a textured pattern (TT6) were used in this study. The insulators were tested under the same polluted condition with ESDD value of 0.64 mg/cm^2 and different fog rates of 4, 7, and 9 l/h. For each insulator design, a series of three tests was conducted, and each test had four flashover ramps. Figure 6-7 shows the average FOV value obtained at each ramp event. It can be observed from the figure below that the FOV of the CONV insulator under a fog rate of 9 l/h is 9 % higher than that value obtained under a low fog rate of 4 l/h. The same trend of this growth is also observed for the TT6 insulator and a 30 % increase in the flashover voltage is recorded.

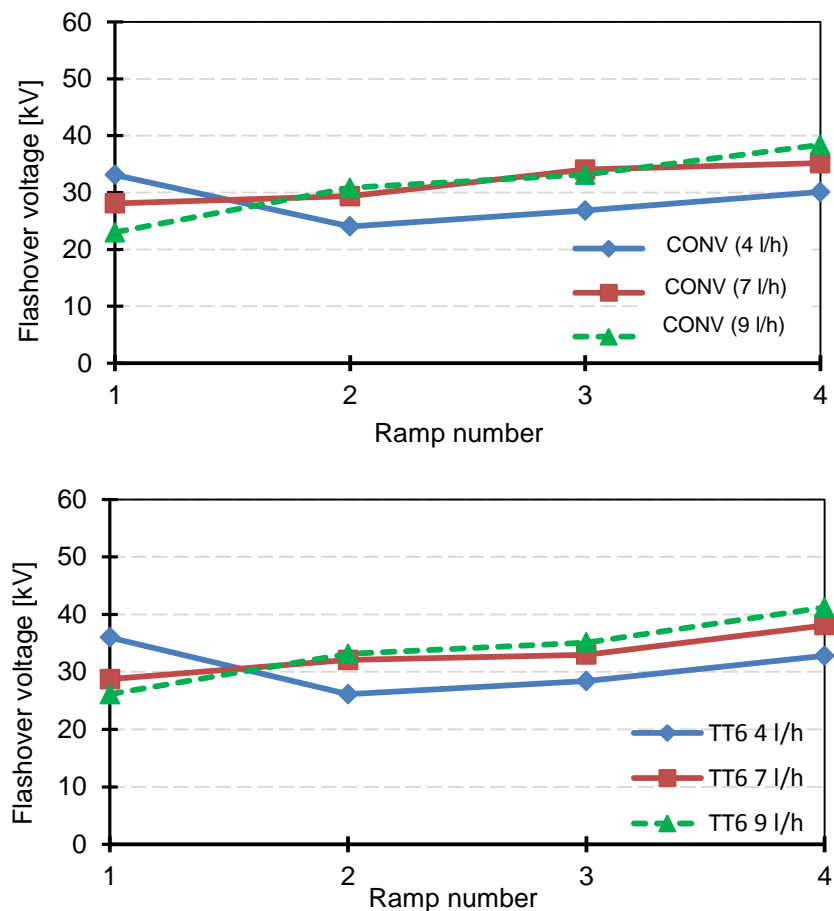


Figure 6-7: Average FOV of 3 test series for CONV and TT6 SiR insulators: effect of wetting rate on FOV. ESDD 0.64 mg/cm^2 . Fog rates 4, 7 and 9 l/h.

It can be seen that the FOV level in the case of 4 l/h does not gradually increase with the testing time but is characterised by a U-trend. In this trend, the second FOV ramp always had the lowest value over the FOV curve. This is because the lower fog rate gives sufficient time for wetting the pollution layer completely. Next, a stable increase in FOV is observed with subsequent ramps similar to the moderate and high fog rate effects.

Regarding the wetting rate impact on the FOV level, the mean FOV of 32.4 kV and 34 kV for CONV and TT6 insulators are greater than those values of 26.4 kV and 30.6 kV obtained under the lower fog rate condition. This result gives an indication that the average FOV is substantially affected by the higher fog rate for both insulator profiles. Furthermore, a greater improvement was gained on the mean FOV under textured design. Therefore, it is essential to choose a suitable fog rate and an appropriate insulator shape to improve the FOV performance of SiR insulators.

6.4.7. Electrical properties calculated associated with FOV

The acquired data of the leakage current and voltage applied waveforms were processed using the LabVIEW program to calculate the other electrical parameters of the test results. These parameters made it possible to characterise each insulator profile and obtain useful information.

Figure 6-8 illustrates the calculated electrical parameters of the root mean square (rms) of the applied voltage and leakage current, the average power dissipation, and the cumulative dissipated energy of a typical ramp voltage test series consisting of five flashover events. The figure shows the derived parameters for the first and the second FOV events (ramp 1 and ramp 2) to evaluate the behaviour of these properties during a ramp voltage test.

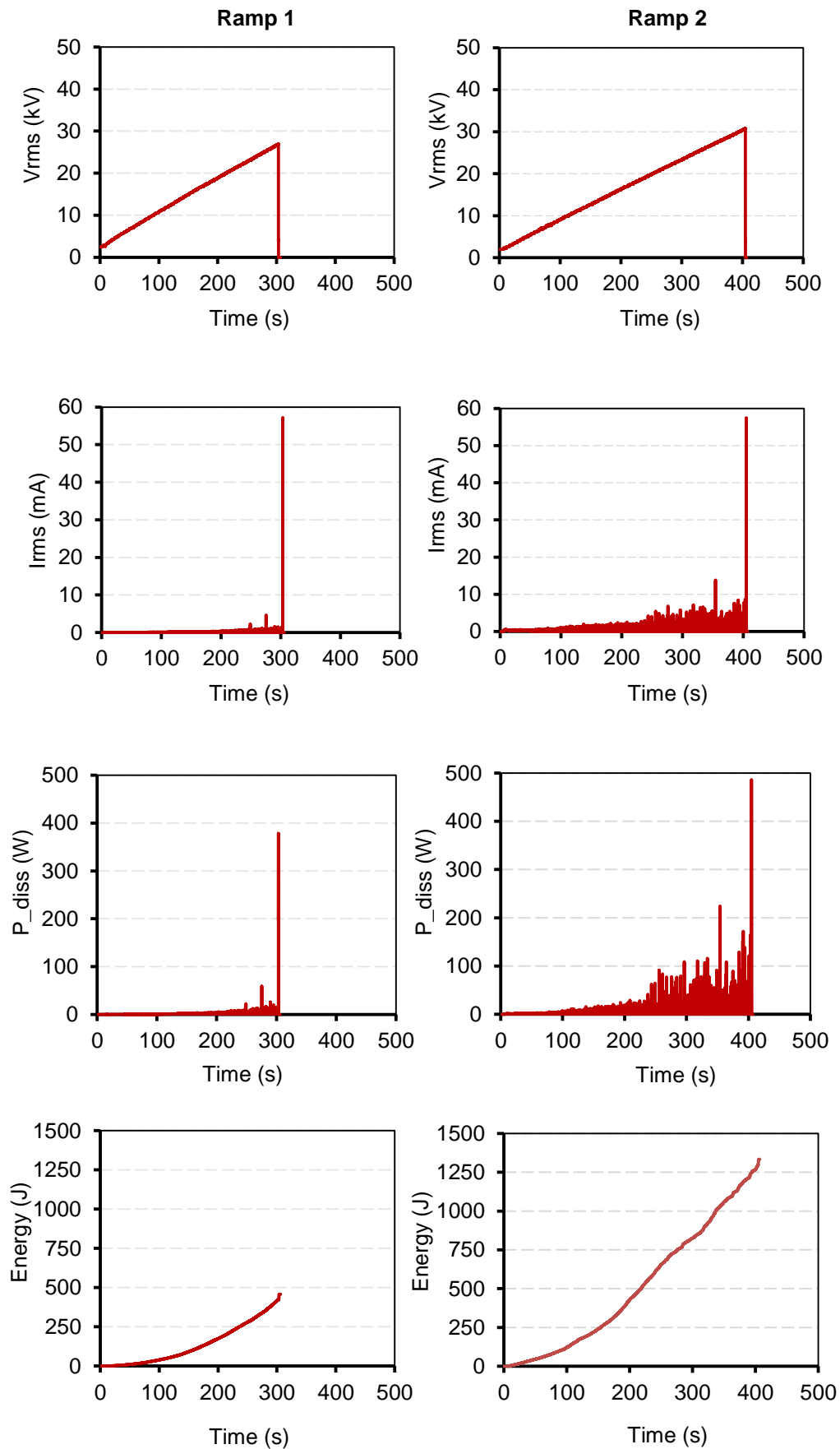


Figure 6-8: Ramp 1 and 2 of test series for CONV insulator under conditions of ESDD (0.64 mg/cm^2) and fog rate (7l/h). Ramp 1: FOV 26.96 kV at 303s; Ramp 2: FOV 30.76 kV at 407s.

As shown in Figure 6-9, the FOV gradually increased from 26.96 kV for the first FOV ramp to 30.76, 34.45, 35.91 and 38.63 kV for ramps 2, 3, 4 and 5 respectively. This growth of the FOV was correlated with the gradual washing off of the pollution layer from the insulator surface.

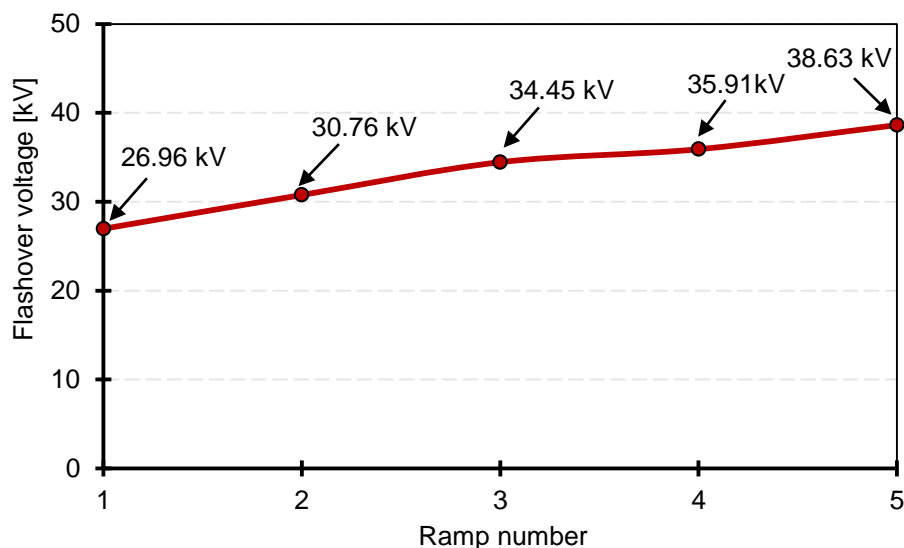


Figure 6-9: Ramp voltage test series for CONV SiR insulator under conditions of ESDD (0.64 mg/cm²) and fog rate (7 l/h).

It is clear that the insulator was most susceptible at the first FOV ramp, and this is attributed to the complete wetting of the pollution layer and the minimum leakage resistance value. For the following ramps, part of the pollution layer was gradually removed during the fog test, and earlier FOV events caused heating, both of which eventually increased the FOV.

It can be seen that the pre-flashover leakage current at the early stage of ramp tests steadily increased with time as the test voltage increased (Figure 6.8). However, it becomes obvious that, for later ramps, where the pollution layer was progressively washed off the insulator, the leakage current at a certain level of voltage gradually decreased. This confirms an inverse relationship between the leakage current and the FOV.

The average power dissipation in the pre-flashover event was significant. The maximum values were obtained in the range between 150 W to 1400 W.

6.4.8. Visual observations of pre-flashover

As shown in Figure 6-11, subsequent captures of discharge activities were recorded using a digital camera during the flashover ramp test. These activities were observed before the flashover event at the voltage level of 34.45 kV.

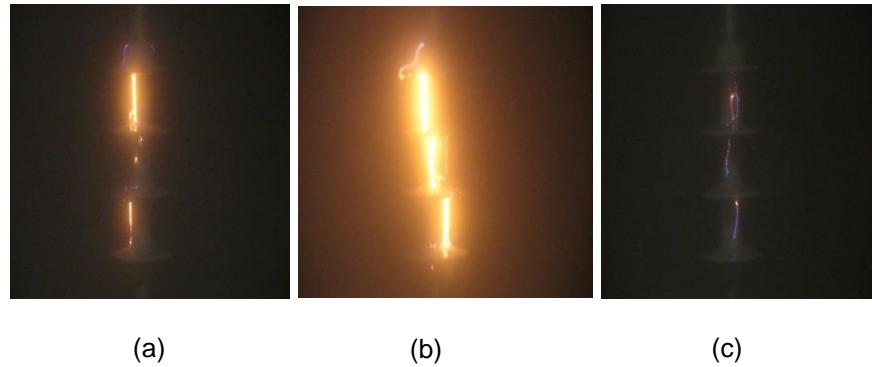


Figure 6-11: Captures images of the conventional insulator during flashover fog test at 32 kV: (a) sparks bridging part of insulator trunk (b) bridging of sheds (c) small streamer discharges.

It is clear from the visual images that the insulator was subjected to severe discharges activities prior to the FOV event. The sparking bridging part of the insulator trunk and the bridging of shed surfaces due to water droplet and streamer discharge activities were clearly revealed. It was also noticed that the frequency of the spark discharges decreased as the voltage reached the flashover event.

6.5. Performance of silicone rubber polymeric insulators under AC and positive DC tests

Outdoor insulation is continuously exposed to the elements and its performance is severely affected by the weather conditions. New anti-dry band designs using textured surfaces have been proposed to achieve better performance under polluted conditions. This section reports a comparative study of SiR polymeric insulators for 11kV systems using artificial pollution tests in accordance with the clean-fog test method specified in IEC 60507. A non-textured polymeric insulator design was selected and used for comparison with an insulator with a textured

surface. Both voltage and leakage current signals were measured and digitized using a high-resolution data acquisition system. The signals were then processed to calculate the other electrical properties of the test results. The rms leakage current and the cumulative dissipated energy were selected to allow a direct comparison to be made between different insulator designs under AC and positive DC voltages. Continuous monitoring of the insulator surface using an IR camera was carried out to evaluate the temperature distribution along the insulator profile and so identify the formation and location of dry regions on the insulator surface.

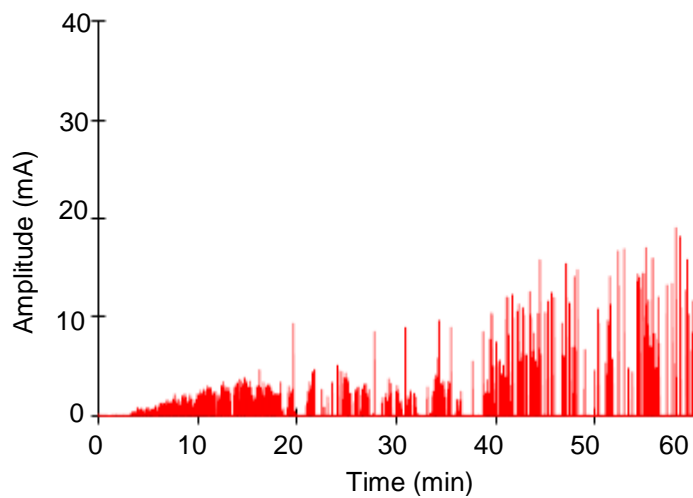
6.5.1. Artificial pollution of tested insulators

SiR insulators with non-textured and textured designs were polluted based on a modified procedure of the IEC 60507:2013 solid layer method, as defined in section 3.7.2. The pollution suspension consisted of tap water (1l), Triton X-100 wetting agent (1 g), kaolin (40 g/l) and an adequate amount of sodium chloride (366 mg) to achieve a volume conductivity value of 11.2 S/m. This value of volume conductivity was chosen as a value that represented heavy pollution conditions. The fog generation rate used was equal to 4 l/h. This rate is sufficient to achieve the maximum conductance of the pollution layer within 20-40 minutes from the instant the fog is applied. The clean insulators were polluted by pouring the contamination onto the insulator surface, ensuring the application on all parts of the insulator surface. Then, the insulator was left to dry for at least 24 hours. The insulator was then mounted in the fog chamber and tested for one hour.

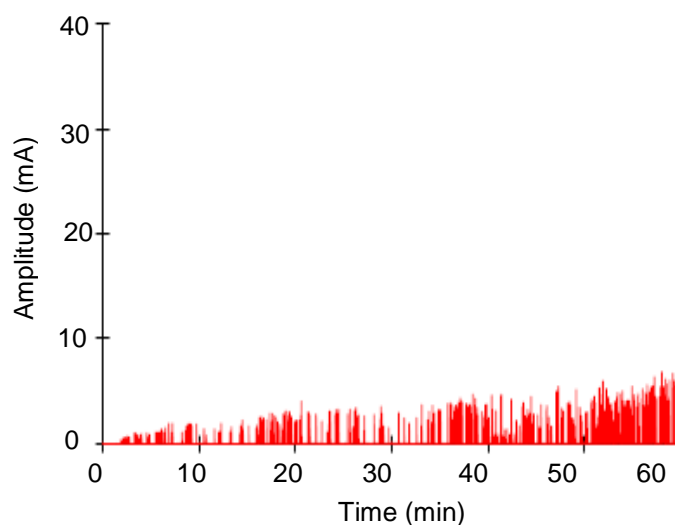
6.5.2. HVAC clean-fog test results

(a) RMS leakage current

Figure 6-12 shows the typical variations of rms leakage current measured for the two insulators. As described earlier, each insulator was tested for one hour. The results show that the amplitude of leakage current generally increases with testing time for both insulators. However, the leakage current magnitudes are greater for the conventional insulator compared with the textured insulator reaching to 17 mA at the end of the test. The maximum leakage current recorded for the textured insulator is lower than 8 mA.



(a) Conventional



(b) Textured

Figure 6-12: Typical variations of rms leakage current for conventional and textured insulators.

(b) Cumulative dissipated energy

Figure 6-13 illustrates the total cumulative dissipated energy for both insulators under AC excitation during the one-hour test. The curve trends for both designs are similar. However, the dissipated energy is much higher by 45 % for the conventional design compared with the textured insulator, reaching 4 kJ at the end of the test.

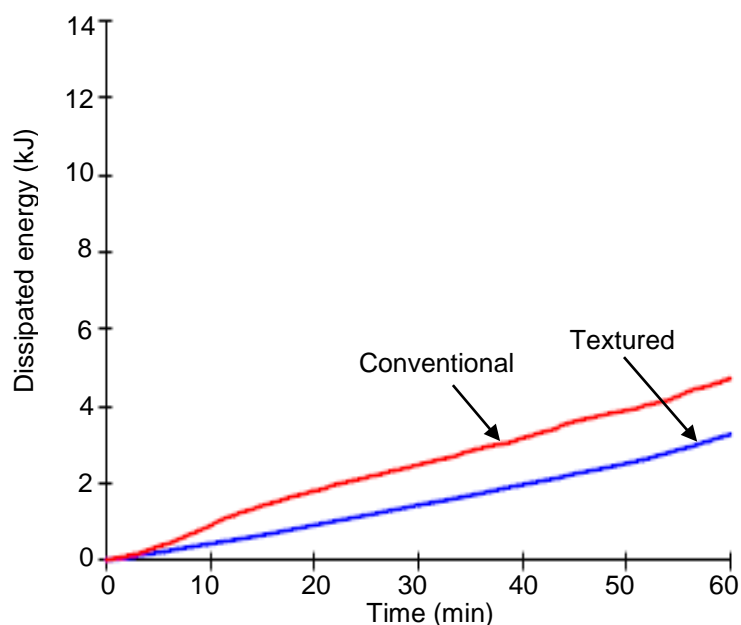
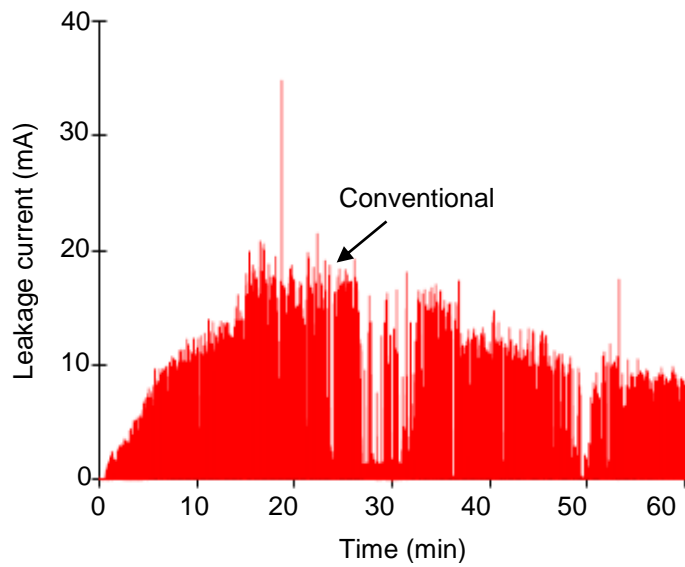


Figure 6-13: Total cumulative dissipated energy during one-hour test under AC energization.

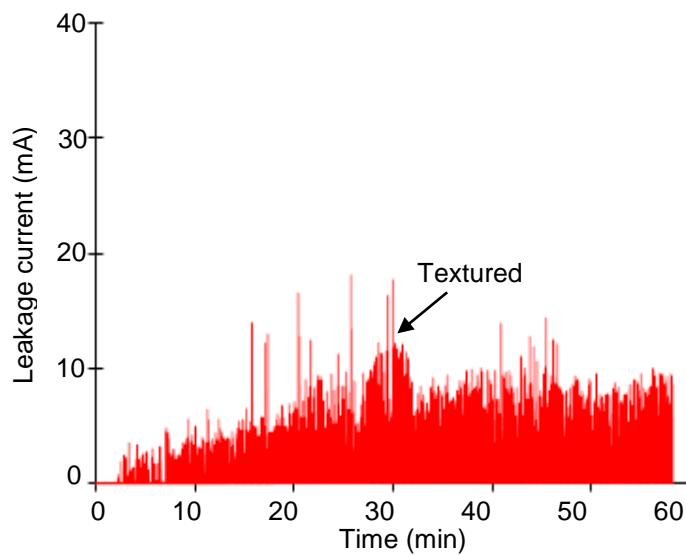
6.5.3. HVDC clean-fog test results

(a) Leakage current

As can be seen in Figure 6-14, the typical variation of leakage current is shown for the two insulators. Both insulators showed a significantly high current during the test. However, the conventional surface exhibited a higher current than did those measured with the textured surface at the beginning of the test. This current was relatively higher by 60 % for the conventional insulator and 50 % for the textured compared with the rms currents obtained under AC excitation. This also gives indication to the severity of the DC energisation on the insulator compared with the AC.



(a) Conventional



(b) Textured

Figure 6-14: Typical variation of leakage current under positive DC excitation.

(b) Cumulative dissipated energy

Figure 6-15 shows the total cumulative dissipated energy for the tested insulators under positive direct voltage energization for the one-hour test. The trends for both insulators are similar. However, the cumulative energy is much higher by 23 % for conventional insulator compared with the textured insulator, reaching

9 kJ at the end of the one-hour test. This result confirms the severity of DC energization for both insulator designs compared with the AC energization.

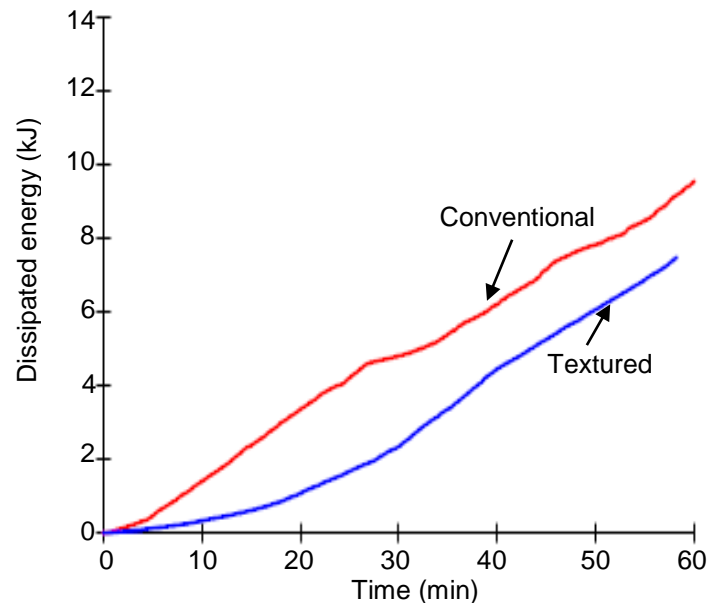


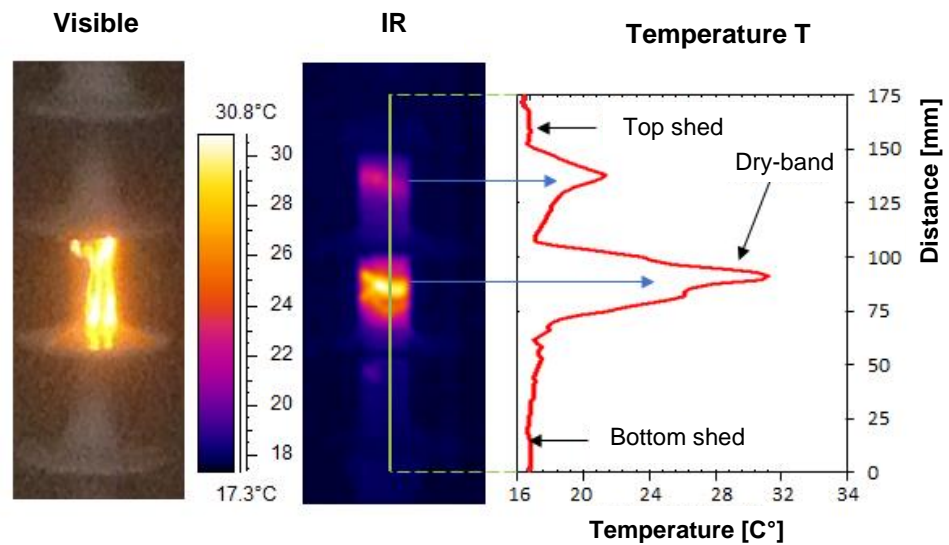
Figure 6-15: Total cumulative dissipated energy during 1-hour test under positive DC energization.

6.5.4. Visual appearance and infrared (IR) observations

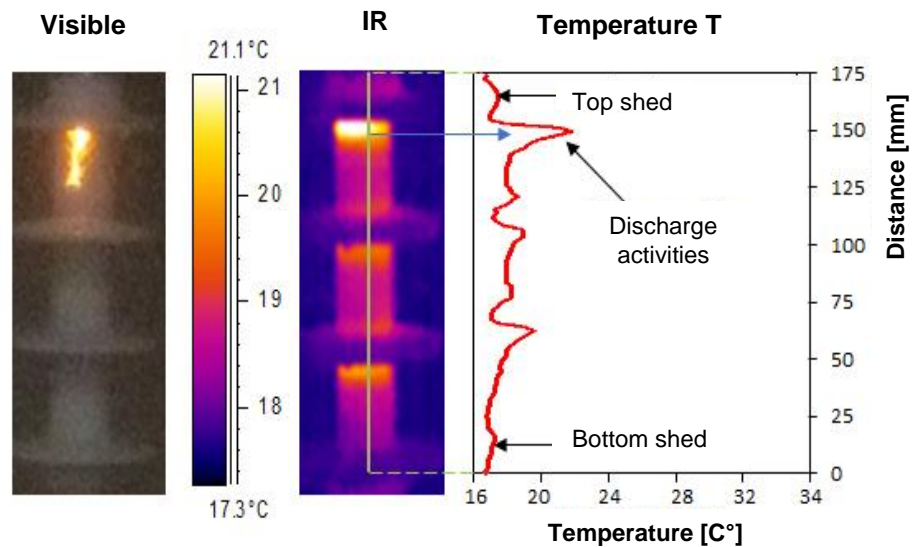
Thermal and visual video records were obtained in order to investigate any indications of aging on the surface of the tested insulators. Figure 6-16 shows a visible image with an infrared record and temperature distribution along the surface profile when a 12 kV voltage is applied to both insulators.

It is clear from the IR captures that the higher temperature was measured on the conventional insulator. The IR record clearly reveals a dry-band formation at the shank region of the conventional surface. The surface temperature profile along the insulator length indicates that the dry-band region was characterised by higher temperature, which reached approximately 31°C. The non-linear conduction behaviour seen on the leakage current over the wet pollution layer was caused by heating due to local power dissipation and drying on the insulator surface. This drying led to dry-band formation on the shank region and expanded until it formed a ring shape, which interrupted the pollution layer conduction.

When the voltage across the dry-band surface was high enough, long discharges were visible, bridging long sections of the insulator creepage length.



(a) Conventional insulator



(b) Textured insulator

Figure 6-16: Visible image, infrared record and temperature distribution along the surface profile.

In the case of a textured insulator, the discharge activity was limited and the surface temperature profile along the insulator was relatively lower compared with the conventional and the highest temperature reached was 21°C. At the end of the test, extensive changes on the insulator surface were observed. In addition, various types of surface degradation, including tracking and erosion,

were detected. As shown in Figure 6-17, surface tracking on the moulding seam of the insulator trunk could be seen. It is well known that tracking on the moulding line can cause substantial damage to a polymeric insulator under severe conditions. In addition, tracking on the surface near both energized and ground ends was also observed. The occurrence of such tracking may have been driven by the local high electric field stress.

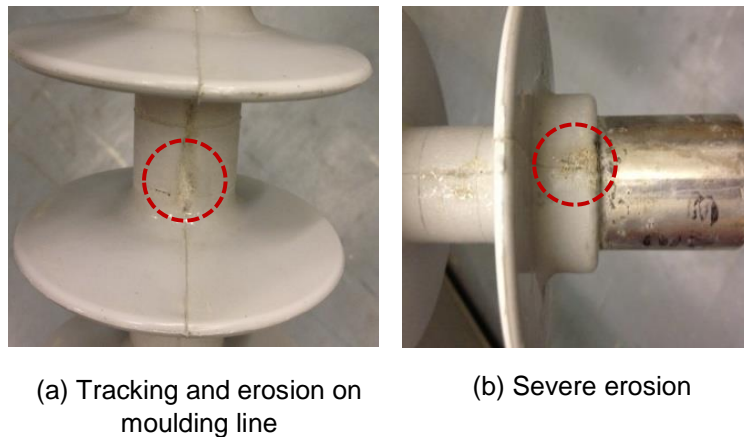


Figure 6-17: The Visual appearance of tested insulators.

6.6. Conclusion

The flashover performance of SiR insulators using clean fog tests based on the modified solid layer method was investigated. An extensive series of high voltage ramp tests under different conditions was performed to investigate the influence of the pollution severity level, wetting rate and insulator profiles on the flashover performance of SiR insulators. For the same wetting rate and insulator design, severely polluted layer has an influence on the FOV and 26 % decrease in the FOV level was found by increasing the pollution severity degree to the 1.15 mg/cm^2 .

For a similar pollution severity level, the mean FOV was substantially increased by increasing the fog flow rate for both insulator designs. An inverse relationship between the flashover voltage and the layer conductance is confirmed and revealed by the U-trend variation of the flashover. The flashover voltage was

significantly decreased with the increase of the pollution layer conductance, which was associated with the controlled wetting of the layer. The flashover voltage was found to progressively recover due to the pollution layer washing.

The flashover performance of the conventional non-textured insulators and textured insulators with different designs were investigated. Textured trunk with 6 mm designs (TT6) showed an improvement of the flashover performance which could reach 16 % compared with the conventional insulator. The same performance of this design (TT6) was also achieved under higher polluted conditions with a lesser improvement of the flashover voltage reaching 14 %. The performance of TT6 design under the severe condition was significantly reduced. It showed a lesser improvement, up to 6 %.

Current records and the electrical properties of the SiR insulator showed that the insulator was most vulnerable to the flashovers at the first ramps. This was attributed to the fully wetting of the pollution layer and the lowest leakage resistance value. For the subsequent ramps, the FOV was gradually increased due to the washing effect of the pollution layer and the heating caused by the former FOVs. This results also showed that the pre-flashover leakage current, at a certain level of voltage, steadily decreased as the FOV increased, which this confirms an inverse relationship between the leakage current and the flashover voltage.

Under AC energization, both leakage current and cumulative energy for conventional insulators were higher compared with textured insulators. The highest amplitude of the leakage current recorded for the conventional design was two times greater than that obtained on the textured. The cumulative dissipated energy was 45 % higher for conventional insulator than the textured. In addition, for both conventional and textured designs, the dissipated energy was approximately two times greater for 12 kV positive DC compared with

12 kV rms AC. This result confirms the severity of positive DC energisation compared with the AC energisation.

For each test, conventional insulator showed regular dry-band formation in the shank region, but this was not always observed for the textured insulator. Texture design was also exhibited very little evidence of discharge activities and lower surface temperature than the conventional. The other observation from the AC and DC tests was that surface degradation, including tracking and erosion, was more severe in the case of the conventional insulator design. This work showed that textured insulator designs can improve the performance of SiR polymeric insulators under AC and positive DC energisations.

CHAPTER 7: GENERAL DISCUSSIONS, CONCLUSION AND FUTURE WORK

The aim of this thesis is to improve the understanding of the performance of conventional and textured SiR insulators under different environmental conditions using AC and positive DC energisations. Discharge activities and dry band arcing events occurring on the surfaces of wet and polluted SiR insulators exposed to different conditions are also examined. The flashover performance and the pollution layer characterisation on the wet-polluted surfaces of different insulator designs are also investigated. Electrical parameters, like leakage current magnitude and accumulated energy, are used as indicators along with the thermal and visual records to assess the performance and the condition of each tested insulator surface.

In this chapter, a summary of the research conclusions is presented along with a brief discussion on the experimental results. Moreover, suggestions regarding the further work for the future research are proposed.

7.1. Performance in the rotating wheel dip tests

These tests were carried out to investigate the aging performance of SiR polymeric insulators using the rotating wheel dip test based on IEC 62730. Both AC and positive DC tests on textured and non-textured insulator designs were performed. A computerised data acquisition system was developed to monitor and save the test voltage and leakage current waveforms. Thermal and visual video records were also conducted in order to reveal any surface heating on the insulator surfaces due to the discharge activity and dry band formation. Surface hydrophobicity tests were performed as described in the STRI hydrophobicity classification guide. To evaluate the localised surface conductance measurement and its variation trends on each insulator surface, an IEC 60507 conductance meter with a spherical probes design was utilised.

The long-term results of the RWDT showed that the textured insulator design has a superior electrical performance in comparison with the conventional design under AC and positive DC energisations. Textured insulator profiles have enhanced surface properties against tracking and erosion with only a minimum loss of material observed. This performance enhancement is attributed to the reduction of the surface current density, which leads to a reduction in the drying and the discharge activity on the insulator surface.

Discharge activity occurring on the hydrophobic surfaces of SiR insulators was investigated. Records using a thermal infrared camera showed that a higher temperature was observable on the conventional surface. Due to a temporary loss of hydrophobicity, leakage current may increase, and the SiR surface is subsequently degraded by the development of dry band arcing. Dry band arcing induces hot spots, which may cause secession of the chemical composition at the surface and, therefore, accelerate the degradation of SiR materials. Continued discharge activity reduces the number of LMW chains on the surface. These changes may lead to a further loss of hydrophobicity, thereby, decreasing the electrical performance.

Textured surface designs also exhibited a lower increase of surface conductance during the test compared with non-textured insulators. This tendency can limit the chance of flashover events and improve overall insulator performance.

The symmetrical model of an 11 kV SiR insulator has been developed for computational studies. The simulation results revealed the high field regions along the leakage path of the insulator with a good correlation with the practical observations on discharge activities. These results also provide useful information about surface heating that could be used to predict the formations of the dry band over the insulator surface.

7.2. Artificial pollution layer characterisation over the insulator surfaces

SiR insulator designs with 4-shed insulators with flat conventional surfaces and with textured patterns (TT or TTS) were polluted based on a modified version of the IEC 60507 solid layer method. The pollution suspension was modified by adding a non-ionic wetting agent (Triton X-100) to increase the wettability of the hydrophobic SiR surface and to improve the uniformity of the pollution layer across the insulator surface.

Based on the clean fog testing method, extensive tests were carried out to characterise the behaviour of the insulator surfaces under different conditions. ESDD and NSDD parameters were determined for different materials and the performance of the conventional design and for first time on the textured design were also assessed. For leakage conductance evaluation, several low voltage tests using AC and positive DC excitations were conducted.

The results of these tests demonstrated that the textured surface design shows a significant improvement in reducing the pollution deposition on the insulation surface. Textured surfaces on rectangular samples do not considerably increase the accumulation of pollutant. This was observed during the ESDD evaluation with an artificial layer, and the increase in dimple size (6 mm). The ESDD values measured for the TXT6 samples were three times lower than that obtained for the CONV samples at different volume conductivities. This confirms that the dimple size of the textured surface has a significant effect on the removal of the contaminant deposition.

In 4-shed insulators, the two materials of SiR insulation has shown very similar ESDD values confirming that the Triton X-100 wetting agent temporarily removing the hydrophobicity properties. Furthermore, textured designs have presented comparable ESDD value with the conventional insulators.

Under both AC and DC voltage tests, the maximum leakage conductance of the tested insulators was measured and an interesting trend of layer conductance was observed with textured designs. This trend was significantly delayed the wetting and this could be useful to delay the growth of the leakage current formation on the insulator surface, thereby, improving the electrical performance.

7.3. Performance under clean fog

7.3.1. Tests procedures

The test procedures for polymeric insulators have been presented based on the proposed test procedure of IEC 60507 solid layer method for ceramic insulators. Extensive tests were carried out to investigate the performance of SiR insulators. These tests included the clean insulator fog tests, the high voltage flashover ramp tests and the clean fog tests with voltage sources of AC and positive DC energisations.

For the former test, the test voltage of 0.87 kV was applied to the insulator for 18 minutes. Then, the test voltage was increased steadily at steps of 4 kV up to 43 kV at which the supply voltage was switched off to avoid flashover. For the method of high voltage ramp, tests were conducted to investigate the flashover performance of SiR insulators by increasing the applied voltage at a rate of 4 kV/min. This increasing rate was sufficient to cause a flashover within 5 to 10 minutes. Tests were performed in a sequence of four voltage ramps, with each ramp completed by the occurrence of a flashover event. The comparison of SiR polymeric insulators for 11kV systems using artificial pollution tests was also investigated. The clean insulator was polluted based on the pollution suspension proposed by Cardiff University. The insulator was left to dry for at least 24 hours then it mounted for the fog chamber and tested for one hour under AC and positive DC energisations.

For the clean insulator fog test, a withstand voltage of the standard insulator was recorded within 30 minutes. No discharge activities or actual flashover events were observed below 40 kV. However, above 40 kV, significant discharge activity was detected and revealed by visual records. The flashover ramp voltage test method was very replicable with consistent results were obtained. The performance under various test conditions was evaluated. Several parameters, such as the leakage current, and the flashover voltage levels, were determined from the experimental measurements to identify any features of aging. Measuring the leakage current and applied voltage waveforms for the full range of the high voltage tests using LabVIEW program allowed the calculation of further electrical parameters. These parameters made it possible to characterise each insulator design and obtain useful information.

Observations using the thermal and visual cameras were also recorded. These recordings provided useful information for the development of discharge activities on the insulator surface and the growth of dry band formation on the silicone rubber insulators.

7.3.2. High voltage ramp tests conclusions

The flashover performance of SiR polymeric insulators during the clean fog tests was investigated. An extensive series of high voltage tests under different conditions was performed. A comparison between the ramp voltage series of conventional (CONV) and 6 mm textured trunk (TT6) insulator designs was performed. The effect of the wetting rate and the pollution severity levels were also investigated.

For the same wetting rate of 9 l/h and the same insulator profile, severely polluted layer has an influence on the flashover voltage (FOV) and 26 % reduction in the FOV was obtained by increasing the pollution degree to the 1.15 mg/cm².

For a similar pollution severity level of 0.64 mg/cm^2 , the mean FOV was significantly increased by increasing the wetting rate for both insulator designs. The average FOV of the CONV insulator at fog rate of 9 l/h was 9 % larger than that obtained under 4 l/h. This growth of the FOV was also obtained for the TT6 insulator and a 30 % increase was achieved. An inverse relationship between the flashover voltage and the layer conductance was found and revealed by the U-curve variation of the flashover. The flashover voltage was substantially decreased with the increase of the pollution layer conductance, which was related with the controlled wetting of the layer. The flashover voltage was found to steadily recover due to the washing effect of the pollution layer. Therefore, the wetting level was found to play an important role in determining the flashover voltage of SiR insulators.

Textured trunk insulators made of 6 mm designs showed an improvement of the flashover performance which might reach 16 % compared with conventional insulators. The same effectiveness of this design (TT6) was also revealed under higher polluted conditions with a lesser improvement of the flashover voltage reaching 14 %. The performance of TT6 design under harsh polluted conditions was considerably reduced. It showed a lower improvement, up to 6 %.

Current measurements and the electrical parameters of the SiR insulator showed that the insulator was most susceptible to the flashover events at the first ramps. This was attributed to the fully wetting of the pollution layer and the smallest leakage resistance value. For the following ramps, the FOV was gradually increased due to the longer exposure of the pollution layer to the washing effect and to the heating caused by the preceding FOVs. This results also revealed that the pre-flashover leakage current, at a certain level of voltage, gradually decreased as the FOV increased, which this confirms an inverse relationship between the leakage current and the flashover voltage.

The results in overall showed that the textured surface design seems to be more effective than the conventional design and can improve the flashover performance of SiR insulators.

7.3.3. Performance of SiR insulators under clean fog test using AC and DC voltages

The performance of SiR insulators was investigated using the clean fog test. Two different insulator designs were used: a conventional smooth insulator and a textured pattern design. Both leakage current and voltage signals were recorded during the test and the post processing procedure was then used to calculate the electrical parameters of the test results. The rms leakage current and the accumulated energy were selected to compare the performance of each insulator under AC and positive DC energisations. Monitoring was also undertaken using thermal and visual records of the insulator surfaces.

Under AC energisation test, the rms leakage current and the cumulative dissipated energy for the conventional insulator was relatively higher compared with the textured design. The highest amplitude of the leakage current measured for the conventional design was two times higher than that recorded on the textured. The cumulative dissipated energy was 45 % bigger for conventional insulator than the textured. Furthermore, for both insulator designs, the dissipated energy was approximately two times higher for positive DC voltage compared with rms AC voltage. This result revealed that positive DC energisation test was more severe than the AC energisation.

During the test, the conventional insulator exhibited very regular dry-band formation in the shank region, but this was not constantly observed for the textured insulator. Texture design was also shown very little evidence of discharge activities and lower surface temperature profile than the conventional. Moreover, the observation from the AC and DC tests revealed that surface

degradation, including tracking and erosion, was more severe in the case of the conventional insulator design. This work concluded that textured insulator designs can improve the performance of SiR polymeric insulators under AC and positive DC energisations.

7.4. Future work

In this study, the performance of high voltage SiR insulation materials was tested in extensive laboratory investigations under AC and DC excitations. However, further investigations are still required to improve the performance of such insulators. The following areas are proposed for future research:

- The tracking wheel test facilities at Cardiff University could be modified to facilitate the long-term testing of textured insulators using AC and DC voltages. The fog chamber could also be adapted to implement the 1000 h salt fog test. Such tests will clearly evaluate the performance of textured designs against tracking and erosions.
- High voltage ramp tests need to be expanded to investigate the flashover performance of different SiR insulator designs (including textured) using HVDC energisation.
- In the field, many complex factors and environmental conditions may affect the performance of textured SiR insulators. It is suggested that further investigations be performed to simulate severe ambient conditions, such as the accretion of ice and dust. The results obtained from both the laboratory tests and the field investigations will clarify the reliability of textured insulators for use in outdoor insulation.

REFERENCES

CHAPTER 1:

- [1-1] W. L. Vosloo, R. E. Macey and C. de Turreil. *The Practical Guide to Outdoor High Voltage Insulators*. Johannesburg, South Africa: Crown Publications CC, July 2004.
- [1-2] CIGRE C4.303, "Outdoor insulation in polluted conditions: Guidelines for selection and dimensioning part 1: General principles and the AC case," 2008.
- [1-3] T. G. Gustavsson, "Silicone Rubber Insulators: Impacts of Material Formulation in Coastal Environment", PhD thesis, Chalmers University of Technology, Sweden, 2002.
- [1-4] S. Venkataraman, R. S. Gorur, and A. P. Mishra, "Impact of weathering on flashover performance of nonceramic insulators," IEEE Trans. Dielectr. Electr. Insul., vol. 15, no. 4, pp. 1073–1080, Aug. 2008.
- [1-5] H. M. Schneider, W. W. Guidi, J. T. Burnham, R. S. Gorur, and J. F. Hall, "Accelerated aging and flashover tests on 138 kV nonceramic line post insulators," IEEE Trans. Power Deliv., vol. 8, no. 1, pp. 325–336, 1993.
- [1-6] R. S. Gorur, H.M. Schneider, J. Cartwright, Y. Beusajour, K. Kondo, S. Gubanski, R. Hartings, M. Shah, J. McBride, C. de Turreil and Z.Szilagyi, "Surface resistance measurements on non-ceramic insulators", IEEE Trans. Power Del, Vol.16, pp. 801 -805, 2001.

- [1-7] Y. Li and C. Huang, "Aging diagnosis of silicone rubber composite insulator based on conduction current test," in 2014 IEEE Conference and Expo Transportation Electrification Asia-Pacific (ITEC Asia-Pacific), pp. 1–5, 2014.
- [1-8] A. Shimada, M. Sugimoto, H. Kudoh, K. Tamura, and T. Seguchi, "Degradation mechanisms of silicone rubber (SiR) by accelerated ageing for cables of nuclear power plant," IEEE Trans. Dielectr. Electr. Insul., vol. 21, no. 1, pp. 16–23, Feb. 2014.

CHAPTER 2:

- [2-1] R. S. Gorur, E. A. Cherney, and J. T. Burnham. *Outdoor insulators, USA*: Ravi S. Gorur, 1999.
- [2-2] J. S. T. Looms. *Insulators for High Voltages*. London, United kingdom: Peter Peregrinus Ltd, 1988, pp. 2-12.
- [2-3] C. Bayliss, and B. Hardy. *Transmission and Distribution Electrical Engineering*. Oxford, UK: Elsevier Ltd, 2007, pp. 163-168.
- [2-4] F. Kiessling, P. Nefzger, J. F. Nolasco, and U. Kaintzyk, *Overhead Power Lines*. Berlin, Heidelberg: Springer Berlin Heidelberg, 2003, pp. 257-270.
- [2-5] T. Fujimura, "The evolution of porcelain insulator technology in Japan," *IEEE Electr. Insul. Mag.*, vol. 11, no. 3, pp. 26–36, May 1995.
- [2-6] E. A. Cherney, "Cement Growth Failure of Porcelain Suspension Insulators," IEEE Trans. Power Appar. Syst., vol. PAS-102, no. 8, pp. 2765–2774, Aug. 1983.
- [2-7] D. A. Swift. "Insulators for outdoor applications" in *Advances in High Voltage Engineering*, 1st ed., vol. 40. A. Haddad and D. Warne, Ed. London, United Kingdom: The Institution of Engineering and Technology, pp. 257-307, 2004.

- [2-8] P. J. Lambeth, "Effect of pollution on high-voltage outdoor insulators," *Proc. Inst. Electr. Eng.*, vol. 118, no. 9R, p. 1107, 1971.
- [2-9] H. M. Schneider, J. F. Hall, G. Karady, and J. Renowden, "Nonceramic insulators for transmission lines," *IEEE Trans. Power Deliv.*, vol. 4, no. 4, pp. 2214–2221, 1989.
- [2-10] J. F. Hall, "History and bibliography of polymeric insulators for outdoor applications," *IEEE Trans. Power Deliv.*, vol. 8, no. 1, pp. 376–385, 1993.
- [2-11] R. S. Gorur, E. A. Cherney, R. Hackam, and T. Orbeck, "The electrical performance of polymeric insulating materials under accelerated aging in a fog chamber," *IEEE Trans. Power Deliv.*, vol. 3, no. 3, pp. 1157–1164, Jul. 1988.
- [2-12] R. Hackam, "Outdoor HV composite polymeric insulators," *IEEE Trans. Dielectr. Electr. Insul.*, vol. 6, no. 5, pp. 557–585, 1999.
- [2-13] V. M. Moreno and R. S. Gorur, "AC and DC performance of polymeric housing materials for HV outdoor insulators," *IEEE Trans. Dielectr. Electr. Insul.*, vol. 6, no. 3, pp. 342–350, Jun. 1999.
- [2-14] S.Vynatheya, N.Vasudev, and R.T.Senthilkumar, "Comparative Performance of Silicone Rubber Insulators with IEC Stipulated Test Methods", 10th IEEE International Conference on the Properties and Applications of Dielectric Material, pp. 1–4, Bangalore, India, 2012.
- [2-15] E. A. Cherney, "Non-Ceramic insulators-a simple design that requires careful analysis," *IEEE Electr. Insul. Mag.*, vol. 12, no. 3, pp. 7–15, May 1996.

- [2-16] R. A. Bernstorff, "Ageing tests of polymeric housing materials for non-ceramic insulators," *IEEE Electr. Insul. Mag.*, vol. 14, no. 2, pp. 26–33, Mar. 1998.
- [2-17] R. S. Gorur, G. G. Karady, A. Jagota, M. Shah, and A. M. Yates, "Aging in silicone rubber used for outdoor insulation," *IEEE Trans. Power Deliv.*, vol. 7, no. 2, pp. 525–538, Apr. 1992.
- [2-18] R. A. Bernstorff, "Ageing tests of polymeric housing materials for non-ceramic insulators," *IEEE Electr. Insul. Mag.*, vol. 14, no. 2, pp. 26–33, Mar. 1998.
- [2-19] H. Deng, R. Hackam, and E. A. Cherney, "Low molecular weight silicone fluid content and diffusion in RTV silicone rubber coating," in *Proceedings of 1995 International Symposium on Electrical Insulating Materials*, pp. 181–184, 1995.
- [2-20] A. E. Vlastos and S. M. Gubanski, "Surface structural changes of naturally aged silicone and EPDM composite insulators," *IEEE Trans. Power Deliv.*, vol. 6, no. 2, pp. 888–900, Apr. 1991.
- [2-21] J. Mackevich and S. Simmons, "Polymer outdoor insulating materials. II. Material considerations," *IEEE Electr. Insul. Mag.*, vol. 13, no. 4, pp. 10–16, Jul. 1997.
- [2-22] J. Mackevich and M. Shah, "Polymer outdoor insulating materials. Part I: Comparison of porcelain and polymer electrical insulation," *IEEE Electr. Insul. Mag.*, vol. 13, no. 3, pp. 5–12, May 1997.
- [2-23] A. Haddad, R. Waters, H. Griffiths, K. Chrzan, N. Harid, P. Sarkar, and P. Charalampidis, "A new approach to anti-fog design for polymeric insulators," *IEEE Trans. Dielectr. Electr. Insul.*, vol. 17, no. 2, pp. 343–350, Apr. 2010.

- [2-24] R. Waters, A. Haddad, H. Griffiths, N. Harid, P. Charalampidis, and P. Sarkar, "Dry-band discharges on polluted silicone rubber insulation: control and characterization," *IEEE Trans. Dielectr. Electr. Insul.*, vol. 18, no. 6, pp. 1995–2003, Dec. 2011.
- [2-25] A. Haddad, and R. Waters, "Insulating Structures," UK Patent 2406225, 2003.
- [2-26] E. A. Cherney, "RTV silicone-a high tech solution for a dirty insulator problem," *IEEE Electr. Insul. Mag.*, vol. 11, no. 6, pp. 8–14, Nov. 1995.
- [2-27] S. M. Gubanski, A. Dornfalk, J. Andersson, and H. Hillborg, "Diagnostic Methods for Outdoor Polymeric Insulators," *IEEE Trans. Dielectr. Electr. Insul.*, vol. 14, no. 5, pp. 1065–1080, Oct. 2007.
- [2-28] K. Kunde, R. Hennings, M. Kuhl, A. Schütz, H. Jansses, and U. Stietzal, "New experience with composite insulators", in *Proc. Cigre Session 1998*, Paper No 15-206, 1998.
- [2-29] T. Kikuchi, S. Nishimura, M. Nagao, K. Izumi, Y. Kubota, and M. Sakata, "Survey on the use of non-ceramic composite insulators," *IEEE Trans. Dielectr. Electr. Insul.*, vol. 6, no. 5, pp. 548–556, 1999.
- [2-30] K. O. Papailiou, "Composite insulators are gaining ground-25 years of Swiss experience," *IEEE Transmission and Distribution Conference.*, vol. 2, pp. 827–833, USA, 1999.
- [2-31] J. Kindersberrer, A. Schutz, H. C. Karner and R. v. d. Huir, "Service Performance, Material Design and Applications of Composite Insulators With Silicone Rubber Housings", *CIGRE 33-303*, pp. 1-5, 1996.
- [2-32] J. T. Burnham and R. J. Waidelich, "Gunshot damage to ceramic and nonceramic insulators," *IEEE Trans. Power Deliv.*, vol. 12, no. 4, pp. 1651–1656, 1997.

- [2-33] T. Sorqvist and A. E. Vlastos, "Outdoor polymeric insulators long-term exposed to HVDC," *IEEE Trans. Power Deliv.*, vol. 12, no. 2, pp. 1041–1048, Apr. 1997.
- [2-34] R. G. Houlgate and D. A. Swift, "Composite rod insulators for AC power lines: electrical performance of various designs at a coastal testing station," *IEEE Trans. Power Deliv.*, vol. 5, no. 4, pp. 1944–1955, 1990.
- [2-35] R. G. Houlgate, D. A. Swift, A. Cimador, E Pourbaix, G. Marrone and P. Nicolini, "Field Experience and Laboratory Research on Composite Insulators for Overhead Lines", CIGRE Paper 15-12,1986.
- [2-36] R. S. Gorur, E. A. Cherney, and R. Hackam, "The AC and DC performance of polymeric insulating materials under accelerated aging in a fog chamber," *IEEE Trans. Power Deliv.*, vol. 3, no. 4, pp. 1892–1902, 1988.
- [2-37] S. M. Gubanski, "Properties of silicone rubber housings and coatings," *IEEE Trans. Electr. Insul.*, vol. 27, no. 2, pp. 374–382, Apr. 1992.
- [2-38] J. M. Seifert and D. Stefanini, "High Pollution Resistant Composite Insulators," *International Conference on High Voltage Engineering and Application*, pp. 32–35, 2008.
- [2-39] E. A. Cherney, R. Hackam, and K. G. Rutherford, "Chemical changes at the surface of RTV silicone rubber coatings on insulators during dry-band arcing," *IEEE Trans. Dielectr. Electr. Insul.*, vol. 1, no. 1, pp. 106–123, 1994.
- [2-40] K. A. Chaou, A. Mekhaldi, and M. Tegar, "Classification of pollution severity on insulator model using Recurrence Quantification Analysis," in *IEEE PES T&D Conference and Exposition*, pp. 1–5, 2014.

- [2-41] J. Hall and T. Paul, "Wind Tunnel Studies of the Insulator Contamination Process," *IEEE Trans. Electr. Insul.*, vol. EI-16, no. 3, pp. 180–188, Jun. 1981.
- [2-42] CIGRE Taskforce 33.04.01: "Polluted insulators: review of current knowledge," CIGRE technical brochure 158, June 2000.
- [2-43] J. H. Mason, F. R. Silva, and M. A. Sens, "DC salt-fog tests on glass and porcelain cap and pin insulators," *Dielectric Materials, Measurements and Applications, Fifth International Conference on*. pp. 139–142, 1988.
- [2-44] T. Cheng and C. Wu, "Performance of HVDC Insulators under Contaminated Conditions," *IEEE Trans. Electr. Insul.*, vol. EI-15, no. 3, pp. 270–286, Jun. 1980.
- [2-45] F. Hirsch, H. V. Rheinbaben, and R. Sorms, "Flashovers of insulators under natural pollution and HVDC," *IEEE Trans. Power Appar. Syst.*, vol. 94, no. 1, pp. 45–50, Jan. 1975.
- [2-46] T. Seta, K. Nagai, K. Naito, and Y. Hasegawa, "Studies on Performance of Contaminated Insulators Energized with DC Voltage," *IEEE Trans. Power Appar. Syst.*, vol. PAS-100, no. 2, pp. 518–527, Feb. 1981.
- [2-47] T. Cheng, C. Wu, F. Zedan, G. Elder, S. Low, J. Rippey, and G. Rodriguez, "EPRI - HVDC Insulator Studies: Part I Field Test at the Sylmar HVDC Converter Station," *IEEE Trans. Power Appar. Syst.*, vol. PAS-100, no. 2, pp. 902–909, Feb. 1981.
- [2-48] A. E. Vlastos, "Transmission line polymeric insulators leak currents and performance", 1992 Cigre Session, paper 15-401, 1992.
- [2-49] K. Naito, "Special aspects of insulators for dc transmission lines and stations", *Int. Colloquium on DC Power Transmission, Cigre Indian National Committee*, 1991.

- [2-50] R. S. Gorur, J. Montesinos, L. Varadadesikan, S. Simmons, and M. Shah, "A laboratory test for tracking and erosion resistance of HV outdoor insulation," *IEEE Trans. Dielectr. Electr. Insul.*, vol. 4, no. 6, pp. 767–774, 1997.
- [2-51] W. T. Starr, "Polymeric outdoor insulation," *IEEE Trans. Electr. Insul.*, vol. 25, no. 1, pp. 125–136, 1990.
- [2-52] R. S. Gorur, E. A. Cherney, and R. Hackam, "Polymer insulator profiles evaluated in a fog chamber," *IEEE Trans. Power Deliv.*, vol. 5, no. 2, pp. 1078–1085, Apr. 1990.
- [2-53] R. A. Ghunem, S. H. Jayaram, and E. A. Cherney, "Erosion of silicone rubber composites in the AC and DC inclined plane tests," *IEEE Trans. Dielectr. Electr. Insul.*, vol. 20, no. 1, pp. 229–236, Feb. 2013.
- [2-54] T. Taniguchi, M. Watanabe, Y. Watanabe, S. Mori, A. Watanabe, and K. Naito, "Electrolytic corrosion of metal hardware of HVDC line and station insulators," *IEEE Trans. Power Deliv.*, vol. 6, no. 3, pp. 1224–1233, Jul. 1991.
- [2-55] I. M. Crabtree, K. Mackey, K. Kito, K. Naito, A. Watanabe, and T. Irie, "Studies on Electrolytic Corrosion of Hardware of DC Line Insulators," *IEEE Trans. Power Appar. Syst.*, vol. PAS-104, no. 3, pp. 645–654, Mar. 1985.
- [2-56] A. W. Bardeen and J. M. Sheadel, "Corrosion as It Affects Insulator and Conductor Hardware [includes discussion]," *Trans. Am. Inst. Electr. Eng. Part III Power Appar. Syst.*, vol. 75, no. 3, p. 1–, Jan. 1956.
- [2-57] J.J. Taylor and A.D. Lantz, Jr., "Insulator Design and Application as Influenced by Difficult Service Environments", *CIGRE Paper*, No. 211, 1960.

- [2-58] C. A. O. Peixoto, L. Pargamin, G. Marrone, and G. Carrara, "Failure of transmission line cap and pin insulators under DC stresses," *IEEE Trans. Power Deliv.*, vol. 3, no. 2, pp. 776–782, Apr. 1988.
- [2-59] I. Kimoto, T. Fujimura, and K. Naito, "Performance of Insulators for Direct Current Transmission Line Under Polluted Condition," *IEEE Trans. Power Appar. Syst.*, vol. PAS-92, no. 3, pp. 943–949, May 1973.
- [2-60] C. H. A. Ely and W. J. Roberts, "Switching-impulse flashover of air gaps and insulators in an artificially polluted atmosphere," *Proc. Inst. Electr. Eng.*, vol. 115, no. 11, p. 1667, 1968.
- [2-61] M. Amin, M. Akbar, and M. Khan, "Aging Investigations of Polymeric Insulators: Overview and Bibliography," *IEEE Electr. Insul. Mag.*, vol. 23, no. 4, pp. 44–50, Jul. 2007.
- [2-62] CIGRE B2-214 "Assessment of the condition of overhead line composite insulators," CIGRE 2012.
- [2-63] R. S. Gorur, "Status assessment of composite insulators for outdoor HV applications," in *Proceedings of 5th International Conference on Properties and Applications of Dielectric Materials*, vol. 1, pp. 35–38, 1997.
- [2-64] L. Paris, L. Pargamin, D. Dumorora, and R. Parraud, "Rating of composite suspension insulators related to the long term mechanical strength of rods," *IEEE Trans. Power Deliv.*, vol. 9, no. 4, pp. 2055–2063, 1994.
- [2-65] R. G. Houlgate and D. A. Swift, "Composite rod insulators for AC power lines: electrical performance of various designs at a coastal testing station," *IEEE Trans. Power Deliv.*, vol. 5, no. 4, pp. 1944–1955, 1990.

- [2-66] V. K. Agarwal, "Aging of multistressed polymeric insulators," *IEEE Trans. Electr. Insul.*, vol. 24, no. 5, pp. 741–764, 1989.
- [2-67] C. A. Spellman, H. M. Young, A. Haddad, A. R. Rowland and R. T. Waters, "Survey of polymeric insulator ageing factors," in 11th International Symposium on High-Voltage Engineering (ISH 99), vol. 4, pp. 160–163, London, UK, 1999.
- [2-68] STRI Guide: "Composite insulator status program: field inspection of composite lineinsulators," STRI Guide 3, 2005.
- [2-69] STRI Guide: "Visual identification of deterioration and damages on suspension composite insulators", STRI Guide 5, 1/1998.
- [2-70] M. Kumosa, L. Kumosa, and D. Armentrout, "Failure analyses of nonceramic insulators. Part 1: Brittle fracture characteristics," *IEEE Electr. Insul. Mag.*, vol. 21, no. 3, pp. 14–27, May 2005.
- [2-71] J. P. Reynders, I. R. Jandrell, and S. M. Reynders, "Review of aging and recovery of silicone rubber insulation for outdoor use," *IEEE Trans. Dielectr. Electr. Insul.*, vol. 6, no. 5, pp. 620–631, 1999.
- [2-72] D. K. Bhana and D. A. Swift, "An investigation into the temporary loss of hydrophobicity of some polymeric insulators and coatings," in *Proceedings of 4th International Conference on Properties and Applications of Dielectric Materials (ICPADM)*, vol. 1, pp. 294–297, 1994.
- [2-73] S. H. Kim, E. A. Cherney, and R. Hackam, "Hydrophobic behavior of insulators coated with RTV silicone rubber," *IEEE Trans. Electr. Insul.*, vol. 27, no. 3, pp. 610–622, Jun. 1992.
- [2-74] H. Hillborg and U. W. Gedde, "Hydrophobicity changes in silicone rubbers," *IEEE Trans. Dielectr. Electr. Insul.*, vol. 6, no. 5, pp. 703–717, 1999.

- [2-75] R. Hackam, "Outdoor high voltage polymeric insulators," in Proceedings of 1998 International Symposium on Electrical Insulating Materials, in conjunction with 1998 Asian International Conference on Dielectrics and Electrical Insulation and 30th Symposium on Electrical Insulating Materials, pp. 1–16, Toyohashi, Japan, 1998.
- [2-76] R. S. Gorur, J. W. Chang, and O. G. Amburgey, "Surface hydrophobicity of polymers used for outdoor insulation," *IEEE Trans. Power Deliv.*, vol. 5, no. 4, pp. 1923–1933, 1990.
- [2-77] E. A. Cherney and R. S. Gorur, "RTV silicone rubber coatings for outdoor insulators," *IEEE Trans. Dielectr. Electr. Insul.*, vol. 6, no. 5, pp. 605–611, 1999.
- [2-78] A. E. Vlastos and E. Sherif, "Experience from insulators with RTV silicon rubber sheds and shed coatings," *IEEE Trans. Power Deliv.*, vol. 5, no. 4, pp. 2030–2038, 1990.
- [2-79] R. Dai, S. Wang, and F. Lu, "RTV silicone rubber hydrophobicity loss and recovery character under AC corona," in *International Conference on Electrical and Control Engineering*, pp. 807–810, Yichang, 2011.
- [2-80] D. A. Swift, C. Spellman, and A. Haddad, "Hydrophobicity transfer from silicone rubber to adhering pollutants and its effect on insulator performance," *IEEE Trans. Dielectr. Electr. Insul.*, vol. 13, no. 4, pp. 820–829, Aug. 2006.
- [2-81] P. Charalampidis, "Characterisation of textured insulators for overhead lines and substations", PhD thesis, High Voltage Energy Systems Group, Cardiff University, 2012.

- [2-82] J. V. Vas, B. Venkatesulu, and M. J. Thomas, "Tracking and erosion of silicone rubber nanocomposites under DC voltages of both polarities," *IEEE Trans. Dielectr. Electr. Insul.*, vol. 19, no. 1, pp. 91–98, Feb. 2012.
- [2-83] A. I. Elombo, J. P. Holtzhausen, H. J. Vermeulen, P. J. Pieterse, and W. L. Vosloo, "Comparative evaluation of the leakage current and aging performance of HTV SR insulators of different creepage lengths when energized by AC, DC+ or DC– in a severe marine environment," *IEEE Trans. Dielectr. Electr. Insul.*, vol. 20, no. 2, pp. 421–428, Apr. 2013.
- [2-84] G. Bruce, S. Rowland, and A. Krivda, "Performance of silicone rubber in DC inclined plane tracking tests," *IEEE Trans. Dielectr. Electr. Insul.*, vol. 17, no. 2, pp. 521–532, Apr. 2010.
- [2-85] T. G. Gustavsson, S. M. Gubanski, H. Hillborg, S. Karlsson, and U. W. Gedde, "Aging of silicone rubber under ac or dc voltages in a coastal environment," *IEEE Trans. Dielectr. Electr. Insul.*, vol. 8, no. 6, pp. 1029–1039, 2001.
- [2-86] E. Nasser, "Some Physical Properties of Electrical Discharges on Contaminated-Surfaces," *IEEE Trans. Power Appar. Syst.*, vol. PAS-87, no. 4, pp. 957–963, Apr. 1968.
- [2-87] A. de la O and R. S. Gorur, "Flashover of contaminated nonceramic outdoor insulators in a wet atmosphere," *IEEE Trans. Dielectr. Electr. Insul.*, vol. 5, no. 6, pp. 814–823, 1998.
- [2-88] G. G. Karady, M. Shah, and R. L. Brown, "Flashover mechanism of silicone rubber insulators used for outdoor insulation-I," *IEEE Trans. Power Deliv.*, vol. 10, no. 4, pp. 1965–1971, 1995.

- [2-89] M. Shah, G. G. Karady, and R. L. Brown, "Flashover mechanism of silicone rubber insulators used for outdoor insulation-II," *IEEE Trans. Power Deliv.*, vol. 10, no. 4, pp. 1972–1978, 1995.
- [2-90] G. G. Karady, "Flashover mechanism of non-ceramic insulators," *IEEE Trans. Dielectr. Electr. Insul.*, vol. 6, no. 5, pp. 718–723, 1999.
- [2-91] W. Que, "Electric field and voltage distributions along non-ceramic insulators", PhD thesis, department of electrical engineering, The Ohio State University, 2002.
- [2-92] STRI. Guide, "Hydrophobicity Classification Guide", 92/1, 1992.
- [2-93] International Electrotechnical Commission TS 62073, Guidance on the measurement of wettability of insulator surfaces, 2003.
- [2-94] INMR article "12 examples of insulator failure", *INMR Transmission and Distribution Magazine*, December 24, 2015, link: "<http://www.inmr.com/examples-insulator-failure/>", accessed on 29 December 2015.
- [2-95] M. Berg, R. Thottappillil, and V. Scuka, "Hydrophobicity estimation of HV polymeric insulating materials. Development of a digital image processing method," *IEEE Trans. Dielectr. Electr. Insul.*, vol. 8, no. 6, pp. 1098–1107, 2001.
- [2-96] A. N. Jahromi, A. H. El-Hag, S. H. Jayaram, E. A. Cherney, M. Sanaye-Pasand, and H. Mohseni, "A Neural Network Based Method for Leakage Current Prediction of Polymeric Insulators," *IEEE Trans. Power Deliv.*, vol. 21, no. 1, pp. 506–507, Jan. 2006.
- [2-97] M. A. R. M. Fernando and S. M. Gubanski, "Leakage current patterns on contaminated polymeric surfaces," *IEEE Trans. Dielectr. Electr. Insul.*, vol. 6, no. 5, pp. 688–694, 1999.

- [2-98] A. De La O, R. S. Gorur, and J. Chang, "AC clean fog tests on nonceramic insulating materials and a comparison with porcelain," *IEEE Trans. Power Deliv.*, vol. 9, no. 4, pp. 2000–2008, 1994.
- [2-99] Jeong-Ho Kim, Woo-Chang Song, Jae-Hyung Lee, Yong-Kwan Park, Han-Goo Cho, Yeong-Sik Yoo, and Kea-Joon Yang, "Leakage current monitoring and outdoor degradation of silicone rubber," *IEEE Trans. Dielectr. Electr. Insul.*, vol. 8, no. 6, pp. 1108–1115, 2001.
- [2-100] P. J. Lambeth, J. S. T. Looms, M. Sforzini, R. Cortina, Y. Porcheron, and P. Claverie, "The Salt Fog Test and its Use in Insulator Selection for Polluted Localities," *IEEE Trans. Power Appar. Syst.*, vol. PAS-92, no. 6, pp. 1876–1887, Nov. 1973.
- [2-101] BS EN 60507, "Artificial pollution test on high-voltage insulators to be used on a.c. systems," British Standard, May 1993.
- [2-102] BS EN 62217, "Polymeric insulators for indoor and outdoor use with a nominal voltage > 1 000 V — General definitions, test methods and acceptance criteria," British Standard, December 2006.
- [2-103] IEC 60587:2007, "Electrical insulating materials used under severe ambient conditions. Test methods for evaluating resistance to tracking and erosion", 2007.
- [2-104] Lightning and Insulator Subcommittee, "Application of Insulators in a Contaminated Environment," *IEEE Trans. Power Appar. Syst.*, vol. PAS-98, no. 5, pp. 1676–1695, Sep. 1979.
- [2-105] B. Macchiaroli and F. Turner, "A New Contamination Test Method," *IEEE Trans. Power Appar. Syst.*, vol. PAS-88, no. 9, pp. 1400–1411, Sep. 1969.

- [2-106] P. Claverie, "Predetermination of the Behaviour of Polluted Insulators," IEEE Trans. Power Appar. Syst., vol. PAS-90, no. 4, pp. 1902–1908, Jul. 1971.
- [2-107] M. Farzaneh and J. F. Drapeau, "AC flashover performance of insulators covered with artificial ice," IEEE Trans. Power Deliv., vol. 10, no. 2, pp. 1038–1051, Apr. 1995.
- [2-108] D. L. Williams, A. Haddad, A. R. Rowlands, H. M. Young, and R. T. Waters, "Formation and characterization of dry bands in clean fog on polluted insulators," IEEE Trans. Dielectr. Electr. Insul., vol. 6, no. 5, pp. 724–731, 1999.
- [2-109] P. Dixit, V. Krishnan, and G. R. Nagabhushana, "Mathematical model to predict flashover voltages of polluted polymeric insulators intended for UHV DC," in 2010 International Conference on High Voltage Engineering and Application, pp. 437–440, 2010.
- [2-110] M. E.-A. Slama, A. Beroual, and H. Hadi, "Experimental and mathematical modeling of the effect of non-soluble and low soluble salts and salts mixture pollution on dc flashover of high voltage insulators," in 2012 Annual Report Conference on Electrical Insulation and Dielectric Phenomena, pp. 757–760, 2012.
- [2-111] M. H. Nazemi and V. Hinrichsen, "Experimental investigations on partial discharge characteristics of water droplets on polymeric insulating surfaces at AC, DC and combined AC-DC voltages," IEEE Trans. Dielectr. Electr. Insul., vol. 22, no. 4, pp. 2261–2270, Aug. 2015.
- [2-112] S. Venkataraman and R. S. Gorur, "Prediction of flashover voltage of non-ceramic insulators under contaminated conditions," IEEE Trans. Dielectr. Electr. Insul., vol. 13, no. 4, pp. 862–869, Aug. 2006.

- [2-113] H. El-Kishky and R. S. Gorur, "Electric field computation on an insulating surface with discrete water droplets," *IEEE Trans. Dielectr. Electr. Insul.*, vol. 3, no. 3, pp. 450–456, Jun. 1996.
- [2-114] C. Muniraj and S. Chandrasekar, "Predictive dynamic arc model of the pre-flashover leakage current on polymeric insulators," in *2011 International Conference on Power and Energy Systems*, pp. 1–5, 2011.
- [2-115] IEC 60815-1:2008, "Selection and dimensioning of high-voltage insulators intended for use in polluted conditions, Part 1 definitions, information and general principles", 2008.
- [2-116] Y. Gao, H. Mei, L. Wang, Z. Guan, and M. Lu, "Feasibility analysis of polymeric material insulator applied to phase to earth insulation of transmission line," in *2014 IEEE Conference on Electrical Insulation and Dielectric Phenomena (CEIDP)*, pp. 357–360, 2014.
- [2-117] N. Vasudev, P. V. V. Nambudri, M. N. Dinesh, K. N. Ravi, and V. Krishnan, "Long term ageing performance of Silicone rubber insulators under different conditions," in *2009 IEEE 9th International Conference on the Properties and Applications of Dielectric Materials*, pp. 276–280, 2009.
- [2-118] G. Haddad, K. L. Wong, and P. Petersen, "Evaluation of the hydrophobic property of composite insulators using Dynamic Drop Test," in *Proceedings of 2014 International Symposium on Electrical Insulating Materials*, pp. 280–283, 2014.
- [2-119] J. P. Holtzhausen, P. J. Pieterse, H. J. Vermeulen, and S. Limbo, "Insulator aging tests with HVAC and HVDC excitation using the tracking wheel tester," in *2010 International Conference on High Voltage Engineering and Application*, pp. 445–448, 2010.

CHAPTER 3

- [3-1] IEC 62730: "HV polymeric insulators for indoor and outdoor use tracking and erosion testing by wheel test and 5 000h test", 2012.
- [3-2] IEC 60815-1:2008, "Selection and dimensioning of high-voltage insulators intended for use in polluted conditions, Part 1 definitions, information and general principles", 2008.
- [3-3] A. Haddad, K. Chrzan, H. Griffiths and R.T. Waters, "A new approach to anti-fog design for polymeric insulators", Intern. Sympos. High Voltage Engineering (ISH), Ljubljana, Slovenia, paper T4-446, 2007.
- [3-4] A. Haddad, H. Griffiths, and R. T. Waters, "Principles of anti-fog design for polymeric insulators", Int. Conf. Solid Dielectr. ICSD, pp. 302–305, 2007.
- [3-5] S. A. Sebo, "Accelerated aging methods for outdoor insulation - Rotating wheel and salt fog chamber tests," in 2010 Annual Report Conference on Electrical Insulation and Dielectric Phenomena, pp. 1–4, 2010.
- [3-6] Wacker Chemie AG. Last access date: October 2015. [Online]. Available: <http://www.wacker.com/>.
- [3-7] National Instruments, LabVIEW user manual, 2003.
- [3-8] Reading and writing TDMS files with NI LabVIEW, Last access date: October 2015. [Online]. Available: <http://www.ni.com/white-paper/3727/en/#toc3>.
- [3-9] IEC 60507:2013, 'Artificial pollution tests on high-voltage ceramic and glass insulators to be used on a.c. systems', 3rd edition.

- [3-10] M. Farzaneh and W. A. Chisholm. *Insulators for Icing and Polluted Environments*. Hoboken, New Jersey: John Wiley & Sons, Inc., 2009, pp. 645–646.
- [3-11] A Muncivi, P. Sarkar, and A. Haddad, “Tracking wheel test facilities”, 44th International Universities Power Engineering Conference, pp. 1-5, Glasgow (UK), 2009.
- [3-12] G. Alice, “Tracking wheel test for dc polymeric insulators”, MSc thesis, Faculty of engineering, Padova University, 2010.
- [3-13] M. Albano, “Conductance meter”, internal technical notes, Cardiff University, 2014.

CHAPTER 4

- [4-1] I. Ramirez-Vazquez, J. Ruiz-Pinales, and J. Salgado-Talavera, “Fractal analysis of nano-reinforced silicone rubber insulators evaluated on a tracking wheel,” *IEEE Electr. Insul. Mag.*, vol. 30, no. 4, pp. 21–27, Jul. 2014.
- [4-2] A. S. Krzma, M. Albano, and A. Haddad, “Comparative performance of 11kV silicone rubber polymeric insulators under Rotating Wheel Dip Test”, 49th International Universities Power Engineering Conference, pp. 1–5, Cluj-Napoca (Romania), 2014.
- [4-3] M. Albano, P. Charalampidis, A. Haddad, H. Griffiths and R. Waters, “Silicone rubber insulators for polluted environments part 2: textured insulators”, *IEEE Transaction. Dielectric and Electrical Insulation*, vol. 21, no. 2, pp. 749–757, 2014.
- [4-4] B. Marungsri, H. Shinokubo, and R. Matsuoka, “Effect of Specimen Configuration on Deterioration of Silicone Rubber for Polymer Insulators

- in Salt Fog Ageing Test”, IEEE Transactions on Dielectric and Electrical Insulation, vol. 13, no. 1, pp. 129–138, 2006.
- [4-5] J. Grasaesom, W. Payakcho, B. Marungsri, and A. Specimen, “Ageing Deterioration of Silicone Rubber Polymer Insulator under Salt Water Dip Wheel Test”, Journal of World Academy of Science, Engineering and Technology, Vol. 56, pp. 211–217, 2011.
- [4-6] I. J. S. Lopes, S. H. Jayaram, and E. A. Cherney, “A Method for Detecting : the Transition from Corona from Water Droplets to Dry Band Arcing on Silicone Rubber Insulators ”, IEEE Transaction. Dielectric and Electrical Insulation, Vol. 9, pp. 964–971, 2002.
- [4-7] G. Heger, H. Vermeulen, J. Holtzhausen, and W. Vosloo, “A comparative study of insulator materials exposed to high voltage AC and DC surface discharges,” IEEE Transaction. Dielectric and Electrical Insulation, vol. 17, no. 2, pp. 513–520, Apr. 2010.
- [4-8] L. H. Meyer, S. H. Jayaram, and E. A. Cherney, “Correlation of Damage, Dry Band Arcing Energy, and Temperature in Inclined Plane Testing of Silicone Rubber for Outdoor Insulation”, IEEE Transaction. Dielectric and Electrical Insulation, vol. 11, no. 3, pp. 424–432, June. 2004.
- [4-9] R. Abd-Rahman, A. Haddad, N. Harid, and H. Griffiths, “Stress control on polymeric outdoor insulators using Zinc oxide microvaristor composites,” IEEE Trans. Dielectr. Electr. Insul., vol. 19, no. 2, pp. 705–713, Apr. 2012.
- [4-10] R. Abd Rahman, N. Harid, and A. Haddad, “Universities Power Engineering Conference (UPEC), 2010 45th International,” Universities Power Engineering Conference (UPEC), 2010 45th International. pp. 1–4, 2010.

Chapter 5

- [5-1] K.O. Papailiou, F. Schmuck, "Silicon Composite Insulators – Material, Design Applications", Springer, 2013, ISBN 978-3-642-15319-8.
- [5-2] A. I. Elombo, J. P. Holtzhausen, H. J. Vermeulen, P. J. Pieterse, and W. L. Vosloo, "Comparative evaluation of the leakage current and aging performance of HTV SR insulators of different creepage lengths when energized by AC, DC+ or DC– in a severe marine environment", IEEE Transaction. Dielectric and Electrical Insulation, vol. 20, no. 2, pp. 421–428, Apr. 2013.
- [5-3] A. Abbasi, A. Shayegani, and K. Niayesh, "Contribution of design parameters of SiR insulators to their DC pollution flashover performance", IEEE Trans. Power Deliv., vol. 29, no. 4, pp. 1814–1821, 2014.
- [5-4] Z. Zhang, X. Jiang, H. Huang, C. Sun, J. Hu, and D. W. Gao, "Study on the wetting process and its influencing factors of pollution deposited on different insulators based on leakage current," IEEE Trans. Power Deliv., vol. 28, no. 2, pp. 678–685, 2013.
- [5-5] A. Pigni, "Most Insulator Failures Result from Improper Selection", INMR T&D, March 18, 2015, link: "<http://www.inmr.com/insulator-failures-result-improper-selection/>", accessed on 25 March 2015.
- [5-6] P. Charalampidis, M. Albano, H. Griffiths, a. Haddad, and R. T. Waters, "Silicone rubber insulators for polluted environments part 1: enhanced artificial pollution tests", IEEE Transaction. Dielectric and Electrical Insulation, vol. 21, no. 2, pp. 740–748, Apr. 2014.
- [5-7] M. Farzaneh, William A. Chisholm "Insulators for Icing and Polluted Environments", John Wiley & Sons, 26 Oct 2009.

- [5-8] M. Leclerc, R.P. Bouchard, Y. Gervais, and D. Mukhedkar, "Wetting Processes on a Contaminated Insulator Surface," IEEE Trans. Power Appar. Syst., vol. PAS-101, no. 5, pp. 1005–1011, 1982.
- [5-9] D.A. Swift, C. Spellman and A. Haddad "Hydrophobicity Transfer from Silicone Rubber to Adhering Pollutants and its Effect on Insulator Performance", IEEE Transaction. Dielectric and Electrical Insulation, Vol. 13, No. 4; 2006.
- [5-10] S. Kumagai and N. Yoshimura, "Hydrophobic transfer of RTV silicone rubber aged in single and multiple environmental stresses and the behavior of LMW silicone fluid", IEEE Trans. Power Deliv., Vol. 18, no. 2, pp. 506–516, 2003.
- [5-11] Z. Jia, H. Gao, Z. Guan, L. Wang, and J. Yang, "Study on Hydrophobicity Transfer of RTV Coatings Based on a Modification of Absorption and Cohesion Theory", IEEE Transaction. Dielectric and Electrical Insulation, Vol.13, no. 6, pp. 1317–1324, 2006.
- [5-12] M. Albano, A. S. Krzma, R. T. Waters, H. Griffiths, and A. Haddad, "Artificial pollution layer characterization on conventional and textured silicone-rubber insulators," in The 19th International Symposium on High Voltage Engineering (ISH), Pilsen, Czech Republic, 2015.

CHAPTER 6

- [6-1] G. Bruce, S. Rowland, and A. Krivda, "Performance of silicone rubber in DC inclined plane tracking tests", IEEE Transactions on Dielectric and Electrical Insulation, vol.17, no.2, pp.521–532, 2010.
- [6-2] J. V. Vas, B. Venkatesulu, and M. J. Thomas, "Tracking and erosion of silicone rubber nanocomposites under DC voltages of both polarities",

IEEE Transactions on Dielectric and Electrical Insulation, vol.19, no.1, pp.91–98, 2012.

- [6-3] M. T. Gencoglu, and M. Cebeci “Computation of AC flashover voltage of polluted HV insulators using a dynamic arc model”, European Transactions on Electrical Power, vol. 19, no. 5, pp. 689–701, 2009.
- [6-4] E. Kuffel, W. S. Zaengl, and J. Kuffel. *High Voltage Engineering, Fundamentals*. Oxford, Great Britain: Butterworth-Heinemann, 2000, pp.509-510.